Cortical experience-dependent plasticity and mesostriatal dopaminergic dysfunction in a mouse model of Angelman syndrome

Thorfinn Riday

A dissertation submitted to the faculty of the University of North Carolina at Chapel Hill in partial fulfillment of the requirements for the degree of Doctor of Philosophy in Curriculum of Neurobiology.

Chapel Hill
2013

Approved by:

Benjamin Philpot PhD

Paul Manis PhD

Ken McCarthy PhD

Flavio Frohlich PhD

William Boyes PhD

ABSTRACT

THORFINN RIDAY: Cortical experience-dependent plasticity and mesostriatal dopaminergic dysfunction in a mouse model of Angelman syndrome
(Under the direction of Bejamin Philpot)

Sensory experience guides development of neocortical circuits. This activity-dependent circuit maturation is required for normal sensory and cognitive abilities, which are distorted in neurodevelopmental disorders. Here we have tested whether experience-dependent cortical modifications require *Ube3a*, an E3 ubiquitin ligase whose dysregulation has been implicated in both autism and Angelman syndrome (AS). Using the visual cortex as a model system for neocortical plasticity, we found that the genetic deletion of UBE3A attenuates activity-dependent synaptic strengthening and weakening in visual cortical slices. Chronic recordings of visual evoked potentials (VEPs) from awake mice also exhibited deficits in critical period ocular dominance plasticity, an *in vivo* assay for experience-dependent synaptic weakening. Stimulus-specific response potentiation (SRP) of VEPs was used as an assay of experience-dependent synaptic strengthening. Contrary to the results observed in *in vitro* slice preparations, we observed developmentally enhanced potentiation of VEPs, including increased power of spontaneous local field potentials (LFP) in AS mice. WT and AS mice achieved similar increases in VEP amplitude with a longer period of visual stimulation, indicating the threshold for potentiation was lower in AS mice. Augmented plasticity and increased spontaneous LFP power were absent from mice maternally

expressing *Ube3a* in inhibitory neurons alone. Our results suggest that sensory experience-dependent cortical potentiation is enhanced in adult AS mice due to reduced inhibition.

Previous studies also suggest that abnormal dopamine neurotransmission may underlie some of the motor deficits exhibited in AS. A clinical trial of levodopa (L-DOPA) in AS is ongoing, although the underlying rationale for this treatment strategy has not yet been thoroughly examined in preclinical models. We found that AS mice exhibited behavioral deficits that correlated with abnormal dopamine signaling. These deficits were not due to loss of dopaminergic neurons or impaired dopamine synthesis. Unexpectedly, AS mice exhibited increased dopamine release in the mesolimbic pathway while also exhibiting a decrease in dopamine release in the nigrostriatal pathway, as measured with fast-scan cyclic voltammetry. These findings demonstrate the complex effects of UBE3A loss on dopamine signaling in subcortical motor pathways that may inform ongoing clinical trials of L-DOPA therapy in patients with AS.

TABLE OF CONTENTS

LIST OF TABLES

LIST OF FIGURES

Chapter 2

Chapter 3

Chapter 4

LIST OF ABREVIATIONS

ACSF	artificial cerebrospinal fluid
AMPA	2-amino-3-(3-hydroxy-5-methyl-isoxazol-4-yl)propanoic acid
APV	(2R)-amino-5-phosphonovaleric acid
AS	Angelman syndrome
BSR	brain stimulation reward
CaMKII	calcium/calmodulin kinase II
D1	dopamine receptor subtype 1
D2	dopamine receptor subtype 2
D3	dopamine receptor subtype 3
DA	dopamine
DAT	dopamine transport blocker
DOPAC	3,4-dihydroxyphenylacetic acid
DR	dark-reared
FSCV	fast-scan cyclic voltammetry
fEPSP	field excitatory postsynaptic potential

HECT	Homologous to the E6-AP Carboxyl Terminus
HEPES	4-(2-hydroxyethyl)-1-piperazineethanesulfonic acid
HPLC	high-performance liquid chromatography
ICSS	intracranial self-stimulation
L-DOPA	levodopa
LTD	long-term depression
LTP	long-term potentiation
MD	monocular deprivation
mEPSC	miniature excitatory post synaptic currents
MFB	medial forebrain bundle
NAc	nucleus accumbens
NMDA	N-methyl-D-aspartate
NR	normally-reared
P	postnatal day
Park2	E3 ubiquitin ligase parkin
Park7	glyoxylase DJ-1
PBS	phosphate-buffered saline

Pink1	PTEN-induced kinase 1, also known as Park6
SDS-PAGE	sodium dodecyl sulfate polyacrylamide gel electrophoresis
SNc	substantia nigra pars compact
SNCA	α-synuclein
SRP	stimulus-specific response potentiation
TH	tyrosine hydroxylase
$Ube3A^{m-/p+}$	maternally-deficient Ube3A heterozygous mouse (AS model mouse)
$Ube3A^{m+/p-}$	paternally-deficient Ube3A heterozygous mouse
VEP	visually evoked potential
VTA	ventral tegmental area
WT	wild-type

CHAPTER 1

1. Introduction

1.1. Angelman Syndrome

Angelman syndrome (AS) is an autism spectrum disorder occurring in 1 in 12,000 to 20,000 births, characterized by profound mental retardation, lack of language, abnormal EEG activity, seizures, disrupted sleep patterns, puppet-like ataxic movements, inappropriate paroxysms of laughter, and hyperactivity (Steffenburg et al., 1996; Kishino et al., 1997a; Peters et al., 2004; Williams et al., 2006; Yashiro et al., 2009) (Table 1-1). AS is caused by the functional loss of the Ube3a gene, found within the 15q11-q13 chromosomal locus, and is maternally imprinted in the brain. The Ube3a gene encodes a HECT domain E3 ubiquitin ligase involved in protein degradation through the ubiquitin-associated proteosome pathway (Kishino et al., 1997b; Sutcliffe et al., 1997b). The UBE3A gene encodes for three protein isoforms generated by differential splicing, however it is not known whether they differ in function or substrate specificity (Yamamoto et al., 1997). Characterization of the endogenous properties and function of Ube3a, and its roles in the pathogenesis of Angelman syndrome, are essential in developing behavioral and pharmacological therapeutics.

1.2. Causes of Angelman Syndrome

The 15q11-13 chromosomal region is a relatively unstable region in which deletions, mutations, and imprinting defects can result is AS. AS is most commonly (65-75%) caused by *de novo* deletions (5-7 Mb) to 15q11-q13 (Williams et al., 2010). 3-7% of individuals

with AS occur when two copies of the paternal chromosomal segment containing UBE3A are inherited (uniparental disomy), with the absence of a maternal copy. Another ~3% of individuals with AS exhibit normal biparental inheritance of the UBE3A allele, but do not express *Ube3a* because of an imprinting defect. Defects in imprinting can occur as a result of abnormal DNA methylation patterns or small deletions in the imprinting center along 15q11-q13, which regulates DNA methylation and imprinting in this region of genes. 5-11% of cases result from mutations in the UBE3A allele, indicating that loss of maternal Ube3a function alone is sufficient for AS. It is interesting to note that while loss of Ube3a function is sufficient for AS, the most commonly associated genetic variation with autism is duplication and triplication of the maternal 15q11-q13 locus containing UBE3A gene (Browne et al., 1997; Mao et al., 2000; Abrahams and Geschwind, 2008; Smith et al., 2011).

1.3. **Ube3a substrates and protein interactions**

Since the initial identification of *Ube3a*, a growing number of proteins have been shown to interact with Ube3a including p53 (Huibregtse et al., 1991), the human homologue A of Rad23 (Kumar et al., 1999), multicopy maintenance protein 7 (Kuhne and Banks, 1998), Src family kinase Blk (Oda et al., 1999), cyclin dependent kinase inhibitor p27 (Mishra et al., 2009), immediate early gene Arc/Arg3.1 (Greer et al., 2010), RhoA guanine nucleotide exchange factor Ephexin5 (Margolis et al., 2010), and even Ube3a itself (Nuber et al., 1998) (Table 1-2). However, the physiological relevance of many of these potential substrates is unknown, and may not all be germane to the body of symptoms encompassed by Angelman syndrome.

Several of these substrates are involved in learning and memory, and may contribute to the cognitive disabilities in AS. The neuronal activity-dependent gene Arc is required for

learning, long-term memory, and homeostatic plasticity (Mabb et al., 2011). Absence of Ube3a increases Arc expression, dysregulating cell surface expression of AMPA receptors by increased endocytosis (Greer et al., 2010), a process thought to be critical in LTP and LTD (Bramham et al., 2008). Ephexin5 interacts with EphrinB upon stimulation by EphB2, leading to activation of RhoA and the suppression of synapse and spine number. Degradation of Ephexin5 is mediated by Ube3a, suggesting that the reduction in spine density observed in AS may be in part attributed to elevated Ephexin5 levels (Margolis et al., 2010; Mabb et al., 2011). Loss of Ube3a increases p27 levels in the cortex, hippocampus and cerebellum (Mishra et al., 2009). It is known that increased p27 in the cortex promotes neuronal differentiation and migration (Nguyen et al., 2006), and therefore may alter cortical cytoarchitecture and function in AS.

Another prominent feature of AS is motor dysfunction and at least two of the identified substrates appear to be involved. There is evidence that Ube3a deficiency reduces degradation of GABA transporter 1 (GAT1). The increase in GAT1 expression leads to lower ambient concentrations of extracellular GABA, which in turn decreases $GABA_A$ receptor-mediated tonic inhibition in cerebellar granule and purkinje cells (Egawa et al., 2012). The attenuated tonic inhibition in the cerebellum contributes to the ataxic-motor dysfunction in AS. In addition to motor dysfunction attributed to the cerebellum, the Ube3a substrate α-synuclein (Mishra et al., 2009) implicates the nigrolstriatal pathway as well in AS. α-Synuclein accumulates in protein inclusions called Lewy bodies, one of the pathophysiological hallmarks of the Parkinson's disease (Kirik et al., 2002). This neurodegenerative disorder results in dopaminergic cell loss in the substantia nigra (SNc). SNc dopaminergic cell loss has been documented in adult AS model mice, in conjunction

with nigrolstriatal-sensitive motor deficits (Mulherkar and Jana, 2010). Parkinsonian symptoms like resting tremor, cogwheel rigidity and bradykinesia have been reported in adults with AS, and were responsive to dopamine replacement therapy (Harbord, 2001).

1.4. **Animal models of Angelman Syndrome**

Mouse models have contributed to the bulk of the neurological knowledge underlying the phenotypes of AS. The earliest AS mouse model was created by parental duplication (partial parental disomy) of the homologous chromosomal region for 15q11-q13, where the UBE3A gene is located (Cattanach et al., 1997). These mice had several characteristics features of AS, including diffuse cortical slow-wave EEG abnormalities, cortical thinning and reduced brain weight, abnormal body weight growth curve, juvenile hyperactivity, and mild ataxia. Employing in situ hybridization, evidence of maternal-specific expression of UBE3A in the mouse brain was demonstrated for the first time (Albrecht et al., 1997).

After establishing UBE3A as the critical gene precipitating in AS (Kishino et al., 1997a), a mouse model was created that specifically targeted the sequence orthologous to human exon 2 of UBE3A via 3kb deletion, rendering the protein product inactive (Jiang et al., 1998). These maternally-deficient heterozygous Ube3a (*Ube3a*$^{m-/p+}$) mice have become the principle mouse model for AS research. Similar to the parental disomy AS model, *Ube3a*$^{m-/p+}$ mice also exhibited ataxia, reduced brain weight and abnormal EEG patterns, including audiogenic-induced seizures. Learning and memory deficits were also observed in the context-dependent fear-conditioning paradigm, consistent with a reduction in hippocampal long-term potentiation (LTP).

A subsequent study found that inhibitory phosphorylation at Thr305 of calcium/calmodulin-dependent protein kinase II (CaMKII) in the hippocampus was

increased, reducing the CaMKII activity (Weeber et al., 2003). The dysregulation of CaMKII was discovered without changes in any other learning-related kinases. This led to the hypothesis that dysregulation of CaMKII was responsible for the reduction in hippocampal LTP, which is dependent on CaMKII activation. A genetic rescue was performed by crossing *Ube3a*$^{m-/p+}$ mice with *CaMKIIT*$^{305/T\ 306V}$ mice, which were deficient in inhibitory CaMKII autophosphorylation (van Woerden et al., 2007). The consequent offspring had comparable levels of CaMKII with wild-type mice. Normal LTP-induction was reinstated, as well as rescuing their performance in a number of behavioral learning paradigms including context-dependent fear-conditioning, Morris water maze tasks, time on the rotarod.

As in humans with AS, the observed motor deficits in the *Ube3a*$^{m-/p+}$ mice have been mostly ascribed to cerebellar dysfunction (Jiang et al., 1998; Cheron et al., 2005; Lalande and Calciano, 2007; Heck et al., 2008; Egawa et al., 2012). In addition to deficits on the rotarod task, *Ube3a*$^{m-/p+}$ mice also exhibited deficits in rope climbing, grip strength, gait, balance on the raised-beam task, and increased licking behavior (Heck et al., 2008). Although most of the studies of *Ube3a*$^{m-/p+}$ mice have attributed all the observed motor deficits to dysfunction of the Purkinje cells in the cerebellum, this has never been rigorously tested. Motor function is also regulated by the spinal cord and basal ganglia. One study of the *Ube3a*$^{m-/p+}$ mice observed abnormalities in the nigrostriatal pathway. In this report it was found that the number of dopamine cells in the SNc were significantly reduced in *Ube3a*$^{m-/p+}$ mice, and credited that loss for the poor performance on more nigralstriatial sensitive behavioral paradigms such as the raised balance beam and pole test (Mulherkar and Jana, 2010).

A second AS mouse model was generated that targeted the human orthologs to exon 15 and 16 of the UBE3A gene (Miura et al., 2002). As with the previous AS mouse model of Jiang et al. (1998), there were deficits in hippocampal-dependent memory tasks, LTP-induction (and impaired neurogenesis), motor coordination, and increased occurrences of seizures (Miura et al., 2002; Mardirossian et al., 2009). EEG recordings revealed abnormal wake/sleep patterns, including reduced time spent in rapid-eye movement (REM), as has been reported in many children with AS (Bruni et al., 2004; Miano et al., 2004; Colas et al., 2005). Electrophysiological recordings from the cerebellum exhibited fast oscillations sustained by increased Purkinje cell firing and rhythmicity (Cheron et al., 2005), as well as a reduction in tonic inhibition mediated by increased GAT1 expression and decreased extracellular levels of GABA (Cheron et al., 2005; Egawa et al., 2012). Treatment with a $GABA_A$ agonist both increased tonic inhibition and reduced cell firing and rhythmicity, resulting in improved performance on the rotarod (Cheron et al., 2005); Egawa et al., 2012).

Although targeted inactivation of maternal UBE3A by itself has been sufficient to cause characteristic AS features in the mouse models of Jiang et al. (1998) and Miura et al. (2002), the predominant form of AS in humans is caused by large deletions to 15q11-13 that also disrupt neighboring genes (Williams et al., 2010). Clinical features of individuals with deletions to 15q11-13 are typically more severe than those with mutations, especially in regards to epilepsy (Smith et al., 1997; Minassian et al., 1998; Moncla et al., 1999; Lossie et al., 2001; Clayton-Smith and Laan, 2003; Mabb et al., 2011). The increased incidence and severity of epilepsy may in part be due to disruptions in the neighboring GABRB3 gene, also known to cause epilepsy (DeLorey et al., 1998). In order to better represent the large deletion class of AS, a mouse model was created with a maternal deletion that spanned 1.6

Mb, disrupting UBE3A, ATP10A, and GABRB3 (Jiang et al., 2010). This AS mouse model recapitulated many of the phenotypes of the two targeted UBE3A models, including impaired motor function and learning and memory deficits. Future comparative studies of the large and micro deletion mouse models of AS will be informative in elucidating the contributing influence of ATP10A and GABRB3 to the severity of AS phenotypes, particularly epilepsy and the abnormal EEG patterns.

An earlier AS mouse model with a transgene-induced mutation that generated a much larger 4 Mb deletion of the 15q11-13 region had been created many years ago (Gabriel et al., 1999). The deletion included UBE3A, ATP10A, GABRB3, GABRA5, GABRG3, P, HERC2, SNURF-SNRPN, NDN, ZFP127. While imprinting of *Ube3a* was confirmed in the cerebellum, no behavioral characterization of the model was ever reported. Another AS mouse model was created which disrupted the AS imprinting center (AS-IC) (Johnstone et al., 2006; Wu et al., 2006)Wu et al., 2006). These models silenced *Ube3a* expression by disrupting the AS-IC, causing maternal *Ube3a* antisense transcription and the repression of *Ube3a* in cis (Johnstone et al., 2006; Wu et al., 2006). Unfortunately, no behavioral descriptions of either AS-IC mouse models have been published to date.

Interestingly, while loss of *Ube3a* expression results in AS, increased expression of *Ube3a* by duplication and triplication of the maternal UBE3A gene is linked to autism (Browne et al., 1997; Mao et al., 2000; Abrahams and Geschwind, 2008; Smith et al., 2011). To study how Ube3a overexpression relates to autism, mice that had two or three maternal copies of UBE3A were created (Smith et al., 2011). As had been found in humans, penetrance of autistic traits such as reduced vocalizations (impaired communication), lack of

social preference (impaired social interactions) and increased grooming (stereotypy) were increased with UBE3A gene dosage.

In addition to the many mouse models of AS, two drosophila models of also been created (Wu et al., 2008; Lu et al., 2009). The drosophila homolog of UBE3A is dUBE3A, and when deleted resulted in impaired motor function, atypical climbing behavior and abnormal circadian rhythms (Wu et al., 2008). The dUBE3A-deficient drosophila exhibited deficits in memory paradigms when training was spaced out, indicating a disruption in long-term memory formation. However, performance on massed training memory paradigms was normal, indicating intermediate-term memory was unaffected. Morphology, dendritic branching was decreased, along with total dendritic length (Lu et al., 2009). Overexpression of dUBE3A also reduced dendritic branching, suggesting a critical role of dUBE3A in regulating dendritic arborization.

Consistent (100%)
Developmental delay, functionally severe
Movement or balance disorder, usually ataxia of gait and/or tremulous movement of limbs. Movement disorder can be mild. May not appear as frank ataxia but can be forward lurching, unsteadiness, clumsiness, or quick, jerky motions
Behavioral uniqueness: any combination of frequent laughter/smiling; apparent happy demeanor; easily excitable personality, often with uplifted hand-flapping or waving movements; hypermotoric behavior
Speech impairment, none or minimal use of words; receptive and nonverbal communication skills higher than verbal ones
Frequent (more than 80%)
Delayed, disproportionate growth in head circumference, usually resulting in microcephaly (≤2 S.D. of normal OFC) by age 2 years. Microcephaly is more pronounced in those with 15q11.2-q13 deletions.
Seizures, onset usually < 3 yrs. of age. Seizure severity usually decreases with age but the seizure disorder lasts throughout adulthood.
Abnormal EEG, with a characteristic pattern, as mentioned in the text. The EEG abnormalities can occur in the first 2 years of life and can precede clinical features, and are often not correlated to clinical seizure events.
Associated (20-80%)
Flat occiput
Occipital groove
Protruding tongue
Tongue thrusting; suck/swallowing disorders
Feeding problems and/or truncal hypotonia during infancy
Prognathia (overbite)
Wide mouth, wide-spaced teeth
Frequent drooling
Excessive chewing/mouthing behaviors
Strabismus
Hypopigmented skin, light hair and eye color (compared to family), seen only in deletion cases
Hyperactive lower extremity deep tendon reflexes
Uplifted, flexed arm position especially during ambulation
Wide based gait with pronated or valgus, positioned ankles
Increased sensitivity to heat
Abnormal sleep wake cycles and diminished need for sleep
Attraction to/fascination with water; fascination with crinkly items such as certain papers and plastics
Abnormal food related behaviors
Obesity (in the older child)
Scoliosis
Constipation

Table 1-1: Developmental and physical findings of Angelman Syndrome (from 2005 consensus criterion document). This information is reprinted from *Facts about Angelman syndrome* (Charles A. Williams, 2009).

Protein	Cellular function	Reference
Ube3a	protein degradation	(Nuber et al., 1998)
P53	neural maturation, axon outgrowth and regeneration, neuronal apoptosis	(Jiang et al., 1998)
Multicopy maintenance protein 7 (MCM7)	involved in initiation of DNA replication	(Kuhne and Banks, 1998)
Human homologue of Rad23A (HHR23A)	DNA repair-enzyme Rad23	(Kumar et al., 1999)
B-cell lymphocyte kinase (BLK)	regulation of Src family kinases	(Oda et al., 1999)
Ubiquilin-1 and -2 (UBQLN1 and -2)	links ubiquitination machinery to the proteasome affecting protein degradation	(Kleijnen et al., 2003), (Kleijnen et al., 2000)
Estrogen receptor	regulate gene transcription	(Li et al., 2006a)
Tuberous sclerosis protein 2 (TSC2)	negative regulator of mTor signaling pathway, neural migration	(Zheng et al., 2008)
α-synuclein	involved in vesicle trafficking, neurodegenerative disorders	(Mulherkar et al., 2009)
Annexin A1 (lipocortin I)	anti-inflammation (protective for neurodegeneration)	(Shimoji et al., 2009)
Promyelocytic leukemia (PML)	regulation of growth inhibition, senescence, apoptosis	(Louria-Hayon et al., 2009)
Cyclin-dependent kinase inhibitor (p27)	neural differentiation, migration	(Mishra et al., 2009)
Sacsin (DNAJC29)	protective against ataxin-1 toxicity	(Greer et al., 2010)
Arc/Arg3.1	regulates level of AMPAR at cell surface	(Greer et al., 2010)
Ephexin5	negatively regulates excitatory synapse number and dendritic spine density	(Margolis et al., 2010)
Ring1B	transcriptional repressor	(Zaaroor-Regev et al., 2010)
Peroxiredoxin 1	role in antioxidant protection	(Nasu et al., 2010)
Mitogen-activated protein kinase 6 (MAPK6)	dendrite development and spine formation	(Martinez-Noel et al., 2012)
Hypoxia-inducible factor 1-alpha inhibitor (HIF1AN)	facilitate metabolic adaptation to hypoxia by regulating HIF1	(Martinez-Noel et al., 2012)
NEURL4	mediates protein-protein interactions, regulation of centrosome	(Martinez-Noel et al., 2012)
GABA Transporter 1 (GAT1)	removes GABA from synaptic cleft	(Egawa et al., 2012)

Table 1-2: Potential *Ube3a* substrates

Genetic manipulation	Phenotypes	Reference for mouse
parental duplication of central region orthologous to15q11-13 (partial parental disomy)	abnormal EEG activity, cortical thinning, juvenile hyperactivity, adult obesity, ataxia	(Cattanach et al., 1997)
deletion of ortholog to exon 2 of maternal UBE3A (3kb deletion)	impaired LTP-induction and learning and memory, abnormal EEG including audiogenic seizures, ataxia, decreased tonic inhibition in the cerebellum, reduced dopamine cell number in SNc	(Jiang et al., 1998)
4 Mb deletion from ZFP127 to HERC2	no behavior or phenotypic data available	(Gabriel et al., 1999)
deletion of orthologs to exon 15 and 16 of maternal UBE3A gene	impaired performance on hippocampal-dependent tasks and LTP-induction, ataxia, increased seizures, abnormal wake/sleep EEG patterns, fast cerebellar oscillations	(Miura et al., 2002)
disruption of AS-IC by deletion to SNRPN	no behavior or phenotypic data available	(Wu et al., 2006)
1.6 Mb deletion to UBE3A, ATP10A, and GABRB3	impaired motor function and learning and memory deficits, spontaneous seizures and abnormal EEG patterns, increased vocalization	(Jiang et al., 2010)

Table 1-3: Angelman syndrome mouse models

CHAPTER 2

2. Ube3a is required for experience-dependent maturation of the neocortex[1]

2.1. Overview

Experience-dependent maturation of neocortical circuits is required for normal sensory and cognitive abilities, which are distorted in neurodevelopmental disorders. We tested whether experience-dependent neocortical modifications require Ube3a, an E3 ubiquitin ligase whose dysregulation has been implicated in autism and Angelman syndrome. Using visual cortex as a model, we found that experience-dependent maturation of excitatory cortical circuits was severely impaired in Angelman syndrome model mice deficient in Ube3a. This developmental defect was associated with profound impairments in neocortical plasticity. Normal plasticity was preserved under conditions of sensory deprivation, but was rapidly lost by sensory experiences. The loss of neocortical plasticity is reversible, as late-onset visual deprivation restored normal synaptic plasticity. Furthermore, Ube3a-deficient mice lacked ocular dominance plasticity *in vivo* when challenged with monocular deprivation. We conclude that Ube3a is necessary for maintaining plasticity during experience-dependent neocortical development and suggest that the loss of neocortical plasticity contributes to deficits associated with Angelman syndrome.

---

[1] Yashiro, K., Riday, T.T., Condon, K.H., Roberts, A.C., Bernardo, D.R., Prakash, R., Weinberg, R.J., Ehlers, M.D., and Philpot, B.D. (2009). Ube3a is required for experience-dependent maturation of the neocortex. Nature neuroscience 12, 777-783.

2.2. Introduction

Angelman syndrome is a severe hereditary mental retardation characterized by outwardly normal development during the first year of life with a profound absence of subsequent cognitive milestones, such as speech (Jiang et al., 1998; Clayton-Smith and Laan, 2003). Angelman syndrome is caused by loss-of-function mutations or deletions in the maternally inherited allele of *UBE3A* (Rougeulle et al., 1997), a gene whose dysregulation is also implicated in autism (Schroer et al., 1998). *UBE3A* encodes a HECT domain ubiquitin E3 ligase that, in the brain, is expressed primarily from the maternal allele as a result of tissue-specific imprinting (Albrecht et al., 1997; Jiang et al., 1998; Dindot et al., 2008). The apparent lack of neurodegeneration (Jiang et al., 1998) and the sharp postnatal onset of symptoms in Angelman syndrome suggest a developmental defect in synaptic circuits (Zoghbi, 2003), whose origin is unknown. Mice that are deficient in maternal Ube3a show genetically reversible impairments in both learning and hippocampal long-term potentiation (LTP) (Jiang et al., 1998; Weeber et al., 2003; van Woerden et al., 2007), indicating deficits in synaptic plasticity. Moreover, recent studies have demonstrated that the ubiquitin proteasome system is involved in synaptic development and plasticity (Yi and Ehlers, 2005, 2007), suggesting that Ube3a-mediated protein degradation may be involved in these processes.

Despite a documented role of Ube3a in learning (Jiang et al., 1998; van Woerden et al., 2007), it is not known how Ube3a affects the neocortex, a brain region that is heavily sculpted through experience-dependent development and whose disruption could explain most Angelman syndrome deficits. Combined with the early postnatal emergence of Angelman syndrome–related deficits and the clinical observations that individuals with Angelman syndrome present behaviors that are consistent with altered sensory processing

(Walz and Baranek, 2006; Williams et al., 2006), the learning deficits associated with Angelman syndrome led us to hypothesize that Ube3a regulates experience-dependent refinement of neuronal circuits dependent on sensory input.

We used the visual cortex as a model system (Kirkwood et al., 1996; Philpot et al., 2001; Fagiolini et al., 2003; Gianfranceschi et al., 2003; Wallace and Bear, 2004; Li et al., 2006b) to study the role of Ube3a in experience-dependent plasticity of the neocortex in a maternally deficient Angelman syndrome mouse model (*Ube3a*$^{m-/p+}$). Our results demonstrate an unexpected role for Ube3a in maintaining synaptic plasticity in the face of sensory processing and suggest a basis for the learning deficits that are associated with Angelman syndrome.

2.3. Results

Reduced maturation of cortical synapses in Ube3a$^{m-/p+}$ mice. Although Angelman syndrome model mice lacking the maternal *Ube3a* allele (*Ube3a*$^{m-/p+}$) show extensive loss of Ube3a as a result of maternal imprinting in many areas of the brain, including the cerebellum, hippocampus and parts of the neocortex (Albrecht et al., 1997; Jiang et al., 1998; Jordan and Francke, 2006; Dindot et al., 2008), it is unknown whether this also occurs in the visual cortex. Immunoblot analysis revealed that paternal deficiency of Ube3a (*Ube3a*$^{m+/p-}$) did not alter Ube3a protein levels in the hippocampus, cerebellum or visual cortex (Figure 2-1A). In contrast, Ube3a expression was markedly reduced in *Ube3a*$^{m-/p+}$ mice compared with wild-type mice in all three brain regions. Consistent with previous observations (Rougeulle et al., 1997; Vu and Hoffman, 1997), this attenuation was brain specific, as Ube3a was highly expressed in the liver of both *Ube3a*$^{m+/p-}$ and *Ube3a*$^{m-/p+}$ mice (Figure 2-1A). We verified maternal imprinting of Ube3a protein using immunohistochemistry. Ube3a immunostaining

was prominent in the visual cortex of wild-type mice, but was only marginally detectable in *Ube3a*$^{m-/p-}$ and *Ube3a*$^{m-/p+}$ mice (Figure 2-1B and Supplementary Figure 2-1). In wild-type mice, cells that were immunopositive for the neuronal marker NeuN (Mullen et al., 1992) stained intensely for Ube3a (Figure 1-1B). Immunoblot analysis of whole cortex homogenates (Supplementary Figure 2-1) and immunohistochemistry (data not shown) revealed that maternal imprinting was a general feature of neocortical Ube3a expression and was not unique to the visual cortex.

To determine the physiological consequences of Ube3a loss on neocortical development, we examined the developmental acquisition of spontaneous excitatory synaptic transmission by recording miniature excitatory postsynaptic currents (mEPSCs) in layer 2/3 pyramidal neurons of visual cortex (see Supplementary Table 2-1 for intrinsic membrane properties of recorded neurons). Consistent with previous findings (Desai et al., 2002; Goel and Lee, 2007), mEPSC amplitudes decreased and frequency increased during development in wild-type mice (Figure 2-1C–E). Just before eye opening (postnatal day 10, P10), mEPSC frequency and amplitude were indistinguishable between wild-type and *Ube3a*$^{m-/p+}$ mice (Figure 2-1C–E). Thereafter, mEPSC frequency failed to develop normally in *Ube3a*$^{m-/p+}$ mice (Figure 2-1C,E). Despite reduced mEPSC frequency relative to wild-type mice (Figure 2-1E), both mEPSC amplitude (Figure 2-1D) and the ratio of AMPA to NMDA responses (Supplementary Figure 2-2) were comparable between wild-type and *Ube3a*$^{m-/p+}$ mice.

Experience-dependent maturation of synapses requires Ube3a. Because mEPSC deficits began to appear after eye opening and the onset of patterned vision (P11–12 in the mouse), we investigated the role of visual experience in regulating the development of spontaneous synaptic activity in *Ube3a*$^{m-/p+}$ mice. Toward this end, we dark-reared animals

from P10 until P25 to deprive them of visual experience after eye opening, and compared mEPSC frequency and amplitude in layer 2/3 pyramidal neurons with that of normally reared mice (Figure 2-2A). Although dark rearing had no measurable effect on mEPSC amplitude in wild-type mice at P25 (Figure 2-2B,C), sensory deprivation strongly attenuated the normal developmental increase in mEPSC frequency in wild-type mice (Figure 2-2B,D). In contrast, dark rearing did not affect mEPSC amplitude (Figure 2-2B,C) or frequency (Figure 2-2B,D) in *Ube3a*$^{m-/p+}$ mice. Consequently, mEPSC frequency in normally reared *Ube3a*$^{m-/p+}$ mice was not significantly different from that of dark-reared wild-type mice ($P = 0.79$; Figure 2-2D). These findings demonstrate that, although Ube3a is not necessary for the initial sensory-independent establishment of synaptic connectivity, it is selectively required for experience-dependent maturation of excitatory circuits.

The decrease in mEPSC frequency raised the possibility that layer 2/3 excitatory synapses are functionally lost in the absence of Ube3a. To examine this further, we used Golgi impregnation to test for experience-dependent differences in dendritic spines (Figure 2-2E), the anatomical site at which most excitatory synaptic connections are made (Nimchinsky et al., 2002). Although the spine density of layer 2/3 visual cortical pyramidal neurons was comparable between dark-reared wild-type and dark-reared *Ube3a*$^{m-/p+}$ mice (Figure 2-2F), it was significantly lower in normally reared *Ube3a*$^{m-/p+}$ mice compared with normally reared wild-type mice ($P < 0.001$; Figure 2-2F), consistent with previous observations in other neocortical regions of normally reared mice (Dindot et al., 2008). Together with our electrophysiological observations, these data demonstrate that *Ube3a*$^{m-/p+}$ mice are defective in the experience-dependent development of excitatory synaptic connections.

Neocortical plasticity is impaired in* *Ube3a*$^{m-/p+}$ *mice. One possible explanation for the lack of experience-dependent synaptic development in *Ube3a*$^{m-/p+}$ mice is defective activity-dependent plasticity at neocortical synapses. We therefore compared the properties of neocortical long-term depression (LTD) and LTP at layer 2/3 synapses in visual cortex of wild-type and *Ube3a*$^{m-/p+}$ mice at both young (~P25) and adult (~P100) ages. Because layer 2/3 pyramidal neurons receive major inputs from layer 4 pyramidal neurons, layer 2/3 field potentials were evoked by layer 4 stimulation (Figure 2-3A). We began by measuring LTD in young mice using a standard stimulation protocol (1 Hz for 15 min). Although LTD was reliably induced in young wild-type mice, it was absent in young *Ube3a*$^{m-/p+}$ mice (Figure 2-3B). We also observed deficits in LTP induction. A relatively weak induction protocol (three 1-s trains of 40-Hz stimulation) elicited LTP in young wild-type mice, but failed to reliably induce LTP in young *Ube3a*$^{m-/p+}$ mice (Figure 2-3C). To test whether the neocortex of *Ube3a*$^{m-/p+}$ mice was capable of expressing LTP, we also applied a strong LTP stimulation protocol (two 1-s trains of 100-Hz stimulation). This protocol consistently induced LTP in both *Ube3a*$^{m-/p+}$ and wild-type mice (Figure 2-3D). Thus, as with LTP deficits in hippocampus (Weeber et al., 2003; van Woerden et al., 2007), the LTP induction machinery is impaired in the visual cortex of *Ube3a*$^{m-/p+}$ mice and this deficit in LTP can be overcome with strong stimulation. Unexpectedly, the impairment in plasticity is bidirectional, as Ube3a was also required for the normal induction of both LTD and LTP (Figure 2-3E), indicating profound synaptic rigidity.

To determine whether the plasticity deficits in Angelman syndrome mice persisted into adulthood, we tested LTD and LTP in adults (~P100). In adult wild-type mice, LTD induced by 1-Hz stimulation was absent, as expected (Kirkwood et al., 1997), whereas LTP

could be induced with strong stimulation (two trains of 100-Hz stimulations; Supplementary Figure 2-3). In adult *Ube3a*$^{m-/p+}$ mice, however, neither of these protocols were effective at modifying synaptic strength (Supplementary Figure 2-3). These results indicate that wild-type mice show attenuated neocortical plasticity as they mature and that this attenuation of plasticity is more severe in the absence of Ube3a (compare Figure 2-3E and Supplementary Figure 2-3). Furthermore, these data indicate that plasticity defects in Angelman syndrome mice persist into adulthood.

Sensory experience dampens plasticity in *Ube3a*$^{m-/p+}$ ***mice.*** Visual experience can alter the ability to induce LTD and LTP (Kirkwood et al., 1996; Philpot et al., 2007). Therefore, we speculated that the LTD and LTP impairments in *Ube3a*$^{m-/p+}$ mice could result from an inappropriately strong downregulation of synaptic plasticity induced by visual experience. In this case, one would expect that mice with no previous visual experience would possess normal synaptic plasticity. We investigated this possibility by measuring LTD and LTP in young wild-type and *Ube3a*$^{m-/p+}$ mice reared in the dark (Figure 2-4A,B). Indeed, visual deprivation in *Ube3a*$^{m-/p+}$ mice restored the normal induction and expression of LTP (induced by the 40-Hz protocol) and LTD (induced by a 1-Hz protocol) (Figure 2-4C,D). Thus, sensory deprivation prevents synaptic plasticity impairments in *Ube3a*$^{m-/p+}$ mice. In other words, *Ube3a*$^{m-/p+}$ mice are born with normal LTD and LTP at neocortical synapses, but ongoing sensory experiences impair the induction/expression of synaptic plasticity in the absence of Ube3a.

To test whether the experience-dependent loss of synaptic plasticity observed by field potential recordings is a result of the loss of plasticity at excitatory synapses, we conducted voltage-clamp recordings of excitatory currents in layer 2/3 pyramidal neurons

(Supplementary Figure 2-4). Consistent with the field potential recordings, 1-Hz stimulation paired with postsynaptic depolarization induced LTD in normally reared young (P25) wild-type mice, but failed to reliably induce LTD in normally reared *Ube3a*$^{m-/p+}$ mice (Supplementary Figure 2-4). Moreover, dark rearing partially recovered LTD in *Ube3a*$^{m-/p+}$ mice to levels comparable to dark-reared wild-type mice (Supplementary Figure 2-4). These data provide further evidence that sensory-driven activity attenuates synaptic plasticity in the absence of Ube3a. In support of this idea, LTD was induced normally in layer 2/3 pyramidal neurons of *Ube3a*$^{m-/p+}$ mice at P10, before eye opening (Supplementary Figure 2-4).

To verify that visual experience, rather than an intrinsic developmental program, caused the loss of plasticity in *Ube3a*$^{m-/p+}$ mice, we investigated the effect of reinstating sensory experience following dark rearing. To this end, we dark-reared mice until ~P25 and then provided them with 1 or 4 d of a normal visual environment (Figure 2-4E). Although LTD was readily induced in the layer 4 to 2/3 pathway of visual cortex in wild-type mice after 1 d of visual experience, LTD appeared to be reduced in *Ube3a*$^{m-/p+}$ mice (Figure 2-4F). After 4 d of visual experience, LTD was completely abolished in *Ube3a*$^{m-/p+}$ mice (Figure 2-4G), indicating that relatively brief (<4 d) visual experience was sufficient to cause a loss of normal plasticity in Angelman syndrome mice (Figure 2-4H).

Late deprivation recovers plasticity in *Ube3a*$^{m-/p+}$ ***mice.*** Can sensory deprivation cause a recovery of plasticity in normally reared *Ube3a*$^{m-/p+}$ mice at later stages, after the ability to induce plasticity has already been driven down by previous sensory experience? To answer this question, we reared wild-type and *Ube3a*$^{m-/p+}$ mice normally until ~P30 (Figure 2-5), as LTD was absent in Angelman syndrome mice by 4 weeks of age (Figure 2-3B), and then measured plasticity (Figure 2-5A) after the mice had been given a late-onset visual

deprivation (LOVD) for 10 d (Figure 2-5B). As an additional control, LTD was also measured in age-matched wild-type mice that had been reared normally until ~P40.

We found that 1-Hz LTD was reduced at ~P40 in normally reared wild-type mice (Figure 2-5C,D), similar to previous observations of a developmental reduction at the field potential level in visual cortex LTD in wild-type animals (Kirkwood et al., 1997; Jiang et al., 2007). Consistent with a recent finding that LOVD restores synaptic plasticity in adult animals *in vivo* (He et al., 2006), LOVD reinstated 1-Hz LTD in wild-type mice (Figure 2-5C,D). Moreover, a similar level of LTD was restored after LOVD in *Ube3a*$^{m-/p+}$ mice (Figure 2-5C,D), suggesting that LOVD recovers LTD even in the absence of Ube3a (Figure 2-5D). The LOVD-induced recovery of LTD was also observed in whole-cell recordings from identified layer 2/3 pyramidal neurons (Supplementary Figure 2-4). Together, these data demonstrate that LOVD can restore synaptic plasticity in *Ube3a*$^{m-/p+}$ mice.

Ocular dominance plasticity is absent in *Ube3a*$^{m-/p+}$ ***mice.*** The severe plasticity deficits recorded in *ex vivo* brain slices suggested that experience-dependent modifications *in vivo* might also be impaired by the absence of Ube3a. We first assessed visual function by recording visual evoked potentials (VEPs) in visual cortex (Figure 2-6). These measurements revealed that both visual acuity (Supplementary Figure 2-5) and baseline ocularity were normal (Figure 2-6B,C), suggesting that *Ube3a*$^{m-/p+}$ mice have grossly normal visual functions.

Next, we investigated *in vivo* plasticity of visual cortical circuits by challenging the mice with monocular deprivation (Figure 2-6A). This sensory manipulation produces a well-characterized ocular dominance shift in wild-type animals and serves as a gauge of critical period plasticity (Wiesel and Hubel, 1963). In the visual cortex, an ocular dominance shift

can be observed most prominently during a critical period, which peaks in the third to fourth postnatal week in mice (Gordon and Stryker, 1996). At these ages, however, both LTD and LTP were impaired in normally reared *Ube3a*$^{m-/p+}$ mice (Figure 2-3). In wild-type mice experiencing normal binocular vision, we observed no marked change in ocularity from P27–P30, as expected (Figure 2-6B). However, 3 d of monocular deprivation beginning from P27 reduced the contralateral bias of wild-type mice (Figure 2-6B), an effect that was particularly robust when comparisons were made between monocularly deprived mice and their age-matched, non-deprived controls (*t* test between monocularly deprived wild-type mice and age-matched control wild-type mice, $P < 0.005$). In these experiments, eye occlusion was always contralateral to the recording electrode. These data indicate that wild-type mice are highly susceptible to altered sensory experience at this age.

Ube3a$^{m-/p+}$ mice experiencing binocular vision had similar ocularity on P27 and P30 (Figure 2-6C). Unlike wild-type mice, the Ube3a-deficient mice showed no response to 3 d of monocular deprivation (Figure 2-6C). The ocularity change observed in wild-type mice was largely a result of monocular deprivation–induced depression of the contralateral VEP response (Figure 2-6D). No change in the contralateral response was observed in *Ube3a*$^{m-/p+}$ mice (Figure 2-6E). These results suggest that the experience-dependent loss of synaptic plasticity that occurs in the absence of Ube3a likewise limits the ability to rearrange cortical circuits during the critical period *in vivo*.

2.4. Discussion

We have identified a critical role for the Angelman syndrome– and autism-linked ubiquitin ligase Ube3a in experience-dependent neocortical development. We found that visual experience failed to strengthen functional connectivity of excitatory neurons in the

visual cortex of *Ube3a*$^{m-/p+}$ mice. The lack of experience-dependent development of excitatory circuits is probably caused by deficits in synaptic plasticity, as both LTP and LTD were severely attenuated in *Ube3a*$^{m-/p+}$ mice. Paradoxically, the plasticity deficit is itself driven by sensory experiences, as sensory deprivation prevented the loss of normal synaptic plasticity, whereas brief sensory experiences could reinstate the plasticity deficit. Therefore, Ube3a is necessary to maintain normal synaptic plasticity during ongoing activity-dependent remodeling. Finally, we found that *Ube3a*$^{m-/p+}$ mice lacked the cortical plasticity that is normally induced by monocular deprivation *in vivo*, demonstrating a role for Ube3a in naturally occurring experience-dependent modifications of neuronal circuits. The neocortical plasticity deficits caused by the absence of Ube3a may thus underlie the learning deficits observed in Angelman syndrome.

Two possibilities could explain the plasticity deficits in *Ube3a*$^{m-/p+}$ mice. First, cooperative excitatory drive may be attenuated in Ube3a-deficient mice, thus increasing the induction parameters for LTD and LTP. This could arise from a decrease in the number of excitatory synapses or their release probability, both of which are consistent with the observed reduction in spine density and mEPSC frequency of layer 2/3 pyramidal neurons. The possibility that *Ube3a*$^{m-/p+}$ mice have abnormal neurotransmitter release might be particularly relevant for the LTD deficit in layers 2/3, as recent evidence suggests that LTD induced at this synapse requires endocannabinoid-mediated reductions in presynaptic neurotransmitter release (Crozier et al., 2007). Future studies are needed to determine whether presynaptic plasticity and/or release mechanisms are disrupted by the absence of Ube3a, and whether this might contribute to the observed plasticity deficits.

Alternatively, the machinery for plasticity induction or expression may itself be compromised in Ube3a-deficient mice, including changes in calcium entry, receptor trafficking or pre/postsynaptic signaling molecules. Indeed, the absence of Ube3a impairs the function of calcium/calmodulin-dependent protein kinase II (CaMKII) (Weeber et al., 2003), an enzyme that normally facilitates LTP induction (Xia and Storm, 2005) in both the hippocampus (Silva et al., 1992) and visual cortex (Kirkwood et al., 1997; Frankland et al., 2001). Thus, although it has not yet been examined in the neocortex, reductions in CaMKII activity in *Ube3a*$^{m-/p+}$ mice might contribute to the observed deficits in neocortical LTP. Notably, the cortical LTP deficit observed in *Camk2a*$^{-/-}$ mice becomes progressively more severe with development (Kirkwood et al., 1997), raising the possibility that the age-dependent increase in the LTP deficits observed in Ube3a-deficient mice may be a consequence of an increasing requirement of CaMKII for LTP induction (Yasuda et al., 2003). Similar to LTP, impairments in LTD could also arise from changes in signaling molecules. One such candidate molecule is protein phosphatase 1, as its enzymatic activity is implicated in LTD induction (Mulkey et al., 1994; Torii et al., 1995) and is attenuated in *Ube3a*$^{m-/p+}$ mice (Weeber et al., 2003). If the plasticity induction mechanisms for LTD and LTP are indeed compromised in the neocortex in the absence of Ube3a, then this could contribute to the observed reductions in spine density.

The ubiquitin-proteasome system is necessary for both LTP (Fonseca et al., 2006) and LTD (Colledge et al., 2003), and our data demonstrate that Ube3a is a critical component of this system. However, the protein substrates of Ube3a, the degradation of which is required to maintain normal synaptic plasticity, remain unknown. Extensive GeneChip analyses of the murine visual cortex have revealed that visual experience affects the expression of many

genes (Majdan and Shatz, 2006; Tropea et al., 2006). If one of these visual experience–induced proteins is a substrate for Ube3a, this protein could be abnormally overexpressed in *Ube3a*$^{m-/p+}$ mice that are given visual experience. Furthermore, if the protein has an ability to suppress synaptic plasticity, experience-dependent accumulation of such a protein would attenuate LTD and LTP in the absence of Ube3a. An ideal substrate of Ube3a that could account directly for the experience-induced plasticity deficits would thus be a protein that is upregulated by activity, but suppresses subsequent synaptic remodeling at high levels.

We suggest that the plasticity deficits observed *in vitro* may contribute to or underlie synaptic learning deficits associated with Angelman syndrome. In support of the idea that Ube3a is required for naturally occurring plasticity during a critical period of development, we found that ocular dominance plasticity was absent in *Ube3a*$^{m-/p+}$ mice (Figure 2-6). Because LTD and monocular deprivation-induced depression of the deprived eye response share a common pathway (Heynen et al., 2003), visual experience–induced loss of LTD could be the direct cause of the lack of ocular dominance plasticity. Consistent with this idea, Ube3a-deficient mice lacked the loss of responsiveness from the deprived eye that is normally observed following brief monocular deprivation.

Functional (Thompson et al., 1999; Van Splunder et al., 2003) and anatomical (Jay et al., 1991) abnormalities in the visual system of individuals with Angelman syndrome are consistent with the observed aberrant development of visual cortical circuits in *Ube3a*$^{m-/p+}$ mice. If the deficits in experience-dependent encoding in the visual cortex can be generalized to other areas of the brain, then these same changes in synaptic physiology may explain the observed deficiencies in learning and cognition in individuals with Angelman syndrome. It is notable that LOVD restored plasticity in *Ube3a*$^{m-/p+}$ mice (Figure 2-5 and Supplementary

Figure 2-4). This demonstration that the physiological substrates of synaptic plasticity remain intact raises the possibility that behavioral or pharmacological manipulations could improve brain function in individuals with Angelman syndrome. Moreover, because it has been speculated that sensory experience–dependent brain development is abnormal in other neurodevelopmental disorders, such as Rett syndrome, Fragile X syndrome and autism (Zoghbi, 2003), our experimental approach may help to elucidate the roles of experience in these disorders.

2.5. Methods

Animals.

Mice deficient in Ube3a, developed previously (Jiang et al., 1998), were obtained through Jackson Laboratory. Mice were bred on a 129S7 background. To obtain heterozygous mice lacking the *Ube3a* gene paternally (m+/p–) or maternally (m–/p+), we crossed a heterozygous male or female mouse with a wild-type female or male mouse, respectively. For most electrophysiological recordings in slices, WT and maternal heterozygous mice were used in three age groups: infant (P8–11, ~P10), young (P21–28, ~P25) and adult (P94–121, ~P100). For LOVD experiments, WT and maternal heterozygous mice at ~P40 (P37–40) were used. Control mice were raised on a 12-h light/dark cycle, whereas dark-reared mice were raised in complete darkness from P9–11 (before eye opening) until ~P25. Light exposure was achieved by transferring dark-reared mice into the control condition at P21–28 and providing 1–4 d in the normal light/dark cycle. LOVD was achieved by transferring NR mice at ~P30 into complete darkness for 10 d. Electrophysiological recordings were obtained from at least three mice for each condition. For *in vivo* electrophysiological recordings, mice were used at ages indicated below. All animal

procedures were performed in compliance with the US Department of Health and Human Services and the animal care guidelines at the University of North Carolina and Duke University.

Immunoblot analysis.

Tissue lysates were prepared in lysis buffer containing 50 mM Tris, 150 mM NaCl, 50 mM NaF, 2 mM EDTA, 2 mM EGTA, 1% Triton X-100 (vol/vol), pH 7.4, and a cocktail of protease and phosphatase inhibitors. Protein concentrations were determined using DC Protein Assay (BioRad). We resolved 20 μg of each lysate on a 7.5% Tris-HCl gel (BioRad) and transferred them to a PVDF membrane. The membrane was probed with antibody to Ube3a (1:1,000, Bethyl Labs) and subsequently with horseradish peroxidase–conjugated polyclonal antibody to rabbit (1:10,000, Cell Signaling). Signals were visualized with ECL Plus reagent (Amersham) and an LAS-3000 Intelligent Dark Box (FujiFilm).

Immunohistochemistry.

Mice were anesthetized with pentobarbital and perfused intracardially with cold phosphate-buffered saline followed by freshly prepared 4% paraformaldehyde in 0.1 M phosphate buffer (pH 7.4). Brains were postfixed in the same solution overnight at 4 °C. Brains were then cut into 50-μm coronal sections using a vibratome (Leica Microsystems). For immunohistochemistry experiments, sections from wild-type, *Ube3a*$^{m-/p+}$ and *Ube3a*$^{m-/p-}$ mice were always processed simultaneously. Sections were incubated in 10 mM sodium citrate buffer (pH 8.65) at 80 °C for 15 min before the immunoreactions. Sections were incubated with rabbit polyclonal antibody to Ube3a (1:500, Bethyl Labs) and mouse monoclonal antibody to NeuN (1:3,000, Chemicon) overnight at 4 °C, and then incubated with Alexa Fluor 488 goat antibody to mouse IgG and Alexa Fluor 568 goat antibody to

rabbit IgG (1:500, Invitrogen). Images were acquired using a Zeiss LSM 510 laser-scanning confocal microscope.

Visual cortical slice preparation.

Mice were anesthetized with an overdose of pentobarbital and decapitated after the disappearance of corneal reflexes. Brains were dissected rapidly and the visual cortex cut coronally at 300 μm (voltage-clamp recordings) or 400 μm (field potential recordings) in dissection buffer containing 75 mM sucrose, 87 mM NaCl, 2.5 mM KCl, 1.25 mM NaH_2PO_4, 26 mM $NaHCO_3$, 10 mM glucose, 7 mM $MgCl_2$, 0.5 mM $CaCl_2$ and 1.3 mM ascorbic acid. Prior to recordings, slices were allowed to recover for 1 h in a submersion chamber containing oxygenated artificial cerebrospinal fluid (ACSF), which consisted of 124 mM NaCl, 3 mM KCl, 1.25 mM NaH_2PO_4, 26 mM $NaHCO_3$, 20 mM glucose, 2 mM $MgCl_2$ and 1 mM $CaCl_2$. For patch-clamp recordings, slices were allowed to recover in a submersion chamber, which was preheated to 35 °C and gradually cooled to room temperature (23 ±1 °C). For field recordings, slices were allowed to recover in a submersion chamber, which was precooled to 5–10 °C and gradually warmed to room temperature (23 ±1 °C).

Voltage-clamp recordings.

For mEPSC recordings, slices were placed in a submersion chamber, maintained at 30 °C and perfused at 2 ml min^{-1} with oxygenated ACSF supplemented with 200 nM tetrodotoxin, 100 μM DL-2-amino-5-phosphonovaleric acid and 50 μM picrotoxin. Neurons were visualized with a Carl Zeiss Axioskop equipped with infrared differential interference contrast optics. Patch pipettes were pulled from thick-walled borosilicate glass. Open tip resistances were 3–5 MΩ when pipettes were filled with an internal solution containing 20 mM KCl, 100 mM potassium gluconate, 10 mM potassium HEPES, 4 mM MgATP, 0.3 mM

NaGTP, 10 mM sodium phosphocreatine and 0.01% Alexa 488 (wt/vol), adjusted with KOH to pH 7.4, and with sucrose to 290–300 mOsm. Voltage-clamp recordings were performed in the whole-cell configuration with a patch-clamp amplifier (Multiclamp 700A, Molecular Devices), and data were acquired with pClamp 9.2 software (Molecular Devices). Input and series resistances were determined throughout the experiment by measuring the response to small intermittent test pulses. Recordings were discarded if the series resistance grew larger than 25 MΩ, or the resting potential was more positive than -60 mV (for the recordings in infant mice, the resting potential was not used as a criterion, as many neurons typically exhibit resting potentials higher than -60 mV). Analysis was restricted to neurons that were anatomically verified by intracellular fills to be pyramidal neurons. MiniAnalysis (Synaptosoft) was used to detect and measure mEPSCs. The threshold to detect mEPSC was set at 5 pA, which is more than 2.5-fold greater than the root mean square of the noise, and mEPSCs with 10-90% rise times more than 3 ms were excluded from the analysis. Analysis of mEPSCs was performed blind to age, genotype and rearing condition.

Whole-cell LTD induction.

Recording conditions were the same as for the mEPSC recordings, except that ACSF was not supplemented with tetrodotoxin, APV, and picrotoxin, and the internal solution contained (in mM): 107 CsOH, 107 Gluconic acid, 20 (K)HEPES, 0.2 (K)EGTA, 3.7 NaCl, 5 QX-314, 4 (Mg)ATP, 0.3 (Na)GTP, 10 Na-phosphocreatine and 0.01% w/v Alexa 488, adjusted to pH 7.2, and with sucrose to 290 mOsm. An empirically determined liquid-junction potential (approximately -14 mV) was corrected. EPSCs were elicited with a two-conductor cluster electrode (FHC) placed in layer 4. Test stimuli (200 μsec) were delivered at 0.033 Hz. The test holding potential was −67 mV (reversal potential for Cl-). Low

frequency stimulus long-term depression (LFS-LTD) was induced by pairing 1 Hz presynaptic stimulation with a brief (100 msec) postsynaptic step depolarization from −67 to −47 mV for each of 200 pulses. Each presynaptic stimulation occurred midway (50 msec) into the step depolarization. Experiments were discarded if input resistance was < 200 MΩ (younger mice) or < 100 MΩ (~P40), if series resistance was > 25 MΩ, or if series resistance changed by >30% during the recording.

Ratio of AMPA receptor to NMDA receptor-mediated currents.

Recording conditions were the same as for the LTD induction experiments except ACSF contained 2 mM MgCl2, 1 μM glycine, and 50 μM picrotoxin, and internal solution contained (in mM): 102 CsOH, 102 Gluconic acid, 5 TEA-chloride, 3.7 NaCl, 20 (K)HEPES, 0.3 (Na)GTP, 4 (Mg)ATP, 0.2 (K)EGTA, 10 BAPTA, 5 N-(2,6-dimethylphenyl carboylmethyl) triethylammonium bromide (QX-314) chloride (Alomone Labs), and 0.01% w/v Alexa 488, adjusted to pH 7.2 and to osmolarity 300 mmol/kg. An empirically determined liquid-junction potential (approximately −16 mV) was corrected. EPSCs were elicited with a two-conductor cluster electrode (FHC) placed in layer 4. Test stimuli (50 μsec) were delivered at 0.066 Hz and evoked EPSCs were recorded at -96 mV and +44 mV. Peaks of an evoked EPSC at -96 mV were considered AMPA receptor-mediated. NMDA receptor-mediated currents were recorded at +44 mV and measured 50 ms after a stimulation artifact, a time when AMPA receptor-mediated currents are largely absent. Experiments were discarded if input resistance was < 200 MΩ or series resistance was > 25 MΩ measured at -96 mV.

Field potential recordings.

Slices were maintained at 30 °C and perfused with ACSF at a rate of 2 ml min^{-1}. A concentric bipolar tungsten stimulation electrode was positioned in layer 4 and a glass recording electrode (1–3 MΩ) that was filled with ACSF was positioned in layers 2/3. The magnitude of responses evoked by a 200-μs pulse was monitored by the amplitude of the field potential. Stimulation intensity was adjusted to elicit half the maximal response, and stable baseline responses were elicited every 30 s. The resulting signals were filtered between 0.1 Hz and 3 kHz, amplified, and captured at 10 kHz using pCLAMP 9.2 software (Molecular Devices). After achieving a stable baseline (<5% drift) for 15 min, slices were stimulated with one of the following three protocols: 100-Hz stimulation for 1 s (repeated two times with a 15-s interval), 40-Hz stimulation for 1 s (repeated three times with 10-s intervals) or 900 pulses at 1 Hz. fEPSP amplitudes were recorded every 30 s for 45 min following cessation of the stimulation protocol. Control and experimental subjects were run in an interleaved fashion. Normalized averaged data were reported as means ±s.e.m. Changes in synaptic strength were measured by comparing the average response amplitudes 30–45 min after conditioning stimulation to the pre-conditioning baseline response.

Morphological analysis by Golgi staining.

Littermates at P25–26 reared in a normal environment (NR WT, n = 4 mice; NR *Ube3a*$^{m-/p+}$, n = 3 mice) or in complete darkness from P10 (DR WT, n = 3 mice; DR *Ube3a*$^{m-/p+}$, n = 4 mice) were used for morphological analysis. Mice were anesthetized with pentobarbital and killed by intracardial perfusion of cold phosphate-buffered saline followed by freshly prepared 4% paraformaldehyde in 0.1 M phosphate buffer (pH 7.4). After post-fixation in the same solution, tissue blocks containing visual cortex were processed according

to a modification of the Golgi-Kopsch technique (Gatenby J.B., 1950). We collected 100-μm-thick serial sections for study. Pyramidal neurons at layer 2/3 of the visual cortex were chosen and spines in 13-μm dendritic segments taken 30–50 μm from the soma were counted under a 100 ×oil-immersion lens. Analyses were performed blind to genotype. Images were taken on a Leica TCS SP2 laser scanning confocal microscope using the 488-nm laser line as a light source. To obtain high-resolution images of impregnated dendrites, we took stacks with a 100 ×objective at 0.3663-μm intervals at 4 ×zoom. Dendritic segments were cropped from the resulting stacks and processed by three-dimensional deconvolution using the AutoQuant software (Media Cybernetics).

Visual evoked potential recordings.

Male and female mice were anesthetized with ketamine/xylazine (120 and 9 mg per kg, respectively; intraperitoneal, Southern Anesthesia) and locally at the scalp incision site with 0.25% bupivacaine (Hospira). Tungsten microelectrodes (FHC) with tip impedances of 0.3–0.5 MΩ were stereotaxically implanted in the binocular zone of the visual cortex: 0.0 mm lambda (anterior/posterior), ±3.00 mm sagittal (medial/lateral) and -0.45 mm depth (dorsal/ventral). Silver reference electrodes were implanted -1.0 mm anterior/posterior to bregma and ±2.00 mm sagittal at a depth just touching the brain surface. Electrodes were secured to the skull with Loctite 455 cyanoacrylate (Henkel).

Electrodes were implanted at P22–23 and animals were habituated 24 h before the first recording session at P27–28. Visual stimuli consisted of full-field diagonal (135° or 45°, reversed on day 3) sine wave gratings at 0.3 cpd and 100% contrast. Visual potentials were evoked monocularly through the eye ipsilateral and contralateral to the recording electrode. Following baseline ocularity VEP recordings, one eye was sutured closed. Mice were

anesthetized with 1.5% isoflurane, lid margins were trimmed and three stitches were applied along the length of the lids using 5-0 silk. Mice were monocularly deprived in the eye contralateral to the recording electrode for 3 d. The stitched eye was then reopened and visual potentials were again evoked monocularly through the eye ipsilateral and contralateral to the recording electrode to measure the ocular dominance shift. To quantify ocular dominance plasticity, we took measurements as a ratio of the contralateral (deprived) to ipsilateral (nondeprived) eye responses (Figure 2-6B,C) or as raw amplitudes (Figure 2-6D,E). As a control for developmental changes, VEP recordings were performed in mice that did not receive monocular deprivation.

Visual acuity.

Measurements were conducted in awake mice at P34. Electrodes were implanted at P22 and animals were habituated to the restraint apparatus 24 h prior to the first recording session. Electrical signals were amplified, band pass filtered (0.3-100 Hz), digitized, and averaged (160 events in two blocks) in synchrony with the stimulus contrast reversal. Peak-to-trough amplitude was measured for transient VEPs in response to abrupt contrast reversal (1 Hz). Visual stimuli consisted of full-field horizontal sine wave gratings [0.05-0.95 cycles per degree (cpd) presented in randomized order] at maximal contrast. Responses to 0% contrast (gray screen) were also recorded as a measure of activity not evoked by patterned visual stimuli. Animals were positioned 20 cm away from a 21" CRT (23 cd/m2 mean luminescence) centered on the midline.

Statistics.

Data are expressed as the means ±s.e.m. Unless otherwise noted, unpaired two-tailed Student's *t*-tests were used to test for statistical significance, which was placed at $P < 0.05$.

The raw values of the data shown in Figures 2-1, 2-2, 2-3, 2-4, 2-5, and 2-6 can be found in Supplementary Table 2-2.

Author Contributions

K.Y., B.D.P. and M.D.E. designed the study and wrote the manuscript. K.Y. conducted immunohistochemistry, Golgi impregnation, whole-cell patch-clamp and field potential experiments. T.T.R. contributed to the field potential studies and conducted VEP experiments. K.H.C. contributed to the Golgi impregnation study and conducted immunoblot experiments. A.C.R. contributed to the whole-cell patch-clamp and field potential studies. D.R.B. contributed to the field potential studies. R.P. contributed to the VEP experiments. R.J.W. directed the Golgi impregnation experiments and helped to prepare the manuscript. M.D.E. and B.D.P. supervised the study.

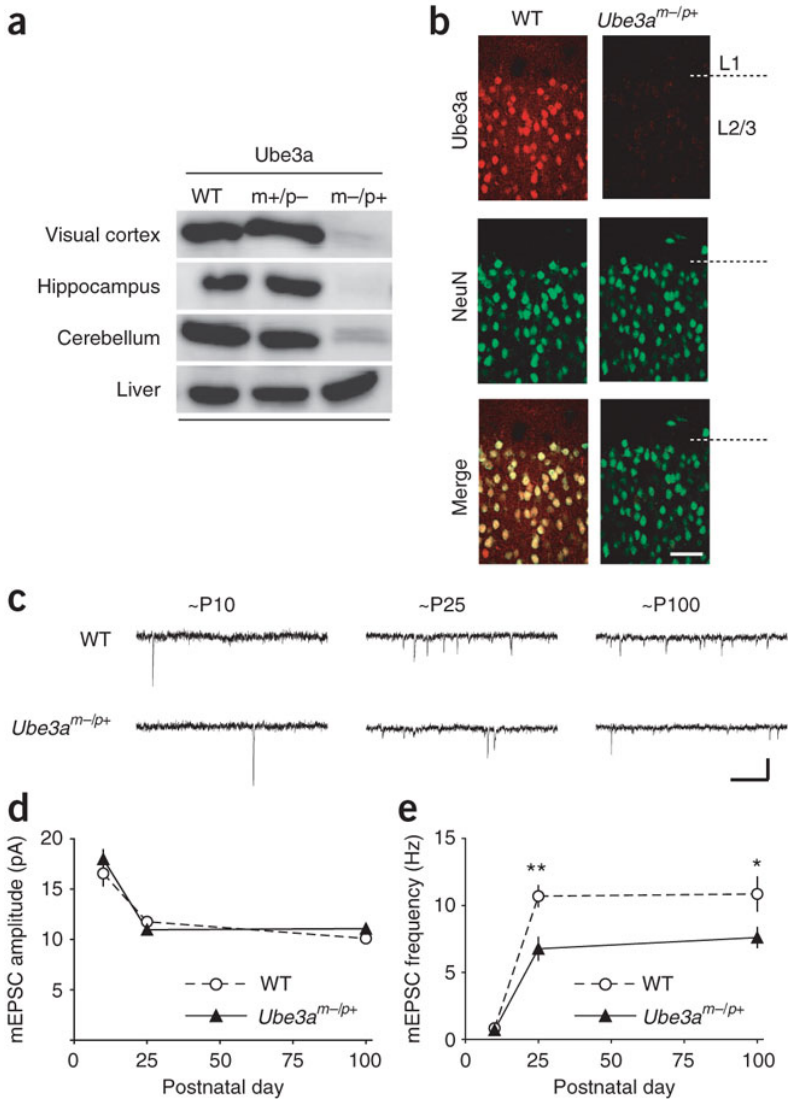

Figure 2-1: Reduced functional maturation of neocortical synapses in Angelman syndrome mice. (**a**) Immunoblot analysis of Ube3a in tissue from young (P26) wild-type (WT), *Ube3a*$^{m+/p-}$ and *Ube3a*$^{m-/p+}$ mice. (**b**) Immunohistochemical analysis of Ube3a expression in the visual cortex from young (P24) WT and *Ube3a*$^{m-/p+}$ mice. Strong Ube3a immunoreactivity was observed in layer 2/3 (L2/3) neurons of WT mice. NeuN antibody stains the cell bodies of neurons. Scale bar represents 50 μm. (**c**) Representative traces of mEPSCs recorded in L2/3 pyramidal neurons from WT or *Ube3a*$^{m-/p+}$ mice at ~P10, ~P25 and ~P100. Scale bars represent 0.2 s and 20 pA. (**d**) Average mEPSC amplitude as a function of postnatal age in WT (P10, $n = 11$ cells; P25, $n = 11$ cells; P100, $n = 12$ cells) and *Ube3a*$^{m-/p+}$ mice (P10, $n = 11$ cells; P25, $n = 12$ cells; P100, $n = 12$ cells). (**e**) Average mEPSC frequency as a function of postnatal age in WT and *Ube3a*$^{m-/p+}$. $^{*}P < 0.05$ and $^{**}P < 0.005$. Error bars represent s.e.m.

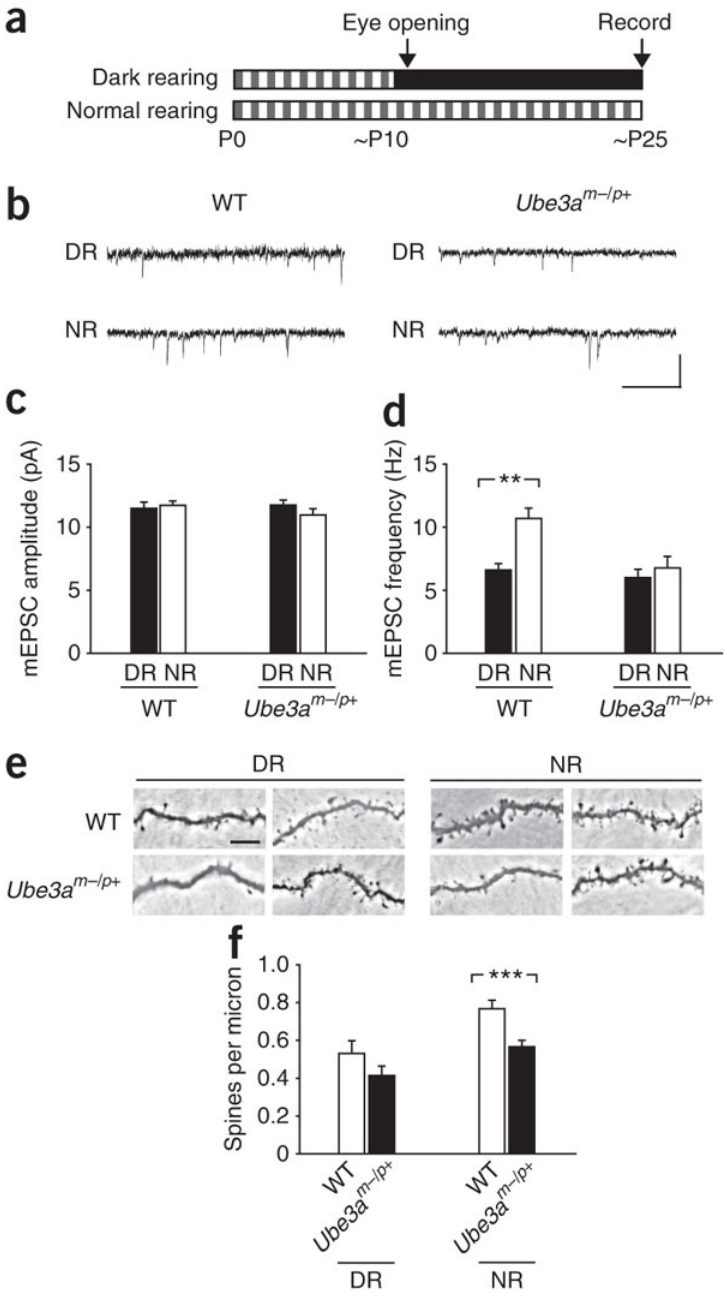

Figure 2-2: Sensory experience augments excitatory synaptic connections in the neocortex of WT mice, but not Angelman syndrome mice. (**A**) Schematic for the rearing conditions. Normally reared (NR) mice were maintained in a 12-h consecutive dark/light cycle, and dark-reared (DR) mice were kept in complete darkness from ~P10. (**B**) Representative traces of mEPSCs recorded in layer 2/3 pyramidal neurons in young WT or *Ube3a*$^{m-/p+}$ mice reared normally or in complete darkness. Scale bars represent 0.2 s and 20 pA. (**C**) Dark rearing did not affect mEPSC amplitude in WT (DR, $n = 12$ cells; NR, $n = 11$ cells; $P = 0.68$) or *Ube3a*$^{m-/p+}$ mice (DR, $n = 14$ cells; NR, $n = 12$ cells; $P = 0.16$). (**D**) Dark rearing significantly reduced mEPSC frequency in WT mice ($P < 0.005$), but did not affect mEPSC frequency in *Ube3a*$^{m-/p+}$ mice ($P = 0.46$). (**E**) Representative images of basal

dendrites of layer 2/3 pyramidal neurons visualized with Golgi staining. Scale bar represents 10 μm. (**F**) Average density of dendritic spines in DR (WT, $n = 25$ cells; *Ube3a*$^{m-/p+}$, $n = 25$ cells; $P = 0.15$) and in NR mice (WT, $n = 33$ cells; *Ube3a*$^{m-/p+}$, $n = 32$ cells; $P < 0.001$). $^{**}P < 0.005$ and $^{***}P < 0.001$. Error bars represent s.e.m.

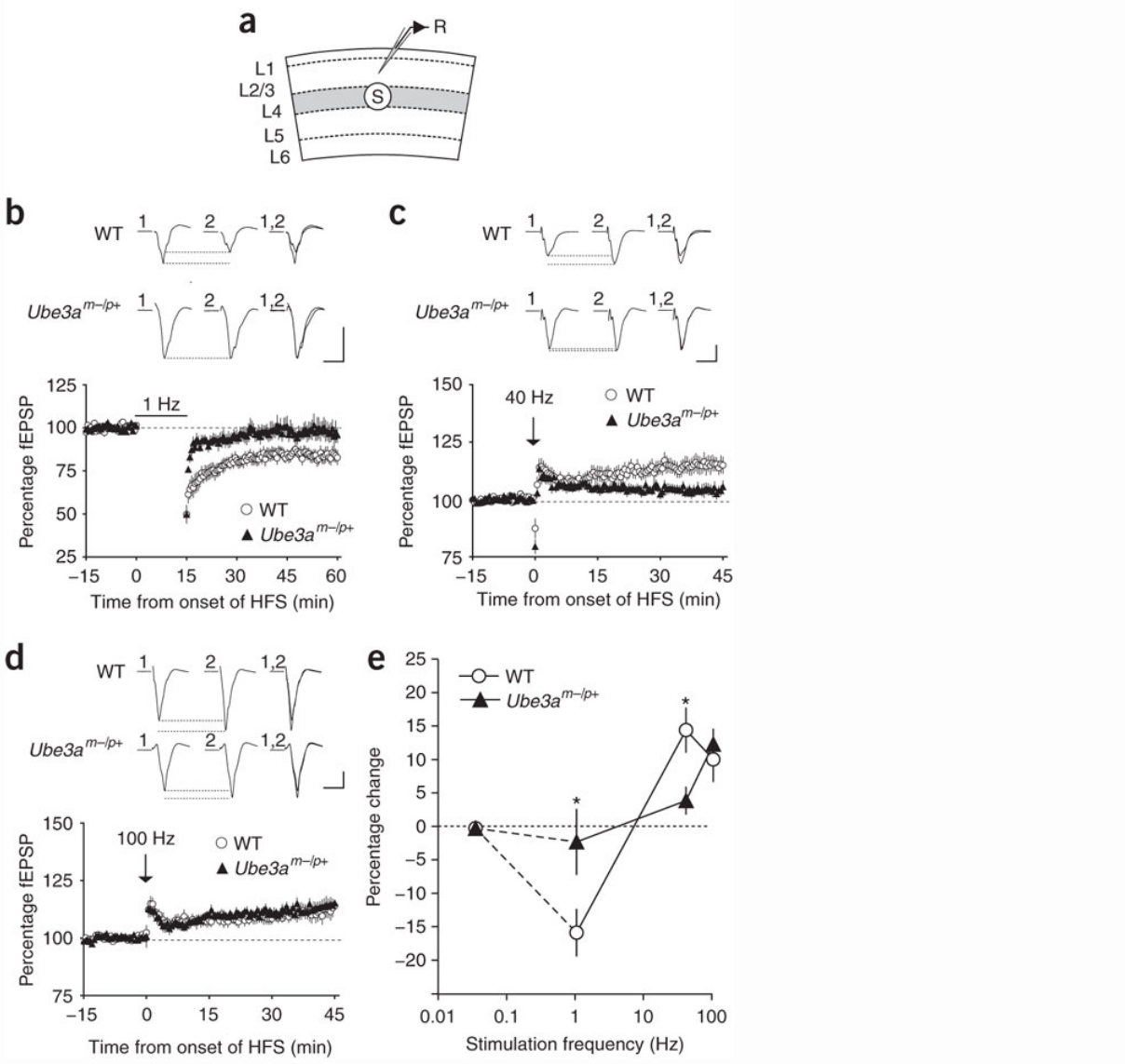

Figure 2-3: Synaptic plasticity is impaired bidirectionally in the neocortex of Angelman syndrome mice. (**A**) Schematic diagram of stimulating (S) and recording (R) configuration. (**B**) Baseline synaptic responses of WT and *Ube3a*$^{m-/p+}$ mice were measured before and after application of conditioning stimuli to the layer 4 (L4) to L2/3 pathway of the visual cortex. Top traces are representative averaged traces of a 15-min baseline (1), 30–45-min period after LTD induction (2) and their overlays (1, 2). Scale bars represent 10 ms and 1 mV. The bottom graph describes the average change in field excitatory postsynaptic potential (fEPSP) on delivery of a 1-Hz stimulus (indicated by the bar). Although 1-Hz stimulation for 15 min induced LTD in young WT mice, it did not change fEPSP amplitudes in *Ube3a*$^{m-/p+}$ mice (WT, $n = 13$ slices; *Ube3a*$^{m-/p+}$, $n = 7$ slices; $P < 0.04$). (**C**) Data are presented as in **B**, except that a stimulus consisting of three 40-Hz trains was delivered (indicated by an arrow). Although this stimulation induced LTP in WT mice, it did not alter fEPSP amplitudes in *Ube3a*$^{m-/p+}$ mice (WT, $n = 12$ slices; *Ube3a*$^{m-/p+}$, $n = 10$ slices; $P < 0.02$). (**D**) Data are

presented as in **C**, except that the stimulus consisted of two 100-Hz trains (indicated by an arrow). This stimulation induced LTP in both genotypes (WT, n = 12 slices; *Ube3a*$^{m-/p+}$, n = 10 slices; P = 0.59). (**E**) Frequency-response functions derived from visual cortex of WT and *Ube3a*$^{m-/p+}$ mice. Data points represent percent changes in fEPSP 30–45 min after the delivery of conditioning stimuli. The data points for 0.033 Hz are inferred from baseline stimulation delivered once every 30 s, which induced no obvious synaptic modifications. $^{*}P$ < 0.05. Error bars represent s.e.m.

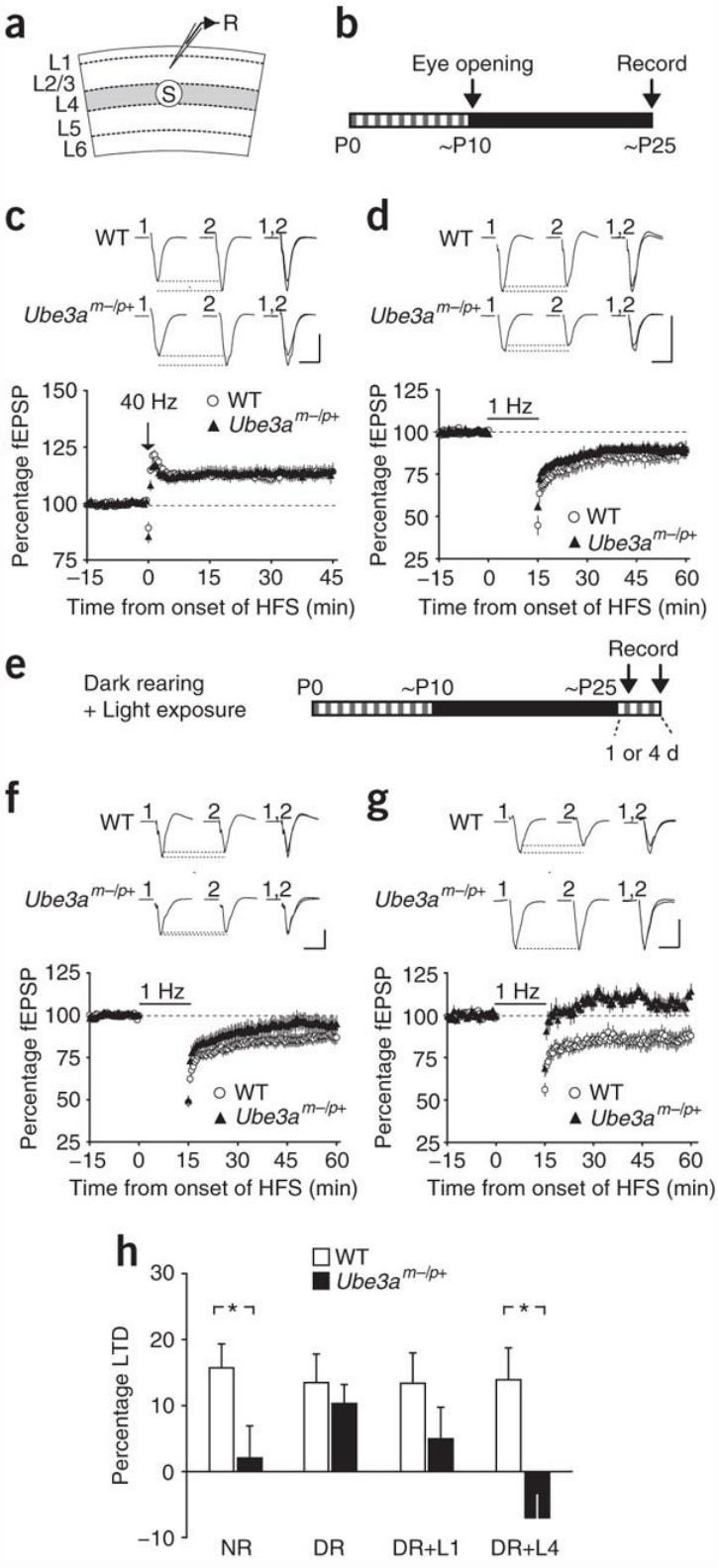

Figure 2-4: Sensory experience eliminates neocortical plasticity in Angelman syndrome mice. (**A**) Schematic of the recording configuration. (**B**) Schematic of the dark-rearing

condition. (**C**) Representative waveforms and averaged data demonstrating that the level of LTP induced with 40-Hz stimulation was comparable between WT (n = 18) and *Ube3a*$^{m-/p+}$ (n = 18) mice reared in complete darkness (P = 0.91). Scale bars represent 10 ms and 0.5 mV. (**D**) The level of LTD was also comparable between WT and *Ube3a*$^{m-/p+}$ DR mice (WT, n = 16 slices; *Ube3a*$^{m-/p+}$, n = 17 slices; P = 0.69). (**E**) Schematic showing the schedule for exposing DR mice to light. (**F**) Dark rearing, followed by 1 d of normal rearing attenuated LTD in visual cortical slices from *Ube3a*$^{m-/p+}$ mice (WT, n = 19; *Ube3a*$^{m-/p+}$, n = 15; P = 0.08). (**G**) After dark rearing, 4 d of normal rearing completely suppressed LTD in visual cortical slices from *Ube3a*$^{m-/p+}$ mice (WT, n = 9; *Ube3a*$^{m-/p+}$, n = 6; $P < 0.01$). (**H**) Visual experience dampened LTD in the visual cortex of *Ube3a*$^{m-/p+}$ mice. Data represent means ± s.e.m. of the percent reduction in fEPSP 30–45 min after the delivery of conditioning stimuli measured in NR and DR mice and in dark-then-light exposed for 1 or 4 d (DR+1L and DR+4L) mice. $^{*}P < 0.05$. Error bars represent s.e.m.

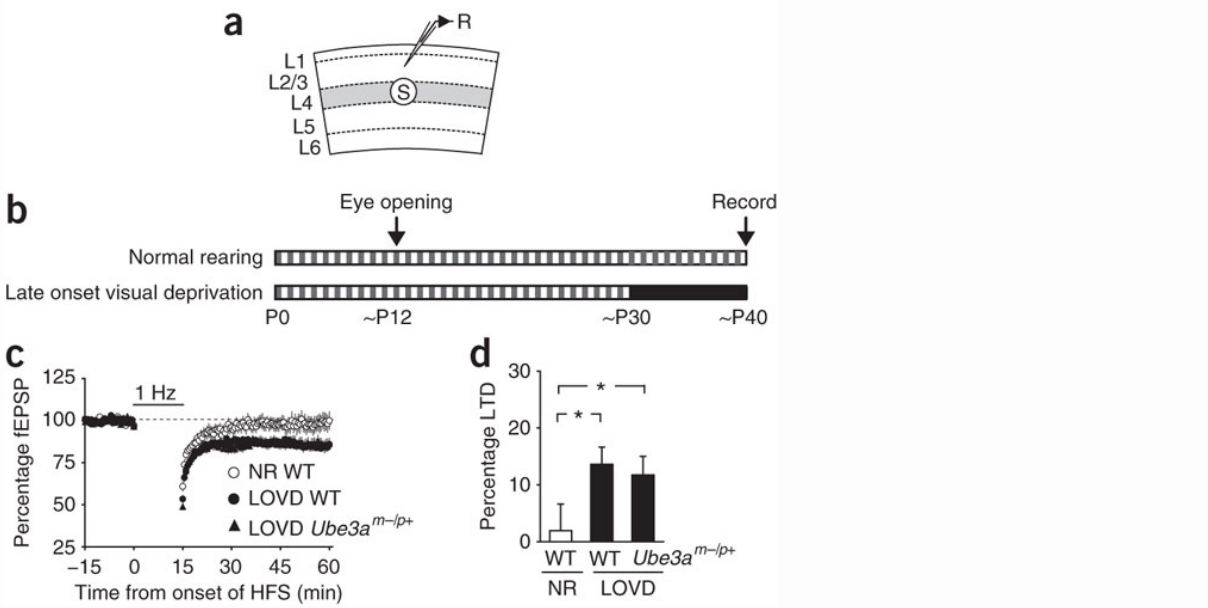

Figure 2-5: LOVD restores synaptic plasticity in Angelman syndrome mice. (**A**) Schematic of the recording configuration. (**B**) Schematic for the LOVD-rearing condition. (**C**) Averaged data demonstrating that LTD was abolished in NR WT mice at ~P40, whereas LTD of a similar magnitude was induced after LOVD in WT and *Ube3a*$^{m-/p+}$ mice (NR WT, $n = 10$ slices; LOVD WT, $n = 10$ slices; LOVD *Ube3a*$^{m-/p+}$, $n = 11$ slices; $P < 0.05$, NR WT was significantly different from both LOVD WT and LOVD *Ube3a*$^{m-/p+}$, one-way ANOVA followed by Tukey). (**D**) Bar graph of data shown in **c**. $^{*}P < 0.05$. Error bars represent s.e.m.

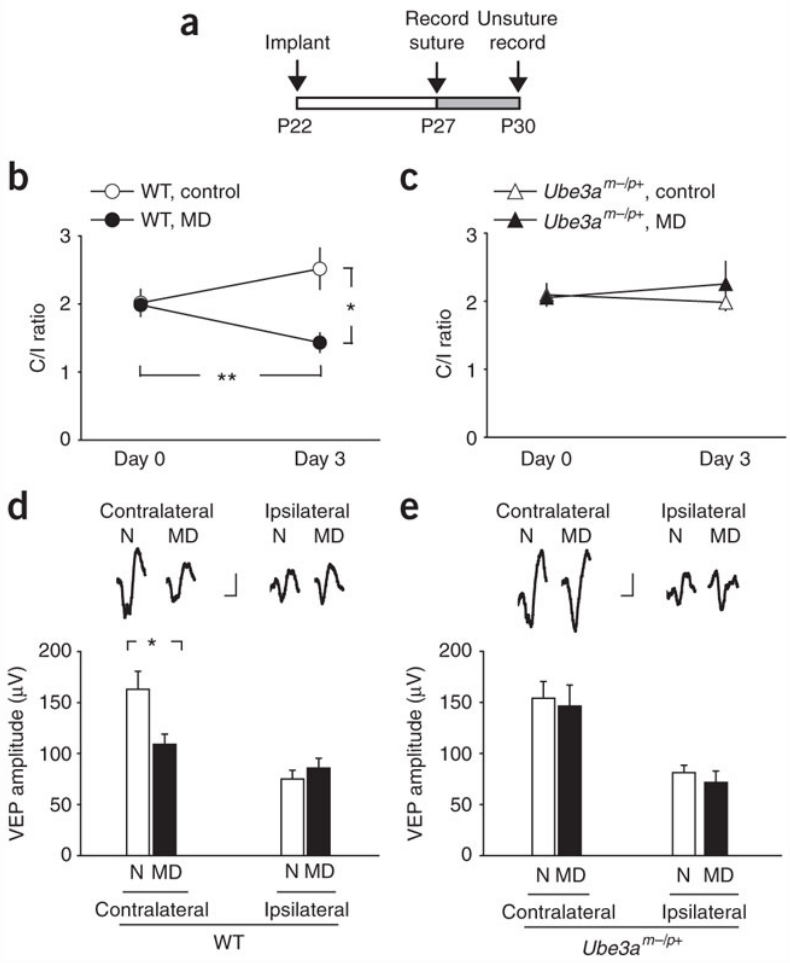

Figure 2-6: Critical period ocular dominance plasticity is absent in Angelman syndrome mice. (**A**) Schedule of the surgery and recording. (**B**) Changes in the ratio of contralateral to ipsilateral eye responses (C/I ratio) in monocularly deprived (MD, n = 13 mice) and nondeprived control WT mice (n = 14 mice) from P27 (day 0) to P30 (day 3). After 3 d of monocular deprivation, the C/I ratio was significantly reduced (paired t test, $P < 0.01$), whereas this reduction was not observed in age-matched nondeprived controls (paired t test, $P = 0.14$). (**C**) C/I ratios in *Ube3a*$^{m-/p+}$ mice (MD = 11 mice, control = 9 mice). Monocular deprivation did not affect the C/I ratio (paired t test, $P = 0.52$). C/I ratio was stable for 3 d in age-matched nondeprived controls (paired t test, $P = 0.53$). (**D**) Monocular deprivation–induced changes in contralateral, but not ipsilateral, VEPs in WT mice. Top traces are representative waveforms of VEPs recorded in WT mice. Scale bars represent 50 μV and 50 ms. The bottom graph describes comparisons of VEP amplitudes between control (N, normal) and MD WT mice. $^{*}P < 0.05$. (**E**) Data is presented as in **D**, except that experiments were conducted in *Ube3a*$^{m-/p+}$ mice. Error bars represent s.e.m.

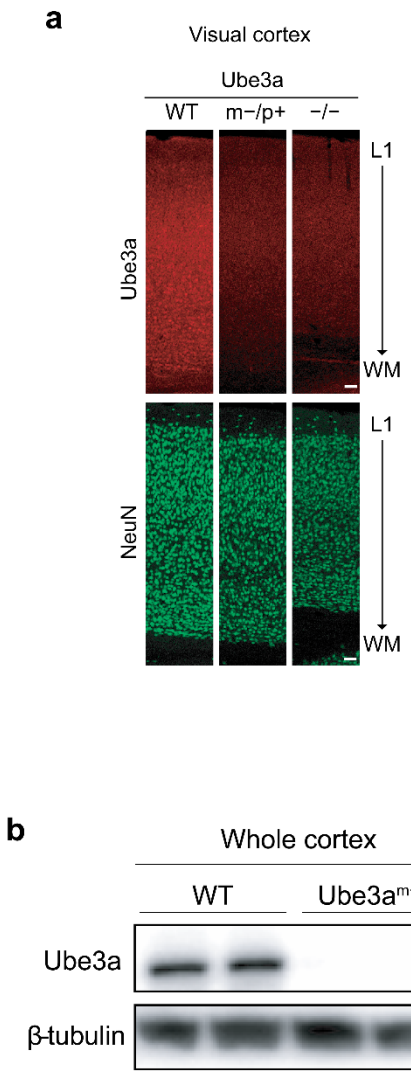

Supplementary Figure 2-1: Maternal expression of Ube3a in the cortex. (**A**) Immunohistochemical analysis of Ube3a expression in the visual cortex from young (P24) WT, *Ube3a*$^{m-/p+}$, and Ube3a m-/p- mice. Whereas strong Ube3a immunoreactivity was observed in all cortical layers except for layer 1 (L1) and white matter (WM) in WT mice, it was very weak in both *Ube3a*$^{m-/p+}$ and Ube3a$^{m-/p-}$ mice. NeuN antibody stains neuronal cell bodies. Scale bars, 100 μm. (**B**), Immunoblot analysis of Ube3a expression in whole cortical lysates from WT and *Ube3a*$^{m-/p+}$ mice at P25-27. Each lane contains cortical lysate from a different mouse. β-tubulin was used as an expression control.

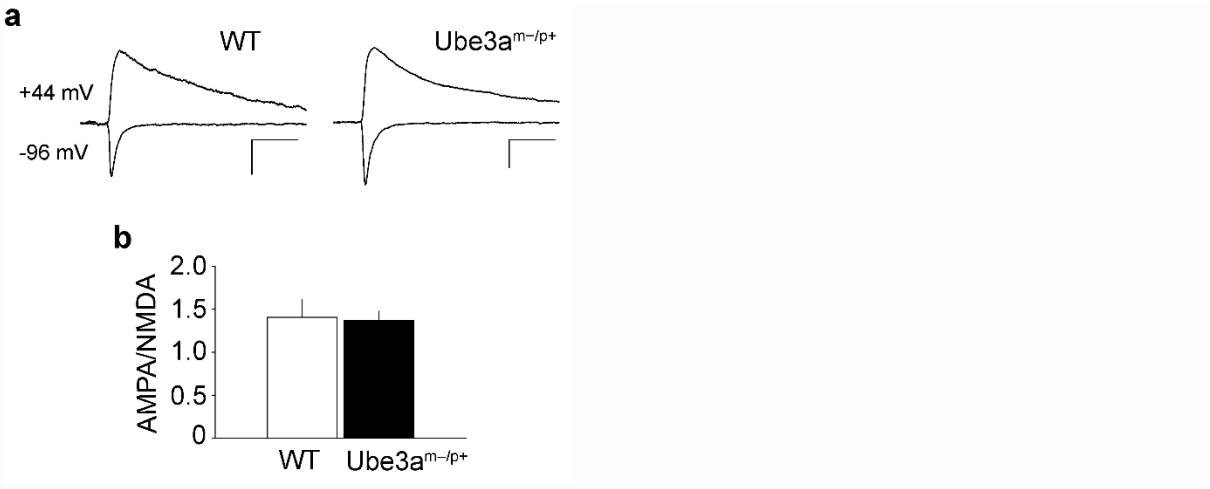

Supplementary Figure 2-2: The ratio of AMPA receptor- to NMDA receptor-mediated currents is normal in Ube3a$^{m-/p+}$ mice. (**A**)**,** Example traces: EPSCs were evoked by stimulating layer 4 and recording in layer 2/3 pyramidal neurons while cells were voltage-clamped at either 96 mV or +44 mV. AMPA receptor-mediated currents were measured at the EPSC peak, while NMDA receptor-mediated currents were recorded at +44 mV and measured 50 msec after the stimulus artifact. Scale bars: WT 50 msec, 50 pA; *Ube3a*$^{m-/p+}$, 50 msec, 100 pA. (**B**)**,** Average AMPA/NMDA current ratios for WT (n = 16 cells) and *Ube3a*$^{m-/p+}$ mice (n = 11 cells), showing no significant difference (WT, 1.4 ± 0.2; *Ube3a*$^{m-/p+}$, 1.4 ± 0.1; p = 0.89).

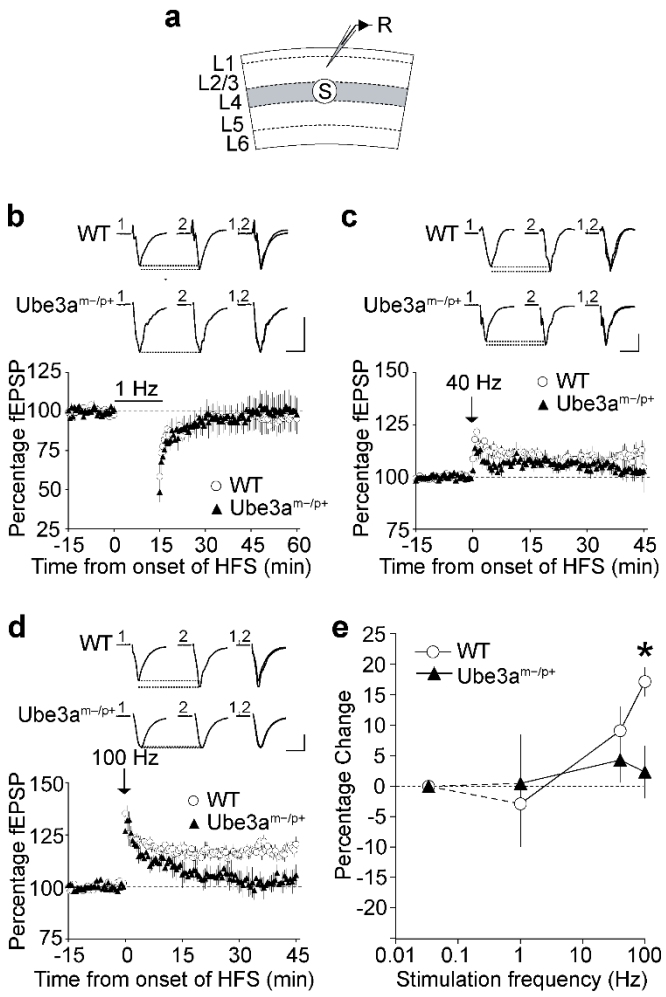

Supplementary Figure 2-3: The absence of Ube3a causes deficits in bidirectional synaptic plasticity in the visual cortex of adult mice. (**A**) Schematic of the recording configuration. (**B**) Synaptic responses of WT (open circle) and *Ube3a*$^{m-/p+}$ (closed triangle) mice were measured before and after application of a conditioning stimulation to the layer 4 (L4) to L2/3 pathway of the visual cortex. LTD was induced with 1 Hz stimulation for 15 min in visual cortex slices from adult mice. Top traces are representative averaged traces of 15 min baseline (1), 30-45 min period after LTD induction, (2) and their overlays (1, 2). Scale bars: 5 ms, 1 mV. Bottom graph describes average change in field EPSP (Percentage fEPSP) upon delivery of a 1 Hz stimulus (indicated by the bar) (WT, 97.1 ± 7.1%; *Ube3a*$^{m-/p+}$, 100.5 ± 8.0%; n = 9, 9; p = 0.75). LTD was not induced in either genotype. (**C**) Same as b, except that plasticity-inducing stimulation consisted of three 40 Hz trains (indicated by an arrow). Whereas this stimulation induced a weak LTP in WT mice, it failed to do so in *Ube3a*$^{m-/p+}$ mice (WT 109.2 ± 4.0%; *Ube3a*$^{m-/p+}$, 104.4 ± 3.7 %; n = 10, 8 slices; p = 0.39)**.** (**D**) Same as c, except that the LTP-inducing stimulation consisted of two 100 Hz trains (indicated by an arrow). Whereas this stimulation induced strong LTP in WT mice, it did not alter fEPSP amplitudes in *Ube3a*$^{m-/p+}$ mice (WT, 117.3 ± 2.4 %; *Ube3a*$^{m-/p+}$, 102.4 ± 4.3%; n

= 6, 7 slices; $p < 0.02$)**.** (**E**), Frequency-response functions derived from visual cortex of WT and *Ube3a*$^{m-/p+}$ mice. Data points represent percent changes in fEPSP 30-45 min after the delivery of conditioning stimulations. The data points for 0.033 Hz are inferred from baseline stimulation **d**elivered once every 30 sec, which induced no obvious synaptic modifications.

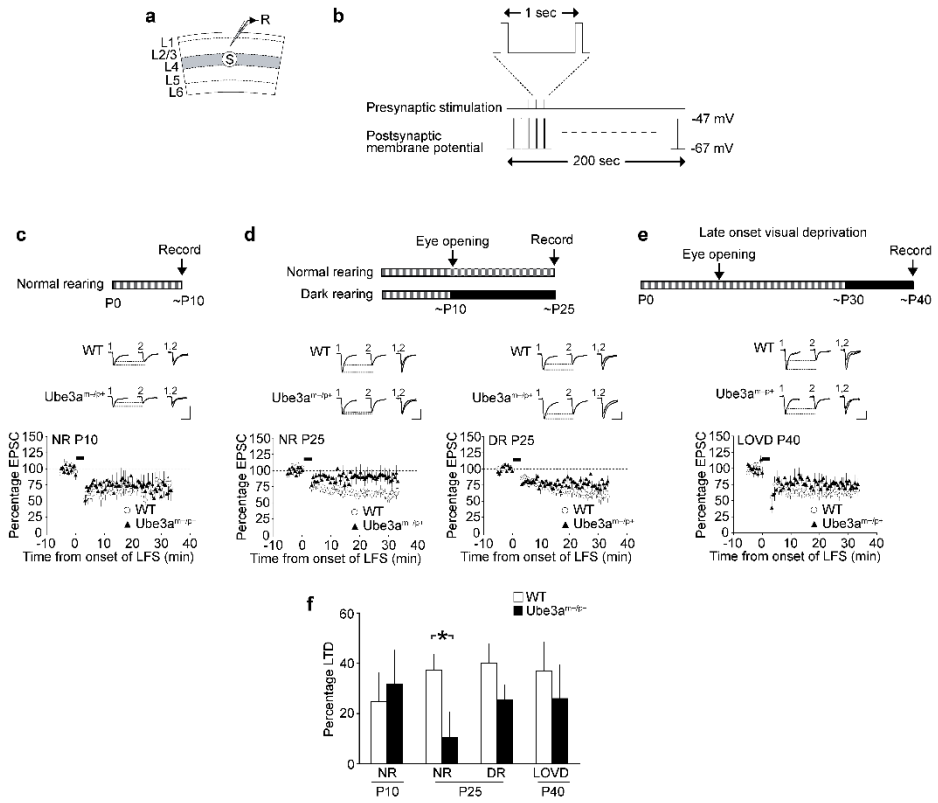

Supplementary Figure 2-4: Experience-dependent loss of LTD at excitatory synapses onto layer 2/3 pyramidal neurons in AS mice. (**A**) Whole-cell recording configuration: EPSCs evoked at layer 4 (L4) were recorded in L2/3 pyramidal neurons. (**B**) LTD induction protocol. (**C**) Baseline synaptic responses of WT (open circle) and *Ube3a*$^{m-/p+}$ (closed triangle) mice were measured before and after application of conditioning stimuli in normally reared (NR) mice at ~P10. A top schematic describes rearing condition. Traces in the middle are representative averaged traces of 5 min baseline (1), 25-30 min period after LTD induction (2), and their overlays (1, 2). Scale bars: 20 ms, 100 pA. Bottom graph describes average change in EPSC (Percentage EPSC) upon delivery of the conditioning stimulus (indicated by the bar). The pairing protocol induced LTD in both WT and *Ube3a*$^{m-/p+}$ mice (Percentage EPSC: WT, 75.3 ± 11.5, n = 8 cells; *Ube3a*$^{m-/p+}$, 68.4 ± 13.5, n = 8 cells; p = 0.71). (**D**) Same as **C**, except that LTD was measured in young (~P25) mice reared normally (left) or in a complete darkness (right). In normally reared mice (NR), whereas the pairing protocol induced LTD in WT mice, it did not alter EPSC amplitudes in *Ube3a*$^{m-/p+}$ mice (Percentage EPSC: WT, 62.3 ± 6.1, n = 11 cells; *Ube3a*$^{m-/p+}$, 90.1 ± 10.1, n = 9 cells; p < 0.03). In dark-reared (DR) mice, LTD was equally induced in both WT and *Ube3a*$^{m-/p+}$ mice (Percentage EPSC: WT, 62.7 ± 9.1, n = 7 cells; *Ube3a*$^{m-/p+}$, 74.7 ± 5.9 , n = 7 cells; p = 0.30). (**E**) Same as **C**, except that LTD was measured in ~P40 mice, provided with late-onset visual deprivation (LOVD). LTD was equally induced in both WT and *Ube3a*$^{m-/p+}$ mice (Percentage EPSC: WT, 63.1 ± 5.4, n = 9 cells; *Ube3a*$^{m-/p+}$, 25.6 ± 9.5, n = 6 cells; p = 0.30). (**F**) Visual experience causes developmental loss of LTD in *Ube3a*$^{m-/p+}$ mice. Data represent means ± SEM of percentage LTD measured 25-30 min after the delivery of conditioning stimuli. Whereas LTD was comparable between WT and *Ube3a*$^{m-/p+}$ mice at P10, it was reduced in young (~P25) *Ube3a*$^{m-/p+}$ mice when they were reared normally. This developmental loss was prevented by DR and LOVD.

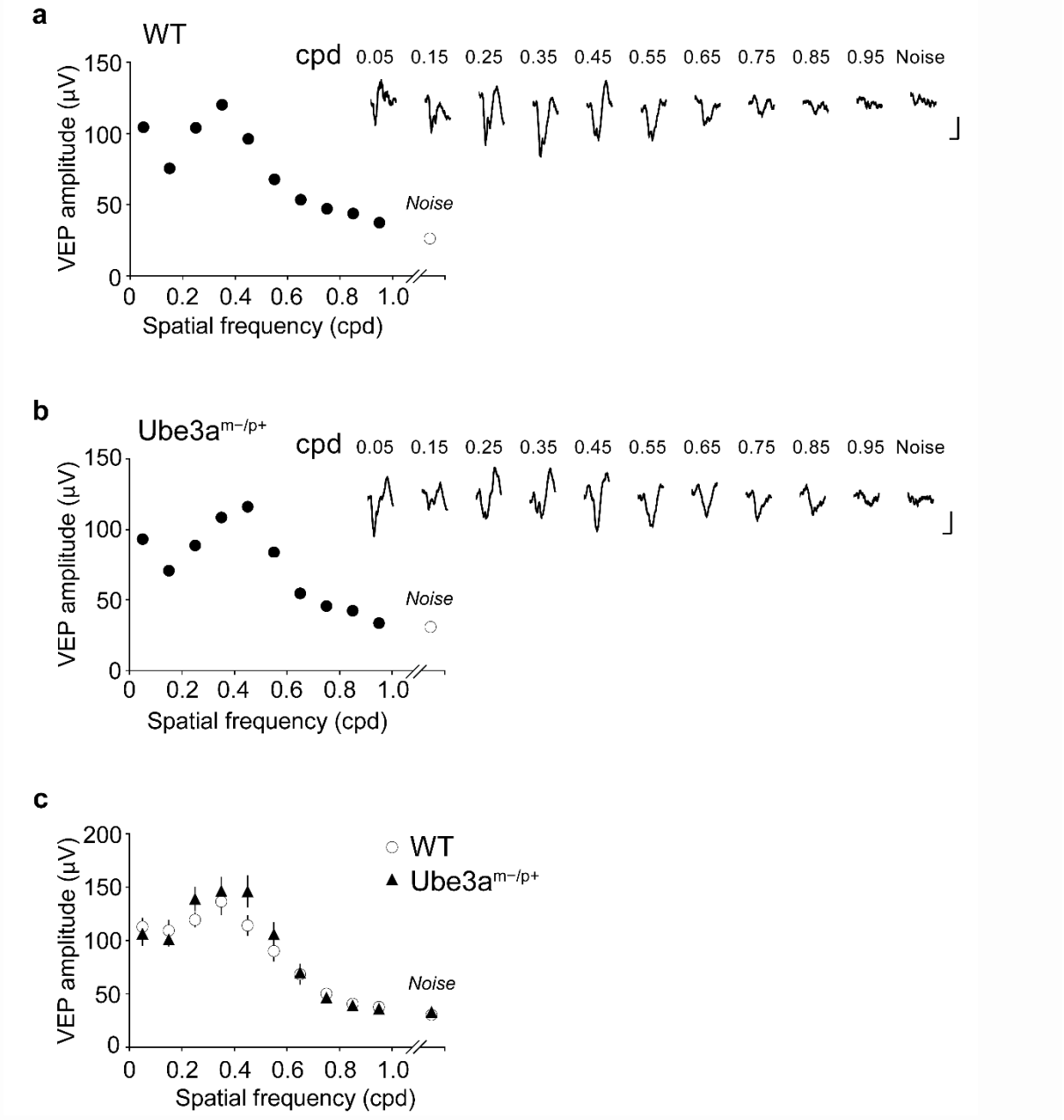

Supplementary Figure 2-5: Normal visual acuity in AS mice. (**A**) Examples of VEP recordings in WT mice. VEPs were evoked by presenting reversing gratings of different spatial frequencies. Closed circles represent amplitudes of VEPs in response to the gratings at maximal contrast. The open circle indicates the amplitude of noise measured at 0% contrast. VEP amplitudes decrease with increasing spatial frequency of stimulus indicated as cycles per degree (cpd). Scale bars: 50 μV, 50 msec. (**B**) Same as a, except that recordings were conducted in *Ube3a*$^{m-/p+}$ mice**.** (**C**) Averaged VEP amplitudes as a function of spatial frequency in WT (n = 15 mice) and *Ube3a*$^{m-/p+}$ mice (n = 13 mice). No statistically significant differences were found between WT and *Ube3a*$^{m-/p+}$ mice ($p > 0.05$, two-way repeated measures ANOVA).

	Infant (P8 – 11)			Young (P21 – 28)			Adult (P98 – 101)		
	WT	Ube3A$^{m-/p+}$	p value	WT	Ube3A$^{m-/p+}$	p value	WT	Ube3A$^{m-/p+}$	p value
Neuron number	11	11		11	12		12	12	
V_m (mV)	-55.5 ± 3.5	-56.8 ± 3.1	0.78	-73.0 ± 1.5	-70.0 ± 1.9	0.24	-75.0 ± 1.4	-72.6 ± 1.7	0.29
Ri (MΩ)	511.2 ± 51.6	487.9 ± 47.5	0.74	114.3 ± 10.1	163.4 ± 13.6	0.01	122.0 ± 1.4	140.7 ± 13.5	0.30
C_m (pF)	66.4 ± 4.1	68.9 ± 2.8	0.61	147.8 ± 5.5	115.2 ± 5.5	0.0004	151.7 ± 8.7	121.6 ± 9.6	0.03
Tau (ms)	1.0 ± 0.1	1.0 ± 1.8	0.32	2.8 ± 0.2	2.3 ± 0.1	0.06	3.1 ± 0.1	2.7 ± 0.2	0.10

	Young WT (P21 – 28)			Young Ube3A$^{m-/p+}$ (P21 – 28)			DR WT vs DR m-/p+
	NR	DR	p value	NR	DR	p value	p value
Neuron number	11	12		12	14		
V_m (mV)	-73.0 ± 1.5	-71.9 ± 1.9	0.48	-70.0 ± 1.9	-73.6 ± 1.4	0.14	0.49
Ri (MΩ)	114.3 ± 10.1	144.7 ± 11.7	0.06	163.4 ± 13.6	156.7 ± 13.3	0.73	0.51
C_m (pF)	147.8 ± 5.5	129.6 ± 8.0	0.08	115.2 ± 5.5	117.1 ± 5.4	0.81	0.26
Tau (ms)	2.8 ± 0.2	2.4 ± 0.2	0.20	2.3 ± 0.1	2.1 ± 0.1	0.43	0.26

Supplementary Table 2-1: Passive membrane properties of layer 2/3 pyramidal neurons in which mEPSC's are recorded. Resting membrane potential (Vm), input resistance (Ri), Membrane capacitance (Cm), and Membrane time constant (Tau) were measured using Mutliclamp (Axon instruments) while cells are voltage-clamped at -70 mV. Significant differences were found in membrane capacitance between the two genotypes of normally reared young and adult mice, and in input resistance of normally reared young mice. These differences may indicate smaller cell size of *Ube3a*$^{m-/p+}$ mice.

Fig 1d: Average mEPSC amplitude.

	P10	P25	P100
WT	16.6 ± 1.2 pA (11 cells)	11.8 ± 0.3 pA (11 cells)	10.1 ± 0.3 pA (12 cells)
Ube3a$^{m-/p+}$	18.0 ± 0.9 pA (11 cells)	11.0 ± 0.4 pA (12 cells)	11.1 ± 0.5 pA (12 cells)
p value	0.36	0.15	0.11

Fig 1e: Average mEPSC frequency.

	P10	P25	P100
WT	0.8 ± 0.2 Hz (11 cells)	10.7 ± 0.8 Hz (11 cells)	10.9 ± 1.3 Hz (12 cells)
Ube3a$^{m-/p+}$	0.7 ± 0.1 Hz (11 cells)	6.8 ± 0.9 Hz (12 cells)	7.5 ± 0.7 Hz (12 cells)
p value	0.52	< 0.003	< 0.03

Fig. 2c: Average mEPSC amplitude.

	WT	Ube3a$^{m-/p+}$
DR	11.5 ± 0.5 pA (12 cells)	11.7 ± 0.3 pA (14 cells)
NR	11.8 ± 0.3 pA (11 cells)	11.0 pA ± 0.4 pA (12 cells)
p value	0.68	0.16

Fig. 2d: Average mEPSC frequency.

	WT	Ube3a$^{m-/p+}$
DR	7.0 ± 0.5 Hz (12 cells)	6.0 ± 0.6 Hz (14 cells)
NR	10.7 ± 0.8 Hz (11 cells)	6.8 ± 0.9 Hz (12 cells)
p value	< 0.005	0.46

Fig 2f: Average density of dendritic spines.

	DR	NR
WT	0.53 ± 0.07 spines/µm (25 cells)	0.77 ± 0.04 spines/µm (33 cells)
Ube3a$^{m-/p+}$	0.41 ± 0.05 spines/µm (25 cells)	0.57 ± 0.03 spines/µm (32 cells)
p value	0.15	< 0.0003

Fig 3b: Average % baseline fEPSP response after 1 Hz stimulation.

	1 Hz stimulation
WT	84.3 ± 3.5 % (13 slices)
Ube3a$^{m-/p+}$	97.9 ± 4.9 % (7 slices)
p value	< 0.04

Fig 3c: Average % baseline fEPSP response after 40 Hz stimulation.

	40 Hz stimulation
WT	114.8 ± 3.3 % (12 slices)
Ube3a$^{m-/p+}$	104.2 ± 2.0 % (10 slices)
p value	< 0.02

Fig 3d: Average % baseline fEPSP response after 100 Hz stimulation.

	100 Hz stimulation
WT	110.4 ± 3.3 % (12 slices)
Ube3a$^{m-/p+}$	112.7 ± 2.2 % (10 slices)
p value	0.59

Fig 4c: Average % baseline fEPSP response after 40 Hz stimulation in dark-reared mice.

	40 Hz stimulation
WT	113.2 ± 2.4 % (18 slices)
Ube3a$^{m-/p+}$	113.6 ± 2.4 % (18 slices)
p value	0.91

Supplementary Table 2-2: Raw values for data presented in manuscript figures 2-1 through 2-6. For statistical analyses, unpaired student t-tests were used unless noted.

Fig 4d: Average % baseline fEPSP response after 1 Hz stimulation in dark-reared mice.

	1 Hz stimulation
WT	86.5 ± 4.3 % (16 slices)
Ube3a$^{m-/p+}$	89.7 ± 2.9 % (17 slices)
p value	0.69

Fig 4f: Average % baseline fEPSP response after 1 Hz stimulation in mice given 1 day of light exposure.

	1 Hz stimulation
WT	86.6 ± 3.8 % (19 slices)
Ube3a$^{m-/p+}$	95.0 ± 4.7 % (15 slices)
p value	0.08

Fig 4g: Average % baseline fEPSP response after 1 Hz stimulation in mice given 4 days of light exposure.

	1 Hz stimulation
WT	86.1 ± 4.8% (9 slices)
Ube3a$^{m-/p+}$	107.0 ± 3.4% (6 slices)
p value	< 0.01

Fig 5c,d: Average % baseline fEPSP response after 1 Hz stimulation.

	1 Hz stimulation
NR WT	98.0 ± 4.7 % (10 slices)
LOVD WT	86.4 ± 3.0 % (10 slices)
LOVD Ube3a$^{m-/p+}$	88.2 ± 3.3 % (11 slices)
p value (one-way ANOVA followed by Tukey)	< 0.05 (NR WT vs. LOVD WT or LOVD Ube3a$^{m-/p+}$)

Fig 6b: C/I ratio in WT mice.

	Deprived (13 mice)	Non-deprived (14 mice)
Day 0	2.0 ± 0.1	2.0 ± 0.2
Day 3	1.4 ± 0.1	2.5 ± 0.3
p value (paired t-test)	< 0.01	0.14

Fig 6c: C/I ratio in Ube3a$^{m-/p+}$ mice.

	Deprived (11 mice)	Non-deprived (9 mice)
Day 0	2.1 ± 0.1	2.1 ± 0.2
Day 3	2.3 ± 0.3	2.0 ± 0.1
p value (paired t-test)	0.52	0.53

Fig 6d: VEP amplitude in WT mice.

	Contralateral	Ipsilateral
Control (14 mice)	163.0 ± 17.6 μV	75.0 ± 8.7 μV
MD (13 mice)	109.1 ± 9.9 μV	85.7 ± 9.7 μV
p value	< 0.05	0.42

Fig 6e: VEP amplitude in Ube3a$^{m-/p+}$ mice.

	Contralateral	Ipsilateral
Control (9 mice)	154.1 ± 16.4 μV	81.2 ± 7.2 μV
MD (11 mice)	146.6 ± 20.5 μV	71.7 ± 11.1 μV
p value	0.77	0.47

Supplementary Table 2-2 (con't): Raw values for data presented in manuscript figures 2-1 through 2-6.

CHAPTER 3

3. Enhanced sensory potentiation in Angelman syndrome mice is abolished by Ube3a expression in inhibitory neurons

3.1. Overview

Sensory experience guides development of neocortical circuits. This activity-dependent circuit maturation is required for normal sensory and cognitive abilities, which are distorted in neurodevelopmental disorders. Here we have tested whether experience-dependent cortical modifications require *Ube3a*, an E3 ubiquitin ligase whose dysregulation has been implicated in both autism and Angelman syndrome (AS). Using the visual cortex as a model system for neocortical plasticity, we have previously found that the genetic deletion of UBE3A causes deficits in critical period ocular dominance plasticity, an *in vivo* assay for experience-dependent synaptic weakening. Because visual cortical slices from *Ube3a*-deficient mice exhibit deficits in activity-dependent synaptic strengthening, we hypothesized that the absence of *Ube3a* might also disrupt experience-driven forms of synaptic strengthening *in vivo*. Using chronic recordings of visual evoked potentials (VEPs), we have found that repeated stimulation of phase-reversing visual stimuli produces a strong potentiation of synaptic responses, consistent with previous studies (Frenkel et al., 2006; Cooke and Bear, 2010). Contrary to our hypothesis, we observed developmentally enhanced potentiation of VEPs, including increased power of spontaneous local field potentials (LFP) in AS mice. WT and AS mice achieved similar increases in VEP amplitude with a longer

period of visual stimulation, indicating the threshold for potentiation was lower in AS mice. Augmented plasticity and increased spontaneous LFP power were absent from mice maternally expressing *Ube3a* in inhibitory neurons alone. Our results suggest that sensory experience-dependent cortical potentiation is enhanced in adult AS mice due to reduced inhibition.

3.2. Introduction

Angelman syndrome (AS) is a neurodevelopmental disorder afflicting 1 in 12,000 individuals, characterized by profound cognitive disability, absent speech, impaired motor coordination, epilepsy and frequent laughter (Steffenburg et al., 1996; Clayton-Smith and Laan, 2003; Williams et al., 2006; Williams et al., 2010). The genetic basis of AS is disruption of maternally inherited *Ube3a* expression on chromosome 15q11-13 (Fang et al., 1999; Ohta et al., 1999; Robinson et al., 2000; Williams et al., 2010). UBE3A encodes an E3 ubiquitin ligase that recognizes and catalyzes the transfer of ubiquitin to its substrates for targeted proteasomal degradation.

Despite the important role of *Ube3a* in the central nervous system, it remains unclear how its loss of expression disrupts cognitive function in AS. Some learning deficits observed in clinical AS have been recapitulated in maternal-deficient *Ube3a* mice. AS mice exhibit deficits in hippocampal-dependent learning and memory paradigms (Jiang et al., 1998; Miura et al., 2002; van Woerden et al., 2007). Electrophysiology experiments carried out in the CA1 Schaffer collateral synapses of the hippocampus have found an increased threshold for long-term potentiation (LTP), the long-believed cellular mechanism that mediates memory (Weeber et al., 2003). Neocortical plasticity is disrupted as well, with higher induction thresholds for both LTP and long-term depression (LTD) of layer IV to II/III synapses in

visual cortical slices (Yashiro et al., 2009). These mechanisms are essential for experience-dependent circuit remodeling of the cortex (Feldman et al., 1999; Malenka and Bear, 2004), demonstrated by blunted LTD-dependent ocular dominance plasticity during the critical period of AS mice (Yashiro et al., 2009; Sato and Stryker, 2010). Although we have previously shown that activity-dependent synaptic weakening is impaired, it remains to be seen if experience driven synaptic strengthening is also impaired.

The present study revisits the visual cortex as a model for cortical development, in order to determine if loss of *Ube3a* impacts sensory experience's ability to strengthen synapses *in vivo*. Using a robust LTP-dependent phenomenon in the primary visual cortex known as stimulus-specific response potentiation (Frenkel et al., 2006; Cooke and Bear, 2010, 2012), we chronically recorded visual evoked potentials (VEP) in awake, head-fixed mice. To our surprise we found that experience-induced augmentation of VEPs was greater, and the threshold for potentiation lower, in Ube3a-deficient mice. This correlated developmentally with a generalized increase in spontaneous local field potential activity. Maternal expression of *Ube3a* in inhibitory neurons alone was sufficient to preclude both electrophysiological abnormalities.

3.3. Results

Normal sensory-driven potentiation in juvenile Angelman syndrome mice. Our previous report, detailing impaired LTP-induction of visual cortical field potentials by tetanic stimulation, suggests the possibility that LTP-induction by natural sensory stimulation may be afflicted as well. To test this hypothesis we bilaterally recorded local field potentials from layer IV in primary visual cortex, in awake, head-fixed mice. VEPs were generated by full-field phase reversing sinusoidal gratings fixed at 100% contrast. The grated sinusoidal bars

varied in width (0.05–0.95 cpd, in 0.1 cpd increments). Presentation of the widest bars (0.05 cpd) triggered the largest VEP responses while the finest bars (0.95 cpds) failed to exert responses discernible from noise (gray screen response). We began recording VEPs at postnatal day 28 (P28), an age when impaired LTP/LTD had previously been observed in vitro in AS model mice (Yashiro et al., 2009).

Eleven days of daily visual stimulation incrementally boosted VEP responses (Figure 3-1A$_1$ and Supplemental Figure 3-1A) to similar extents in both wild-type (WT) and AS model (*Ube3a*$^{m-/p+}$) mice (Figure 3-1A$_2$), indicating that experience-dependent plasticity was intact. On day twelve, the now familiar stimulus (Xº) was rotated (Xº + 90º). The new orthogonal stimulus evoked smaller VEPs, equivalent to those on day one (Figure 3-1A$_3$, $p > 0.05$), demonstrating that the exhibited potentiation in both genotypes was entirely exclusive to the familiar stimulus (Xº). By the fourth day of the novel stimulus (Xº + 90º), the VEP response had surpassed that of the familiar stimulus (90º), and continued to increase on the subsequent days (Supplemental Figure 3-1A). This suggests that the rate of potentiation to the novel stimulus had been enhanced by the previous experience with the familiar stimulus (Xº). To assess the stability of the potentiated visual response, mice were left in their home cages for 7 weeks (until P100) following the eleventh day of stimulus Xº + 90º. Upon reevaluation of stimulus Xº + 90º at P100, the VEP amplitude had remained elevated, and did not increase with further days of stimulation, confirming the response was still saturated (Supplemental Figure 3-2). These results imply that experience-dependent strengthening, specificity and stability of the circuit are functioning normally in juvenile *Ube3a*$^{m-/p+}$ mice.

Threshold for potentiation is lower in adult Angelman Syndrome mice. Because our previous data had shown that the LTP-induction threshold was even more severe at P100

(Yashiro et al., 2009), we were interested to see if SRP was altered in adult *Ube3a*$^{m-/p+}$ mice. Using the same experimental protocol applied at P28 revealed that by P100 sensory-driven VEP potentiation was markedly larger in *Ube3a*$^{m-/p+}$ mice, and significantly larger at P300 relative to WT mice (Figure 3-1A$_2$, Supplemental Figure 3-1B and 3-1C). Interestingly, in adult mice (P100 and P300) the novel stimulus Xº + 90º (day 12), generated a significantly greater VEP response than stimulus Xº on day 1 (Figure 3-1A$_3$). Although this robust form of perceptual learning persists into late-adulthood, it may be less stimulus-selective.

To further understand the enhanced SRP in adult *Ube3a*$^{m-/p+}$ mice, we examined how quantity of visual stimulation influenced the magnitude of potentiation. Animals were either briefly or heavily stimulated daily, with 100 or 1100 phase reversals respectively, at 1 Hz and 0.05 cpd (Figure 3-1B$_1$ and Supplemental Figure 3-3). Visual responses developed to a greater extent in *Ube3a*$^{m-/p+}$ mice compared to WTs when daily stimulation was brief (Figure 3-1B$_2$). However, 1100 phase reversals elicited a similar degree of potentiation in WT and *Ube3a*$^{m-/p+}$ mice. While the longer period of stimulation had a greater effect on WT VEP responses, *Ube3a*$^{m-/p+}$ mice responded similarly to both 100 and 1100 phase reversals, implying the visual response had been saturated by 100 phase reversals. Brief stimulation also only led to SRP that was entirely stimulus-specific in WT mice (Figure 3-1B$_3$). Complete specificity was absent in both genotypes following 1100 phase reversals.

Power of spontaneous local field potentials increases developmentally in Angelman syndrome mice. We recorded spontaneous local field potential (LFP) activity to assess the state of the visual cortical network, because sensory evoked activity may be influenced by ongoing cortical activity (Arieli et al., 1995; Arieli et al., 1996; Fellinger et al., 2011). The fast-fourier transform (FFT) function was used for spectral analysis of LFPs, recorded from

the same microelectrodes used in VEP recordings, prior to the outset of the visual plasticity paradigm. Power spectral analysis revealed that spontaneous visual cortical activity was depressed in the alpha, beta and gamma bands of juvenile (P28) *Ube3a*$^{m-/p+}$ mice (Figure 3-2A). However, as *Ube3a*$^{m-/p+}$ mice matured, the level of spontaneous activity rose across all frequency bands relative to WT mice (Figure 3-2B and 3-2C). Activity within the delta, theta and alpha frequency bands was significantly greater in *Ube3a*$^{m-/p+}$ mice at both P100 and P300, and no longer attenuated in the beta-gamma range.

Augmented LFP activity and plasticity absent in mice expressing Ube3a in inhibitory neurons. Several recent studies have found evidence for a developmental loss of inhibition in *Ube3a*-deficient mice that parallels the increase in spontaneous LFP activity and plasticity that we have identified (Egawa et al., 2012; Wallace et al., 2012). Considering that reduced inhibition may lead to overall increased excitation, possibly elevating spontaneous LFP activity and plasticity, we investigated the effect of maternal expression of *Ube3a* in inhibitory neurons. *Ube3a* expression was limited to inhibitory neurons by crossing GAD2-CRE transgenic and *Ube3a*-loxP-STOP-loxP mice (GAD2-CRE:*Ube3a*$^{stop/+}$).

Immunofluorescence studies were carried out with anti-Ube3a and anti-GABA to confirm *Ube3a* recombination was restricted to inhibitory neurons (Figure 3-3A). FFT analysis was performed on spontaneous LFP activity within the primary visual cortex of adult (P100) GAD2-CRE:*Ube3a*$^{stop/+}$ mice. Delta activity was significantly lower in GAD2-CRE:*Ube3a*$^{stop/+}$ mice relative to WTs, however power at higher frequency bands (theta, alpha, beta, and gamma) was normal (Figure 3-3B). When sensory experience-dependent plasticity was tested, we found that the magnitude and stimulus-specificity of potentiation was equivalent in WT and GAD2-CRE:*Ube3a*$^{stop/+}$ mice (Figure 3-3C). Repeated

presentation of stimulus Xº + 90º (days 12-22) conversely, failed to increase VEP amplitude in GAD2-CRE:*Ube3a*$^{stop/+}$ mice to the same extent as in WT mice (Supplementary Figure 3-4).

3.4. Discussion

Disruption of memory and plasticity has been an area of great interest in Angelman syndrome (AS) research over the past 15 years. Numerous studies have described attenuated LTP of electrically evoked field potentials in *Ube3a*$^{m-/p+}$ mice, both within CA1 hippocampus and the primary visual cortex (Jiang et al., 1998; Miura et al., 2002; Weeber et al., 2003; van Woerden et al., 2007; Yashiro et al., 2009; Sato and Stryker, 2010; Baudry et al., 2012; Kaphzan et al., 2012). This study is the first to provide evidence of an augmented form of synaptic plasticity in AS, known as stimulus-specific response potentiation (SRP). SRP is an experience-dependent enhancement, in part, of the thalamocortical synapses in the primary visual cortex. This enhancement is manifested by an increase in the visual evoked potential (VEP) response, and has many of the attributes of conical LTP. It is long lasting, can be prevented by either blocking NMDA receptors or inhibiting AMPA receptor insertion, and its maintenance is abolished by inhibition of PKMζ, a kinase that maintains NMDA-dependent LTP (Frenkel et al., 2006; Cooke and Bear, 2010). These properties suggests that this type of endogenous plasticity is a naturally occurring form of thalamacortical LTP.

When we examined the SRP phenomenon in juvenile AS model mice no deficits were found. The rate and magnitude of VEP potentiation was indistinguishable from WT mice, and very stable. There was no sign of decline in the potentiated response even after 7 weeks without visual stimulation. Speculating that the increase in LTP-induction threshold, observed *in vitro* at P25, might be too small to influence SRP, we examined adult *Ube3a*$^{m-/p+}$

mice reported to have more severely impaired LTP (Yashiro et al., 2009). However, by P100 *Ube3a*$^{m-/p+}$ mice were exhibiting a greater gain in VEP responses from day-to-day stimulation, than were WT mice. The magnitude of this gain appeared to have fully matured by P100 and persisted into late-adulthood (P300). SRP potentiation was the same in adult AS mice whether being stimulated daily with 100 or 1100 phase reversals. On the other hand, WT mice showed greater potentiation with 1100 phase reversals, equivalent to *Ube3a*$^{m-/p+}$ mice. This suggests that *Ube3a*$^{m-/p+}$ mice may in fact have a lower threshold for this form of experience-dependent plasticity. This is surprising because in slice *Ube3a*$^{m-/p+}$ mice have a higher LTP-induction threshold for layer IV to II/III synapses in the primary visual cortex (Yashiro et al., 2009).

Emergence of the VEP enhancement in *Ube3a*$^{m-/p+}$ mice corresponds with a general increase of spontaneous local field potential (LFP) activity. Young *Ube3a*-deficient mice have a reduction of power across the alpha, beta and gamma bands. By adulthood that reduction is gone, replaced by increased power in the delta, theta and alpha bands. While oscillations in narrow frequency bands of LFP activity correspond to a wide variety of behavioral and cognitive states (Basar et al., 2001; Kahana, 2006), less is known about the significance of broadband shifts in activity such as those observed in the *Ube3a*$^{m-/p+}$ mice. Increases in broadband LFP activity have been shown to correspond to increased neuronal spiking (Manning et al., 2009; Miller, 2010). This leads us to speculate that the lower broadband power observed in young *Ube3a*$^{m-/p+}$ mice may be due to reduced population spiking, which transitions into an overactive state in adulthood. An important test will be to see if single-unit recordings confirms this, and to determine the relative contributions of inhibitory/excitatory neuronal spiking. This plays into evidence of an excitatory/inhibitory

imbalance in AS, where reduced cortical excitation in juvenile *Ube3a*$^{m-/p+}$ mice (Yashiro et al., 2009), is reversed by an aggregative loss of inhibition observed both in the cerebellum and cortex (Egawa et al., 2012; Wallace et al., 2012).

To determine whether inhibitory decline, due to loss of *Ube3a*, was impacting the SRP enhancement, we utilized CRE recombinant mice that expressed maternal *Ube3a* exclusively under the GAD65 promoter, a marker for inhibitory neurons. Indeed, limiting *Ube3a* expression to inhibitory neurons was sufficient in preventing an exaggerated experience-dependent VEP response. Restoration of *Ube3a* in inhibitory neurons also eliminated elevated broadband LFP activity. There was a curious decrease of delta power in the GAD2-CRE:*Ube3a*$^{stop/+}$ mice which may reflect a complex interplay between inhibitory and dysfunctional *Ube3a*-deficient excitatory neurons.

Our findings fit the growing literature of evidence for an increased excitation to inhibition ratio in autism (Rubenstein and Merzenich, 2003; Bourgeron, 2009; Yizhar et al., 2011). Fragile X syndrome (Fmr1 KO) mice exhibit cortical hyperexcitability due to decreased excitatory drive onto inhibitory neurons (Gibson et al., 2008). Excitatory drive onto inhibitory neurons is normal is AS model, however the reciprocal drive of inhibitory synapses onto excitatory neurons is developmentally reduced in the cortex (Wallace et al., 2012). Network dynamics in AS are further complicated because excitatory neurotransmission is also substantially reduced, leading to a cortical LTP deficit, at least *in vitro* (Yashiro et al., 2009). It appears that the net balance of excitation/inhibition in adult AS may be in favor of reduced inhibition. The reduction of inhibitory tone by the disruption of GABA synthesis has been shown to increase experience-dependent OD plasticity in the visual cortex of adult rats (Harauzov et al., 2010). This rise in adult plasticity is

accompanied by improved synaptic strengthening, but not synaptic weakening, suggesting the OD shift may have occurred because of enhanced open eye potentiation. SRP may similarly be enhanced in AS mice due to a net increase excitation, which is not present when *Ube3a* expression is limited to inhibitory cells. One of the consequences of the hyper-plastic adult *Ube3a*$^{m-/p+}$ mice was a lower threshold for nonspecific VEP potentiation evoked by a novel visual stimulus. These modifications to experience-dependent plasticity may underlie some of the sensory processing disturbances reported in AS (Walz and Baranek, 2006). Treatment with the administration of a GABAergic agonist has been effecting in restoring inhibitory function in the cerebellum of AS, including ameliorating some of the motor deficits (Cheron et al., 2005; Egawa et al., 2012). It would be interesting to see if administration of a GABAergic agonist might be equally effective in restoring normal experience-dependent plasticity in the adult visual cortex.

3.5. Material and Methods

Animals

Male and female C57BL6/J WT and maternally deficient Ube3a mice were generated by crossing paternally deficient Ube3a females with WT males. Juvenile, adult and late adult mice ranged from P27-29, P90-120, P255-310 respectively. Mice were kept on a 12-hour dark/light cycle and given ad libitum access to food and water. All experimental animal procedures were carried out according to the NIH *Guide for the Care and Use of Laboratory Animals* and the Society for Neuroscience *Policy on the Use of Animals in Neuroscience Research* and were approved by the Institutional Animal Care and Use Committee at the University of North Carolina at Chapel Hill.

Transgenic male and female GAD2-Cre;lox-Stop-lox-ube3a mice were utilized to obtain maternal expression of Ube3a in interneurons. Mice were on a mixed C57BL6/J background and ranged from P90-120.

Surgery for in vivo recordings

Mice were anesthetized with ketamine / xylazine (120 mg: 9 mg/kg; Bioniche Pharma / AnaSed) delivered intraperitoneally, and 0.25 % bupivacaine (Hospira) was locally applied to the scalp incision site. Sharpened tungsten microelectrodes (0.3-0.5 MΩ impedance range; FHC) were bilaterally implanted into the binocular zone of V1, ±3.00 mm lateral of lamda and -0.45 mm ventral from brain surface. Silver reference electrodes were implanted ±2.00 mm lateral and -1.0 mm posterior of bregma, on the brain surface. A head-restraint holding post was placed on the skull surface, anterior to the reference electrodes, and all were secured to the skull with cyanoacrylic (Henkel). Mice were given at least 48 h to recover before being habituated to the head-restraint apparatus for 45 min.

EEG recordings

EEG recordings were taken 24 hr after the initial habituation to the head-restraint, in the absence of visual stimulation. The first 10 min of recording were discarded (habituation period) and the following 25 min utilized for EEG analysis. All recordings were amplified 1000x, and high and low band filters set to 0.1 Hz and 100 Hz respectively (Grass Technologies). Data were acquired and digitized at 4096 Hz into Spike2 (Cambridge Electronic Design). Spectral analysis was performed using a Fast Fourier Transform (FFT size 8192; Hanning Window), and grouped into the following EEG bands: delta (1-3.5 Hz), theta (4-7.5 Hz), alpha (8-12 Hz), beta (13-20 Hz) and gamma (21-50 Hz).

Visual Evoked Potentials (VEP)

VEPs were recorded 24 hr after EEG recordings (48 hr after head-restraint habituation). Mice were placed 20 cm from a 21 inch CRT computer monitor (80 cd/m^2) and visually stimulated with 1 Hz square-wave reversing sinusoidal gratings oriented at either 0º or 90º (Vision Research Graphics). Visual stimuli were presented in groups of 34 consecutive reversals followed by a 10 sec break (black screen). VEP responses were calculated as the trough to peak amplitude of 102 averaged presentations.

Stimulus-Selective Response Potentiation (SRP)

To characterize SRP across development (P28, P100, P300), each mouse was presented with a randomized array of visual stimulation consisting of 102 presentations of 0.05, 0.15, 0.25, 0.35, 0.45, 0.55, 0.65, 0.75, 0.85 and 0.95 cpd, including 2.84 cpd and the gray screen response as controls. The array of visual stimuli were all presented in one orientation (0º or 90º) for 11 consecutive days. On the 12th day the grating orientation was rotated 90º and maintained for another 10 consecutive days until the 23rd day when the orientation was reverted back to the starting orientation.

To assess the effect of presentation number on SRP, mice were presented with either 102 or 1122 grating reversals at only 0.05 cpd. For mice receiving 1122 presentations, the VEP amplitude was determined from the average of the first 102 reversals.

Histology and Immunohistochemistry

Mice were deeply anesthetized with sodium pentobarbital (60 mg/kg i.p.) prior to transcardial perfusion with room temperature phosphate-buffered saline (PBS) immediately followed by room temperature phosphate-buffered 4% paraformaldehyde (pH 7.3). Perfused brains were removed from their skulls and postfixed overnight at 4°C prior to being

cryoprotected via sequential 12-hour incubations in 10%, 20%, and 30% sucrose in PBS (pH 7.5). Cryoprotected brains were frozen on dry ice and cut into 40 □m-thick sections with a sliding microtome (Thermo Scientific, Kalamazoo, MI, USA). Sections were stored in a cryopreservative solution (by volume: 45% PBS, 30% ethylene glycol, 25% glycerol) at -20°C until they were processed for free-floating immunohistochemistry.

For immunofluorescent staining, sections were rinsed several times in PBS before blocking in PBS plus 5% normal goat serum and 0.02% Triton-X-100 (NGST) for 1 hour at room temperature. Blocked tissue sections were incubated in primary antibodies (1:1000 rb anti-GABA, Sigma-Aldrich; 1:200 ms anti-Ube3a, Sigma-Aldrich) diluted in NGST for 48 hours at 4°C. Sections were then rinsed several times in PBS containing 0.02% Triton-X-100 (PBST) before incubation in secondary antibodies (also diluted in NGST) for 1 hour at room temperature. In most experiments, 4',6-diamidino-2-phenylindole (DAPI, Invitrogen D1306) was added during the secondary antibody incubation at a concentration of 700 ng/mL for nuclear counterstaining. Images of brain sections were acquired with a Zeiss LSM 710 confocal microscope equipped with ZEN imaging Software (Zeiss, Jena, Germany).

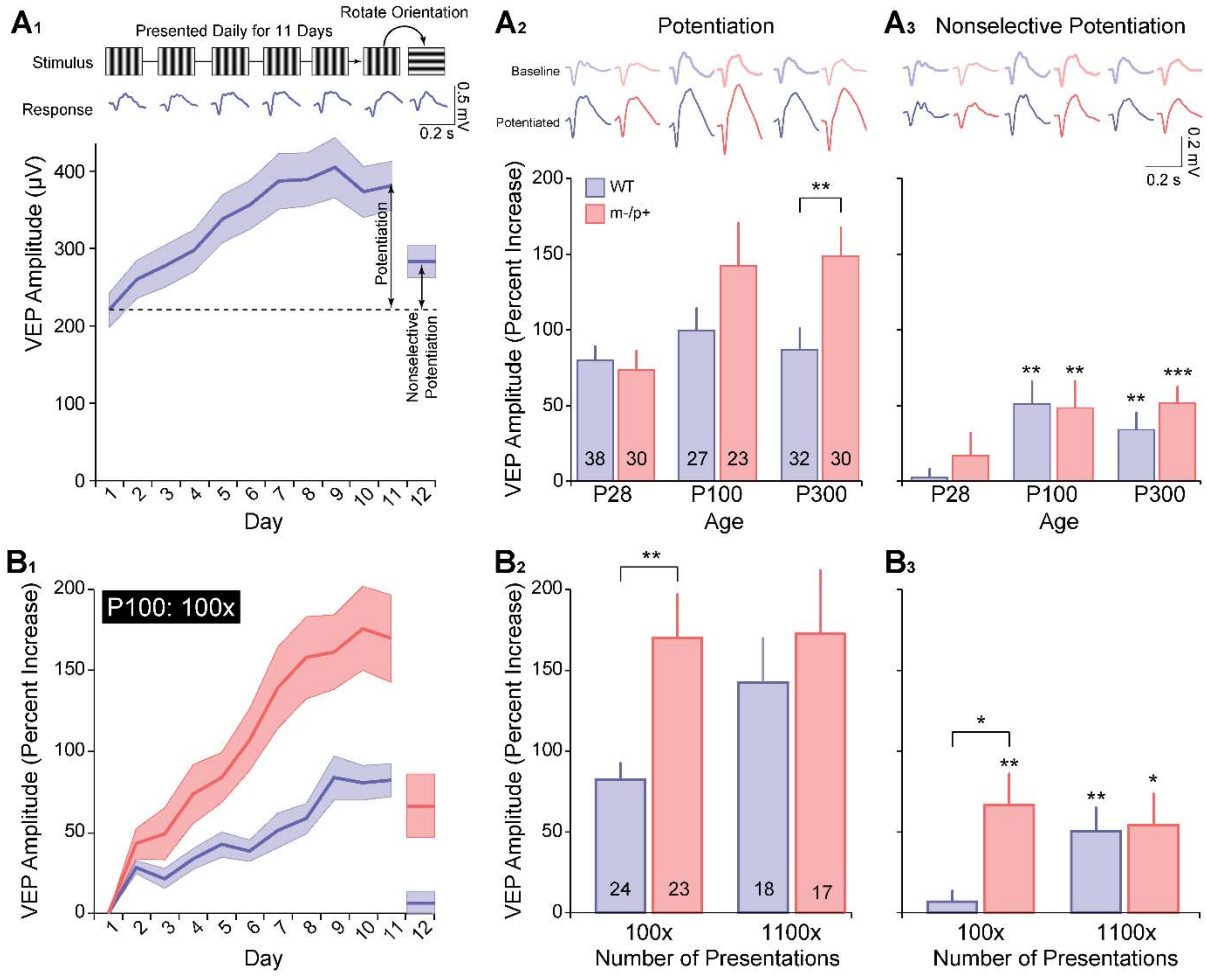

Figure 3-1: Adult experience-dependent potentiation is enhanced in Angleman syndrome mice. (**A1**) Visual-evoked potentials (VEP) were recorded bilaterally from layer IV of primary visual cortex in awake, head-fixed mice. Animals were visually stimulated with phase-reversing sinusoidal gratings (Xº) for eleven consecutive days, triggering a gradual potentiation in the VEP amplitude. The stimulus-selectivity of the enhanced response is demonstrated on the twelfth day when the now-familiar stimulus is rotated 90º (Xº + 90º). Traces are representative VEP waveforms from a single WT mouse, while the line graph represents the average VEP amplitude of all WT mice tested at P100. (**A2**) Traces are the average VEP waveform of all WT (blue) and *Ube3a*$^{m-/p+}$ (red) mice, on day one (baseline) and eleven (potentiation) of visual stimulation, among three different age groups (P28, P100, P300). Juvenile (P28) *Ube3a*$^{m-/p+}$ mice exhibited a similar magnitude of potentiation to WTs following eleven days of visual stimulation, but was significantly enhanced in adulthood ($p < 0.01$). (**A3**) Average WT and *Ube3a*$^{m-/p+}$ VEP waveform on days one (baseline) and twelve (potentiated). Adult mice exhibited significantly more stimulus-nonselective response potentiation (SNRP), absent in the juvenile mice. There were no genotype differences. (**B1**) The average percent increase in VEP amplitude following modest

daily visual stimulation (100 phase reversals) at P100. (**B_2**) The potentiation threshold was significantly lower in *Ube3a*$^{m-/p+}$ mice when presented 100 phase reversals daily, but comparable with more rigorous stimulation (1100 phase reversals). (**B_2**) Presenting 100 phase reversals daily only induced SNRP in *Ube3a*$^{m-/p+}$ mice, while SNRP was obtained in both genotypes with 1100 phase reversals daily.

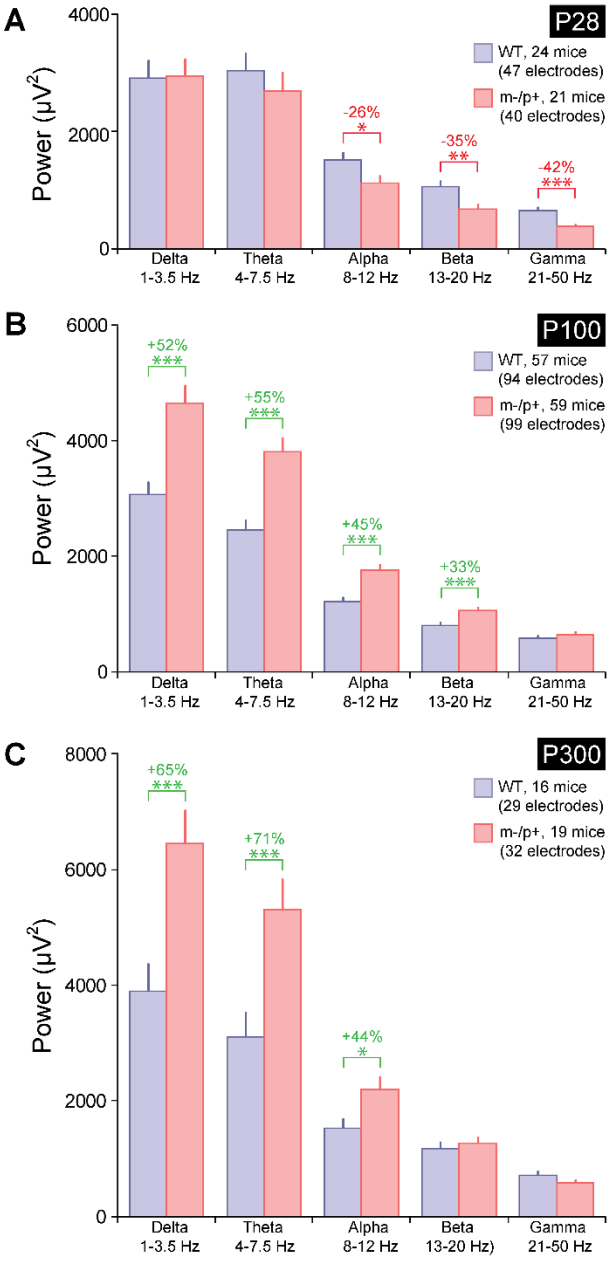

Figure 3-2: Developmental rise in visual cortical EEG power in Angelman syndrome mice. (**A**) Spontaneous EEG activity was recorded from V1, prior to visual stimulation paradigm. Juvenile *Ube3a*$^{m-/p+}$ mice exhibit significantly less power in the alpha, beta and gamma bands. **(B)** Adult (P100) *Ube3a*$^{m-/p+}$ mice reveal a general increase in power across all frequency bands relative to WTs, with significantly greater levels of power in delta, theta, alpha and beta bands. **(C)** The increase in power is preserved in late adulthood (P300) in *Ube3a*$^{m-/p+}$ mice.

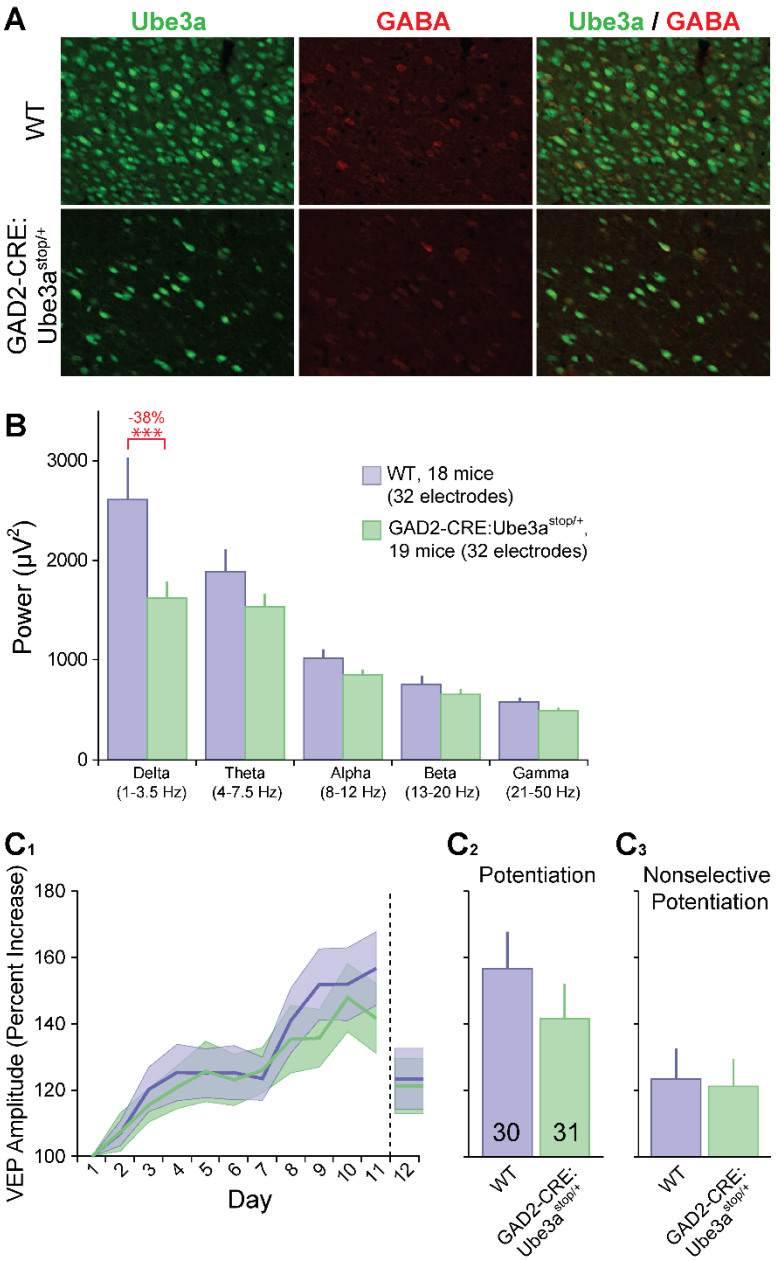

Figure 3-3: Increased EEG activity and enhanced potentiation is abolished by *Ube3a* expression in inhibitory neurons. (**A**) Immunohistochemistry from sagittal sections through the visual cortex at P100. GAD2-CRE:*Ube3a*$^{stop/+}$ mice only express *Ube3a* maternally in *GABA* producing inhibitory neurons. **(B)** Maternal expression of *Ube3a* in inhibitory neurons led to reduced power in the delta frequency band. **(C_1)** Following eleven days of visual stimulation **(C_2)** WT and GAD2-CRE:*Ube3a*$^{stop/+}$ mice displayed comparable degrees of VEP potentiation, **(C_3)** as well as SNRP.

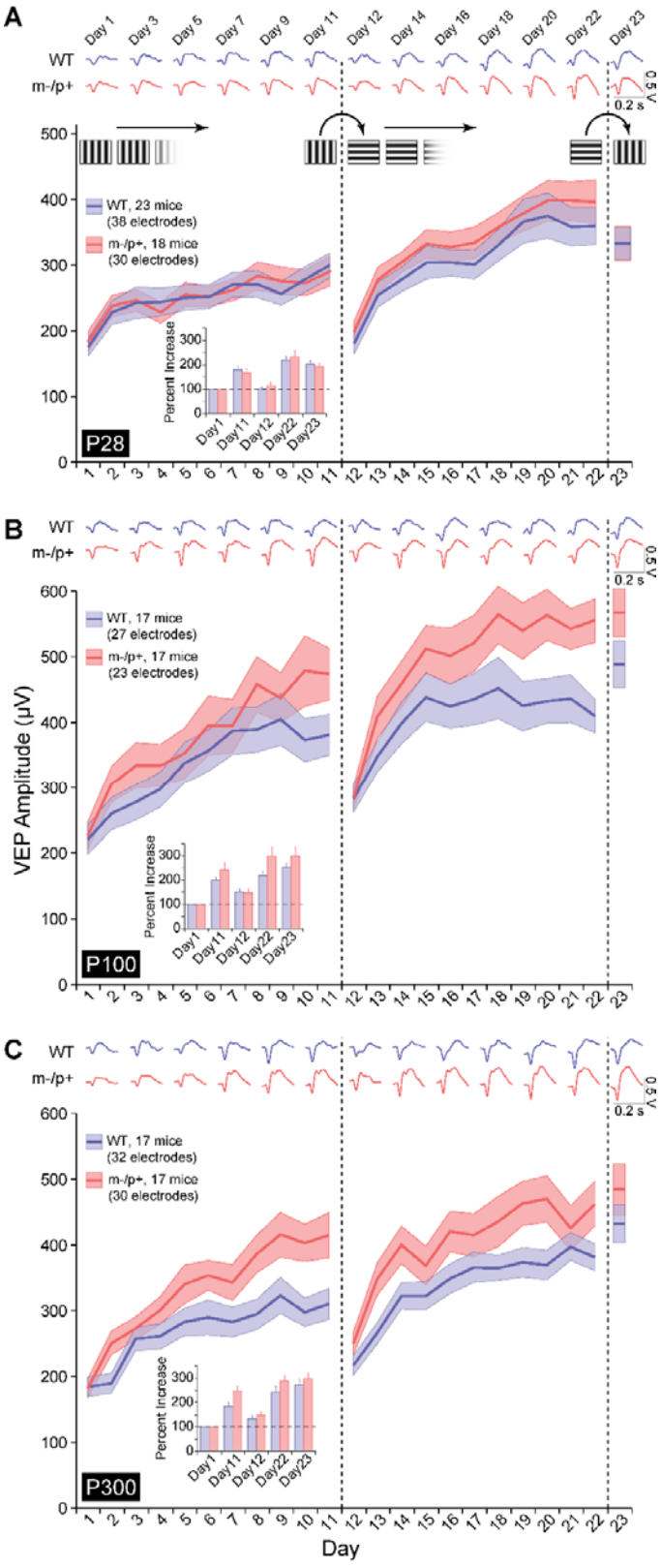

Supplemental Figure 3-1: Developmentally enhanced VEP potentiation in Angleman syndrome mice. (**A**) Traces represent example VEP waveforms from an individual WT

(blue) and *Ube3a*$^{m-/p+}$ (red) mouse over 23 days of visual stimulation. The graphs represent the average VEP amplitude with the percent increase from day one in the insets. Phase reversing sinusoidal gratings (Xº) were presented for eleven days, resulting in a potentiated response. On day 12 the grating orientation was reversed (Xº + 90º), representing a novel stimulus, presented for an additional 11 days, and then reverted back to the original orientation to demonstrate retention of potentiation. **(B)** There is a trend towards greater potentiation in adult (P100) *Ube3a*$^{m-/p+}$ mice following 11 days of visual stimulation. The enhanced potentiation becomes more apparent in the *Ube3a*$^{m-/p+}$ mice on days 12-22 with introduction of the novel stimulus (Xº + 90º). **(C)** The enhanced potentiation is more apparent the later-adult (P300) *Ube3a*$^{m-/p+}$ mice.

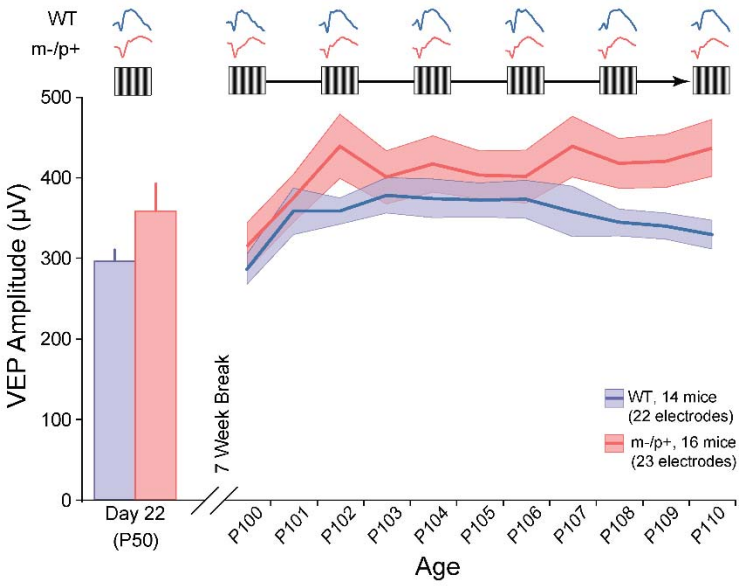

Supplemental Figure 3-2: Potentiated response is maintained for 7 weeks. (**A**) Traces are representative waveforms from an individual WT and *Ube3a*$^{m-/p+}$ mouse. Mice visually stimulated for 23 days starting at P28 (subset of mice from Supplementary Figure 3-2A), were left in their homecages for 7 weeks until P100, and visually reevaluated. After the 7 week break, mice from both genotypes maintained potentiated VEP responses, which could not be increased any further with subsequent days of visual stimulation.

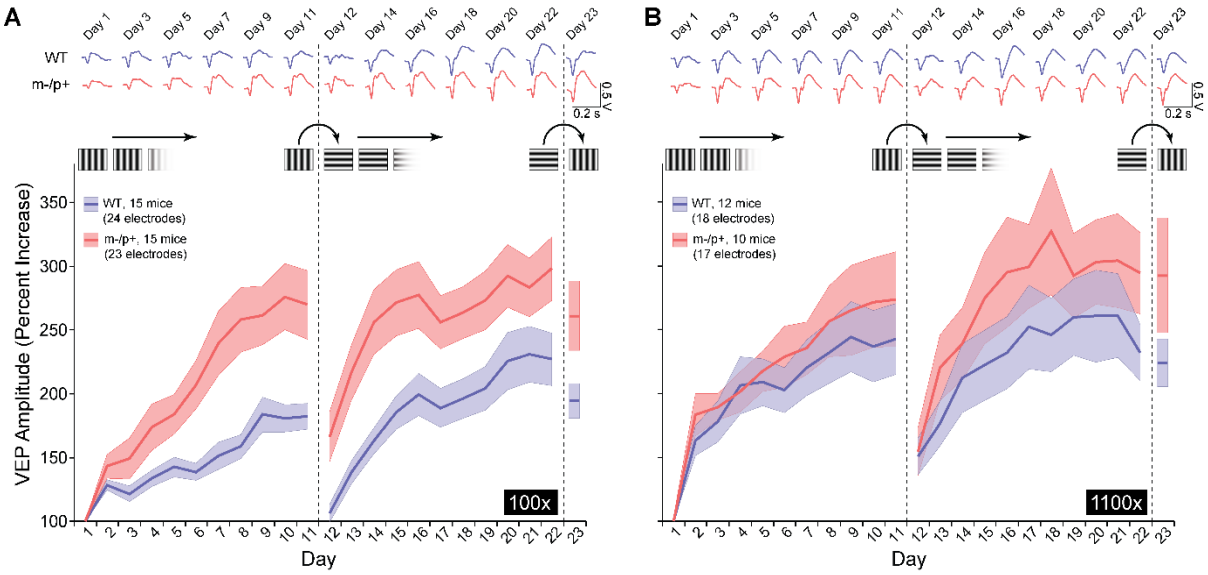

Supplemental Figure 3-3: Lower threshold for potentiation in adult Angelman syndrome mice. Adult (P100) mice were either stimulated with **(A)** 100 or **(B)** 1100 phase reversals of 0.05 cpd daily. (**A**) The representative VEP waveforms are from an individual WT (blue) and *Ube3a*$^{m-/p+}$ (red) mouse, and line graphs signify the average of both genotypes. Ube3a-deficient mice exhibited greater potentiation (days 1-11, 12-22) that was also less stimulus-specific (day 12), relative to WTs, when daily stimulation was brief (100 phase reversals). **(B)** However, both the magnitude and specificity of the VEP response were comparable between *genotypes* when the duration of stimulation was increased (1100 phase reversals).

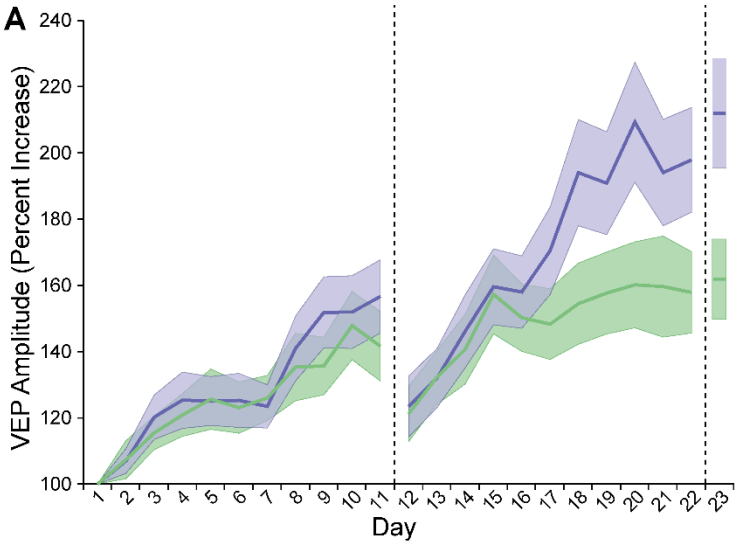

Supplemental Figure 3-4: *Ube3a* expression in inhibitory neurons attenuates sensory potentiation. (A) WT and GAD2-CRE:*Ube3a*$^{stop/+}$ mice displayed comparable degrees of VEP potentiation to stimulus Xº (day 1-11). Presentation of the novel stimulus Xº + 90º (day 12-22) to GAD2-CRE:*Ube3a*$^{stop/+}$ mice, failed to raise VEP responses to the same extent as WT mice. Blue (WT) and green (GAD2-CRE:*Ube3a*$^{stop/+}$) line graphs represent the average VEP responses for each group. Shaded regions denote S.E.M.

CHAPTER 4

4. Pathway-specific dopaminergic deficits in a mouse model of Angelman syndrome[2]

4.1. Overview

Angelman syndrome (AS) is a neurodevelopmental disorder caused by maternal deletions or mutations of the ubiquitin ligase E3A (*UBE3A*) allele and characterized by minimal verbal communication, seizures, and disorders of voluntary movement. Previous studies have suggested that abnormal dopamine neurotransmission may underlie some of these deficits, but no effective treatment currently exists for the core features of AS. A clinical trial of levodopa (L-DOPA) in AS is ongoing, although the underlying rationale for this treatment strategy has not yet been thoroughly examined in preclinical models. We found that AS model mice lacking maternal *Ube3a* (*Ube3a*$^{m-/p+}$ mice) exhibit behavioral deficits that correlated with abnormal dopamine signaling. These deficits were not due to loss of dopaminergic neurons or impaired dopamine synthesis. Unexpectedly, *Ube3a*$^{m-/p+}$ mice exhibited increased dopamine release in the mesolimbic pathway while also exhibiting a decrease in dopamine release in the nigrostriatal pathway, as measured with fast-scan cyclic voltammetry. These findings demonstrate the complex effects of UBE3A loss on dopamine

[2] Riday, T.T., Dankoski, E.C., Krouse, M.C., Fish, E.W., Walsh, P.L., Han, J.E., Hodge, C.W., Wightman, R.M., Philpot, B.D., and Malanga, C.J. (2012). Pathway-specific dopaminergic deficits in a mouse model of Angelman syndrome. The Journal of clinical investigation 122, 4544-4554.

signaling in subcortical motor pathways that may inform ongoing clinical trials of L-DOPA therapy in patients with AS.

4.2. Introduction

Angelman syndrome (AS) is a neurodevelopmental disorder characterized by intellectual disability, profound language impairment, seizures, and a propensity for a happy disposition (Steffenburg et al., 1996; Peters et al., 2004; Williams et al., 2006). AS results from loss of function of the maternally inherited *UBE3A* allele at the 15q11-q13 locus (Knoll et al., 1989; Williams et al., 1990; Kishino et al., 1997a; Rougeulle et al., 1997; Vu and Hoffman, 1997; Mabb et al., 2011). The *UBE3A* gene encodes a HECT domain E3 ubiquitin ligase (UBE3A, also known as E6AP) involved in protein degradation through the ubiquitin-proteasome pathway (Kishino et al., 1997a; Sutcliffe et al., 1997a). Clinical treatment of AS commonly includes pharmacotherapy for seizures, problem behaviors, and motor dysfunction (Pelc et al., 2008). Although treatments for AS are limited, a case study of 2 adults with AS found that levodopa (L-DOPA) administration dramatically improved resting tremor and rigidity (Harbord, 2001), leading to a clinical trial of L-DOPA in individuals with AS (Tan, 2012).

There are few published studies validating the rationale for using L-DOPA to treat parkinsonian features in AS. AS model mice lacking maternal *Ube3a* (*Ube3a*$^{m-/p+}$ mice) were reported to have reduced dopamine cell number in the substantia nigra pars compacta (SNc) by 7 to 8 months of age (Mulherkar and Jana, 2010). In *Drosophila*, UBE3A has been shown to regulate GTP cyclohydrolase I, an essential enzyme in dopamine biosynthesis (Ferdousy et al., 2011). However, little is known about the function of mesolimbic or nigrostriatal dopamine pathways in AS, which have vital roles in several of the behaviors or motor

symptoms commonly managed with pharmacotherapy, including hyperactivity, impulsivity, tremor, and rigidity. A survey of psychoactive drugs used in patients with AS reported that the majority responded poorly to stimulant medications (Philpot et al., 2011), most of which act by increasing available extracellular dopamine levels.

We examined dopamine-dependent behaviors as well as dopamine synthesis, content, and release in the mesolimbic and nigrostriatal pathways of AS model mice. *Ube3a*$^{m-/p+}$ mice were more sensitive to brain stimulation reward (BSR) but less sensitive to the effects of drugs that increase extracellular dopamine in behavioral measures of both reward and locomotion. Surprisingly, we found increased dopamine release in the mesolimbic system but decreased release in the nigrostriatal system. These changes in dopaminergic function were not accounted for by differences in dopaminergic cell number or differences in tyrosine hydroxylase levels or dopamine content in the terminal fields of the nucleus accumbens (NAc) or dorsal striatum. Our findings raise the possibility that similar effects on dopaminergic systems may occur in humans and may inform ongoing and future clinical trials of L-DOPA in individuals with AS.

4.3. Results

Ube3a*$^{m-/p+}$ *mice are more sensitive to rewarding electrical brain stimulation.

Activity of mesolimbic dopaminergic neurons in the midbrain ventral tegmental area (VTA) is critical for the perception of reward (Cooper and Breese, 1975; Wise, 2002). To determine whether loss of UBE3A alters mesolimbic dopamine function, *Ube3a*$^{m-/p+}$ and WT mice were implanted with stimulating electrodes in the medial forebrain bundle (MFB) and trained to perform operant intracranial self-stimulation (ICSS) by turning a wheel (Supplemental Figure 1A). Thresholds for perception of BSR were determined before and after

administration of drugs that increase extracellular dopamine levels (Figure 4-1A). *Ube3a*$^{m-/p+}$ mice showed a leftward shift of the baseline charge-response curve (Figure 4-1B), indicating that these mice required less charge than WT littermates to sustain the same degree of wheel turning (Figure 4-1C; $U = 59.0$, $P < 0.001$). There was no difference in the maximum rate of operant responding between genotypes (Figure 4-1D), demonstrating that voluntary motor function required for ICSS was unimpaired in *Ube3a*$^{m-/p+}$ mice. *Ube3a*$^{m-/p+}$ mice also sustained a lower reward threshold for longer than WT littermates (16–30 minutes, $P < 0.001$; 31–45 minutes, $P < 0.001$; 46–60 minutes, $P = 0.026$; Figure 4-1E).

Ube3a*$^{m-/p+}$ *mice are less sensitive to dopaminergic manipulation of BSR. Drugs that enhance extracellular dopamine availability increase the potency of BSR, measured as a lowered BSR threshold (Supplemental Figure 4-1, B and C). To determine whether the increase in reward sensitivity in *Ube3a*$^{m-/p+}$ mice was due to changes in dopamine neurotransmission, we investigated the effects of pharmacological manipulation on BSR threshold. The nonselective monoamine reuptake blocker, cocaine, similarly lowered BSR thresholds in both genotypes at the peak of its effect from 0 to 15 minutes after i.p. administration (Figure 4-2, A and B, and Supplemental Figure 4-2A), but the reward-potentiating effects of cocaine decayed more slowly in *Ube3a*$^{m-/p+}$ mice (Figure 4-2C). Maximum operant response rates showed a greater increase following cocaine administration in WT mice at 10.0 mg/kg cocaine (31–45 minutes, $P = 0.028$) and 17.0 mg/kg cocaine (31–45 minutes, $P = 0.001$; Supplemental Figure 4-3A), indicating that cocaine effects on operant motor behavior are reduced in *Ube3a*$^{m-/p+}$ mice. The highly selective dopamine transporter (DAT) blocker GBR 12909 reduced reward threshold similarly to cocaine but remained active for over 2 hours following administration. GBR 12909 lowered reward threshold

significantly less in *Ube3a*$^{m-/p+}$ mice, revealing a more pronounced difference in potentiation of BSR than that seen with cocaine (10.0 mg/kg, $P = 0.002$; 17.0 mg/kg, $P < 0.001$; Figure 4-1F and Supplemental Figure 2B). The ability of GBR 12909 to increase the maximum operant response rate was also reduced in *Ube3a*$^{m-/p+}$ mice at 10.0 mg/kg (76–90 minutes, $P = 0.032$; 91–105 minutes, $P = 0.018$) and 17.0 mg/kg (76–90 minutes, $P = 0.015$; 91–105 minutes, $P = 0.004$; Supplemental Figure 4-3B).

To assess possible differences in dopamine receptor sensitivity in the NAc and other forebrain targets, we measured the potency of selective dopamine receptor antagonists in reducing BSR. We found that the D1 receptor antagonist SCH 23390 elevated BSR thresholds similarly in both genotypes (Figure 4-2D and Supplemental Figure 4-2C). The motor depressant effect of SCH 23390 on maximum operant response rate was also similar between WT and *Ube3a*$^{m-/p+}$ mice (Figure 4-2G and Supplemental Figure 4-3C), suggesting that dopamine acting through D1 receptors was unaffected by loss of UBE3A. The reward threshold-elevating effects of the D2/3 receptor antagonist raclopride (Figure 4-2E) and D2-selective receptor antagonist L741,626 (Figure 4-2F) were also similar between genotypes (see also Supplemental Figure 4-2, D and E). However, the depressant effect of both raclopride (16–30 minutes, 0.178 mg/kg, $P = 0.005$; 0.3 mg/kg, $P < 0.001$; Figure 4-2H and Supplemental Figure 4-3D) and L741,626 (46–60 minutes, 5.6 mg/kg, $P < 0.001$; Figure 4-2I and Supplemental Figure 4-3E) on maximum operant response rate was blunted in *Ube3a*$^{m-/p+}$ mice.

Ube3a*$^{m-/p+}$ *mice are less sensitive to cocaine-stimulated locomotor activity. To further assess dopamine-related behavior in *Ube3a*$^{m-/p+}$ mice, we performed locomotor sensitization experiments using cocaine (5.6, 10.0, or 17.0 mg/kg i.p.) as a tool to evaluate

both acute locomotor stimulation and adaptation to repeated drug exposure (Figure 4-3). Cocaine has a rapid onset of action, with brain concentrations peaking approximately 5 minutes after injection, and a half-life of approximately 15 minutes (Benuck et al., 1987). Therefore, we used the total activity in the first 15 minutes following injection to compare cocaine-stimulated locomotor activity between genotypes. Total locomotion over the 15 minutes following saline injection was lower in *Ube3a*$^{m-/p+}$ mice (531 ± 51 cm) than in WT mice (916 ± 79 cm; $U = 266$, $P < 0.001$), consistent with decreased motor activity previously described in *Ube3a*$^{m-/p+}$ mice (Allensworth et al., 2011). Although a low cocaine dose (5.6 mg/kg; Figure 4-3A) was sufficient in both genotypes to induce locomotor sensitization, defined as greater distance traveled on the challenge/last day compared with that on the first day of administration ($P < 0.001$), we found *Ube3a*$^{m-/p+}$ mice to be less sensitized than WT mice (day 4, $P = 0.02$; day 5, $P = 0.031$; challenge, $P = 0.031$; Figure 4-3D). An intermediate cocaine dose (10.0 mg/kg; Figure 4-3B) increased locomotion more in WT mice than in *Ube3a*$^{m-/p+}$ mice for 5 consecutive days after the first day of exposure (day 2, $P = 0.009$; day 3, $P = 0.012$; days 4–6, $P < 0.001$), although this difference was no longer significant on cocaine challenge after 7 days (Figure 4-3E). The largest cocaine dose tested (17.0 mg/kg; Figure 4-3, C and F) stimulated comparable locomotion on the second day of exposure in both genotypes, suggesting that the reduced cocaine effect in *Ube3a*$^{m-/p+}$ mice was not due to a reduction in maximum cocaine potency or a ceiling effect.

Neuroanatomical and biochemical markers of dopamine are unaltered in Ube3a$^{m-/p+}$ mice. Projection neurons within the VTA and SNc express both UBE3A and tyrosine hydroxylase (TH), the rate-limiting enzyme in dopamine biosynthesis. We performed immunohistochemistry to confirm maternal imprinting of *Ube3a* in the VTA and SNc

(Figure 4-4A) and then quantified TH-positive neurons with design-based stereology in the VTA and SNc. We found no differences in the estimated dopamine cell number in either region at P100 (Table 4-1 and Figure 4-4B). We performed Western blots for TH in the NAc and dorsal striatum as a measure of biosynthetic capacity in dopaminergic terminal fields originating from neurons in the VTA or SNc, respectively. TH protein levels were similar between *Ube3a*$^{m-/p+}$ and WT mice in the NAc and striatum (Table 4-2 and Figure 4-4C). HPLC on tissue homogenates showed no difference in total dopamine content in *Ube3a*$^{m-/p+}$ mice in the NAc or dorsal striatum (Table 4-2 and Figure 4-4D). Furthermore, tissue concentrations of DOPAC, the primary acid metabolite of dopamine (Figure 4-4E), and dopamine/DOPAC concentration ratios (Figure 4-4F) were comparable between genotypes.

Dopamine transmission is enhanced in the NAc and reduced in the dorsal striatum of Ube3a$^{m-/p+}$ mice. We performed fast-scan cyclic voltammetry (FSCV) in the NAc and dorsal striatum to determine whether the loss of UBE3A affected phasic dopamine transmission in these limbic and motor terminal regions, respectively (Figure 4-5). Stimulation of the MFB resulted in greater dopamine release in the NAc of *Ube3a*$^{m-/p+}$ mice across all stimulus frequencies (Figure 4-5A and Supplemental Figure 4-4A), with higher maximum extracellular dopamine concentrations obtained at 30 to 60 Hz (30 Hz, $P = 0.05$; 40 Hz, $P = 0.008$; 50 Hz, $P = 0.045$; 60 Hz, $P = 0.004$; Figure 4-5, C, E, and G). In contrast to that in the NAc, we found reduced dopamine release across all stimulus frequencies (Figure 4-5B and Supplemental Figure 4-4B), with lower maximum extracellular dopamine concentration in the dorsal striatum of *Ube3a*$^{m-/p+}$ mice at 30 to 50 Hz (30 Hz, $P = 0.006$; 40 Hz, $P = 0.002$; 50 Hz, $P = 0.015$; Figure 4-5, D, F, and H). Modeling of the FSCV data did not reveal any differences in dopamine uptake following stimulation in either the NAc or

dorsal striatum (data not shown). Administration of the DAT blocker GBR 12909 prior to stimulation caused similar changes to the time course of extracellular dopamine concentrations in the NAc and dorsal striatum (Figure 4-5, I and J), suggesting no differences in dopamine reuptake between genotypes.

4.4. Discussion

The principal findings of this study are that *Ube3a*$^{m-/p+}$ mice, a model of AS, exhibit increased mesolimbic dopamine release but decreased nigrostriatal dopamine release and decreased behavioral sensitivity to drugs that enhance extracellular dopamine availability. Release of accumbal dopamine is critical to the rewarding effects associated with both BSR and drugs of abuse as well as natural incentives such as food and sex (Wise and Rompre, 1989). We used ICSS as an experimental model to directly assess motivation and reward and to minimize effects from potential sensory processing abnormalities (Wise, 2002; Walz and Baranek, 2006). We found that *Ube3a*$^{m-/p+}$ mice required significantly less electrical stimulation to attain the same level of responding for BSR as in controls and were able to maintain a higher degree of responding for BSR over time, consistent with the increased dopamine release in the NAc following MFB stimulation that we observed with FSCV. Increased extracellular dopamine could result from slower dopamine uptake, but no differences in accumbal dopamine clearance were observed with FSCV by either modeling of uptake kinetics or by administration of GBR 12909, a selective DAT blocker. This suggests that the increase in extracellular dopamine in the NAc is the result of increased release. However, *Ube3a*$^{m-/p+}$ mice were also less sensitive to the reward-potentiating effects of the DAT-selective reuptake blocker GBR 12909 on BSR. While this suggests that loss of UBE3A may affect dopamine receptor signaling in the NAc, the attenuated response could

not be accounted for by differences in D1 or D2 receptor activity, since antagonism of both receptors elevated reward thresholds equally in both genotypes.

In contrast to that in the NAc, electrically stimulated extracellular dopamine was significantly reduced in the dorsal striatum of *Ube3a*$^{m-/p+}$ mice. As in that in the NAc, we observed no differences in striatal dopamine clearance with FSCV by either modeling of uptake kinetics or by administration of GBR 12909, indicating normal DAT function. This suggests that extracellular levels of dopamine are lower in dorsal striatum as a result of reduced release. One of the primary local regulators of dopamine release is negative feedback through D2 autoreceptors on dopaminergic terminals. Although D2 antagonism did not differentially affect BSR threshold in *Ube3a*$^{m-/p+}$ mice, the inhibitory potencies of both the D2/D3 antagonist raclopride and the D2-selective antagonist L741,626 in reducing maximum operant response rate were significantly lower, suggesting decreased D2 receptor function. Mice lacking D2 receptors exhibit some similarities to *Ube3a*$^{m-/p+}$ mice, including decreased cocaine-stimulated locomotion (Chausmer et al., 2002; Welter et al., 2007) and increased extracellular dopamine in the NAc following MFB stimulation (Rouge-Pont et al., 2002), the latter effect due to decreased D2 autoreceptor function (Bello et al., 2011). However, in contrast to *Ube3a*$^{m-/p+}$ mice, D2-deficient mice are also less sensitive to BSR alone (Elmer et al., 2005), suggesting that the increased sensitivity to BSR and the changes in dopamine release in the NAc and dorsal striatum that we observed in *Ube3a*$^{m-/p+}$ mice may be due to alterations in other signaling pathways not yet investigated.

Interestingly, some of the changes that we observed in *Ube3a*$^{m-/p+}$ mice resemble those found in mouse models of human mutations in patients with autosomal recessive familial Parkinson's disease. Mice lacking either PTEN-induced kinase 1 (*Pink1*, also known

as *Park6*; ref. (Kitada et al., 2007)) or the novel glyoxylase DJ-1 (*Park7*; refs. (Goldberg et al., 2005; Lee et al., 2012)) exhibit decreased electrically evoked striatal dopamine release in the absence of changes in dopaminergic cell number or dopamine synthesis and metabolism. Decreased spontaneous locomotion is observed with both mutations but is not evident in PINK1-deficient mice until late adulthood (Gispert et al., 2009). Conversely, mice deficient in the E3 ubiquitin ligase parkin (*Park2*) exhibit increased striatal dopamine release while also showing decreases in both spontaneous and drug-stimulated locomotion without changes in dopaminergic cell number, striatal TH, or striatal dopamine content (Goldberg et al., 2003; Itier et al., 2003). In contrast to loss of UBE3A, in which dopamine reuptake appears to be functionally normal, loss of either PINK1 or parkin is associated with decreased striatal DAT levels and function, while mice deficient in DJ-1 have normal DAT levels but increased dopamine reuptake and decreased behavioral and physiological sensitivity to D2 receptor agonists (Goldberg et al., 2005). Of note, while radionuclide imaging has confirmed loss of presynaptic dopamine in the striatum of patients with PINK1- (Khan et al., 2002), DJ-1– (Dekker et al., 2003), and parkin-associated early-onset Parkinson's disease (Scherfler et al., 2004), no similar imaging findings or clinical measures of monoamines and their metabolites in cerebrospinal fluid have been published in studies of patients with AS.

Converging lines of evidence suggest that defects of the ubiquitin-proteasome pathway may underlie some forms of human movement disorders, particularly those involving neurodegenerative processes (Ross and Pickart, 2004). For example, some early-onset forms of Parkinson's disease are caused by loss-of-function mutations in genes encoding parkin, PINK1, and DJ-1, while mutations in the gene encoding α-synuclein (*SNCA*) have been found in both autosomal dominant and sporadic forms of the disease. As

mentioned, parkin itself is an E3 ubiquitin ligase, which together with PINK1 and DJ-1 forms a complex to promote ubiquitination and degradation of parkin substrates (Xiong et al., 2009). Parkin has been shown to specifically ubiquitinate and increase proteasomal turnover of a number of proteins, including O-glycosylated α-synuclein (αSp22; ref. (Shimura et al., 2001)), which when overexpressed are toxic to monoaminergic neurons (Zhang et al., 2000; Imai et al., 2001; Choi et al., 2003; Ko et al., 2005; Wang et al., 2008). Misfolded α-synuclein or excessive levels of α-synuclein are associated with dopaminergic cell death in Parkinson's disease and can inhibit ubiquitin-proteasomal activity (Tanaka et al., 2001; Snyder et al., 2003). Data from cell culture suggest that α-synuclein may be a substrate for UBE3A, but there is no evidence for elevated α-synuclein levels in the absence of UBE3A in vivo (Mulherkar et al., 2009), consistent with normal numbers of midbrain dopaminergic neurons in *Ube3a*$^{m-/p+}$ mice. Increasing α-synuclein expression reduces dopamine release by interfering with vesicle recycling before neurodegeneration occurs, consistent with the reduced dorsal striatal dopamine release we observed in *Ube3a*$^{m-/p+}$ mice (Nemani et al., 2010). It has been shown that dopaminergic VTA neurons are resistant to the toxic effects of α-synuclein overexpression (Maingay et al., 2006), but it is unknown whether or how α-synuclein affects dopamine release in the NAc. In light of these observations, our data further support the possibility that disorders of ubiquitination can lead to functional changes in neural circuits in the absence of neurodegeneration (Shenoy and Lefkowitz, 2003; Hislop and von Zastrow, 2011).

L-DOPA is a mainstay of therapy for Parkinson's disease but can be accompanied by significant adverse effects. For example, patients with early-onset Parkinson's disease with parkin mutations are exquisitely sensitive to L-DOPA but are also significantly more likely to

develop limiting dyskinesias and psychiatric complications while on L-DOPA therapy (Khan et al., 2003). In patients with Parkinsonism, replacement therapy with L-DOPA or directly acting dopaminergic agonists is aimed at ameliorating motor symptoms mediated by the dorsal striatum. However, such therapy consistently leads to adverse effects on reward-mediated behaviors involving the NAc (Macdonald and Monchi, 2011). These observations, together with our findings that dopaminergic dysfunction in AS may be pathway specific, raise a cautionary note for ongoing clinical trials of L-DOPA in individuals with AS. Such studies may benefit from additional outcome measures, particularly neuropsychiatric indices, to ensure that L-DOPA treatment does not lead to unanticipated outcomes in patients with AS.

4.5. Methods

Animals. Male C57BL6/J WT and maternally deficient *Ube3a*$^{m-/p+}$ mice were used in all instances. These mice were generated from pairings of paternally deficient females with WT males. Age of mice ranged from P90 to P120. Mice used for ICSS were implanted at P65.7 ± 7.8 days and fully trained for the start of behavioral assessment with cocaine at P105.5 ± 18.1 days; raclopride at P131.3 ± 17.9 days; L741,626 at P155.3 ± 16.7 days; SCH 23390 at P164.5 ± 16.2 days; or GBR 12909 at P197.3 ± 12.7 days. Animals were kept on a 12-hour-dark/light cycle and given ad libitum access to food and water. All experiments (with the exception of Western blots) were performed blinded to genotype.

ICSS. ICSS was performed as detailed previously (Fish et al., 2010). Briefly, mice (26 WT and 27 *Ube3a*$^{m-/p+}$ mice) were anesthetized (120 mg/kg ketamine, 9 mg/kg xylazine; Hospira), and 0.25% bupivacaine (Hospira) was applied to the scalp incision site. A stainless steel monopolar stimulating electrode (0.28-mm diameter; Plastics One) was stereotaxically

implanted into the MFB at the following coordinates relative to bregma: anterior/posterior (A/P) –1.3 mm; medial/lateral (M/L) +1.1 mm; dorsal/ventral (D/V) from skull surface –5.0 mm (Paxinos G, 2001). Stimulating electrodes were insulated with polyamide, leaving approximately 0.25 mm of the tip exposed. The electrical ground was an uninsulated stainless steel wire (0.125-mm diameter) wrapped around a stainless steel screw threaded into the skull. Electrode assemblies were secured to the skull with dental cement.

Following 1 week of recovery, mice were trained on a continuous (FR-1) schedule of reinforcement by the delivery of rewarding electrical stimulation (BSR) in a sound-attenuated operant chamber (Med Associates) equipped with a wheel manipulandum. Each quarter turn of the wheel was reinforced by 500 ms of unipolar cathodal square-wave current paired with illumination of the house light as a secondary reinforcer. Mice were presented 15 descending stimulation frequencies in discrete 0.05 inverse log steps, ranging from 126 to 25 Hz (100-μs pulse width). Each frequency trial lasted 1 minute and consisted of a 5-second priming phase of noncontingent stimulation; 50-second active phase, during which BSR was available; and ended with a 5-second time out, during which further responses received no additional stimulation. The minimum current intensity required to maintain responding (minimum of 40 responses per minute) for the highest 3 to 5 frequencies was determined for each individual mouse and kept constant for the duration of the experiment. For SCH 23390, raclopride, and L741,626 experiments, the current was adjusted to maintain responding for the top 8–12 frequencies. Each test session consisted of 45 minutes (15 frequencies for 3 repetitions) before injection and 60 minutes after injection. For GBR 12909 and L741,626, mice were placed into their home cage for 30 minutes following injection, followed by either 90 minutes (6 series repetitions for GBR 12909) or 75 minutes (5 series repetitions for

L741,626) of access to BSR. BSR thresholds before injection (50% of maximum asymptotic response rate [EF50]) were calculated from the average of the second and third series (the first series was considered a "warm-up" and was discarded) and used as daily baselines for comparison to BSR thresholds after injection.

Changes in BSR threshold were evaluated following i.p. injection of cocaine (1.0, 3.0, 5.6, 10.0, 17.0 mg/kg, calculated as the free base; 26 WT and 27 *Ube3a*$^{m-/p+}$ mice; Sigma-Aldrich), raclopride (0.03, 0.1, 0.178, 0.3 mg/kg; 9 WT and 12 *Ube3a*$^{m-/p+}$ mice; Sigma-Aldrich), L741,626 (1.0, 1.78, 3.0, 5.6 mg/kg; 6 WT and 9 *Ube3a*$^{m-/p+}$ mice; Sigma-Aldrich); SCH 23390 (0.003, 0.01, 0.03, 0.1 mg/kg; 8 WT and 12 *Ube3a*$^{m-/p+}$ mice; Sigma-Aldrich); GBR 12909 (1.0, 3.0, 10.0, 17.0 mg/kg; 7 WT and 9 *Ube3a*$^{m-/p+}$ mice; Sigma-Aldrich); and normal saline or distilled water (vehicle for 741,626). All mice were assessed with cocaine and then divided into 2 groups, with one group of mice being tested with raclopride and L741,626 and the other group being tested with SCH 23390 and GBR 12900. Each dose was replicated 1–2 times and averaged for each mouse's behavioral response.

Locomotor behavior. Locomotion was measured in unlit sound-attenuated chambers (27.3 cm × 27.3 cm; Med Associates) and quantified by beam breaks of a 16 × 16 photobeam infrared array. Mice were placed in the chamber for 15 minutes of habituation, injected i.p. with normal saline or cocaine, and locomotion after injection was monitored for 45 minutes. Animals were habituated to the chamber and injection stress (saline) for 4 days, and the fourth day was used as baseline locomotor activity. Following baseline determination, mice were injected with cocaine daily, and cocaine-stimulated locomotor activity was assessed for 6 consecutive days. Following 6 days of cocaine abstinence, during which animals remained in their home cages, locomotion after cocaine challenge was evaluated on day 7. 36 WT and

36 *Ube3a*$^{m-/p+}$ mice were divided into 3 separate groups of 12, receiving either sensitizing doses of 5.6, 10.0, or 17.0 mg/kg cocaine for the entirety of the experiment.

TH immunohistochemistry. Mice (6 WT and 5 *Ube3a*$^{m-/p+}$ mice) were deeply anesthetized (120 mg/kg pentobarbital, i.p.) and perfused transcardially with 0.1 M PBS (pH 7.4), followed by 4% paraformaldehyde in 0.1 M PBS. All brains were post-fixed by submersion in the same fixative for 24 hours and then cryoprotected in 10% sucrose for 24 hours followed by 30% sucrose for 24 hours. Brains were sectioned (40 μm, coronal) on a sliding microtome and stored in cryoprotectant (1.0% polyvinylpyrrolidone [w/v], 30% sucrose [w/v], and 30% ethylene glycol [v/v] in 0.1 M PBS). Endogenous peroxidase activity was quenched with 1% hydrogen peroxide in 0.1 M PBS for 30 minutes at room temperature. Sections were blocked in 5% normal goat serum (NGS) and 2% Triton X-100 in 0.1 M PBS for 24 hours at room temperature and then incubated in rabbit α-rat TH primary antibody (1:2,000; AB152, Millipore) in 2% NGS and 2% Triton for 4 days at 4°C. Sections were washed (3 times) in 0.1 M PBS and incubated with HRP-conjugated goat α-rabbit secondary antibody (1:250; 31460, Thermo Scientific) in 2% NGS and 2% Triton at room temperature for 3 hours. Reaction product was visualized with a DAB Peroxidase Substrate Kit (SK-4100; Vector Laboratories). Sections were mounted on potassium dichromate/gelatin-subbed slides and counterstained with cresyl violet for Nissl.

Stereological quantification of cell numbers. The total number of TH-positive cells in the SNc and VTA was estimated with design-based stereology using StereoInvestigator v9.14 (MBF Bioscience) on a Microphot FXA microscope (Nikon). Every other section (section interval = 2) was immunostained and counted, yielding on average 12 midbrain sections per animal. The borders of the SNc and the VTA at all rostrocaudal levels in the

midbrain were delineated at low (×4) magnification based on the standard mouse atlas (Paxinos G, 2001). For purposes of this study, the VTA and SNc were divided by a line connecting the medial border of the medial lemniscus, dorsally, to the medial edge of the corticospinal tract, ventrally, in all sections. Counting frames (50 μm × 50 μm) were randomly placed and systematically moved through a sampling grid (120 μm × 120 μm) by the software via a motorized stage (Ludl Electronic Products). An optical disector height of 12.0 μm, flanked by 2.0-μm guard zones on top and bottom, was applied to all counting frames based on average section shrinkage estimates. Bright-field counting under direct visualization was performed at ×100 oil magnification (NA = 1.4). Estimates of the total numbers of TH-immunostained neurons were calculated using the optical fractionator method (West, 1999). For all estimates, coefficients of error ≤ 0.10 were accepted (Gundersen and Jensen, 1987). Using this protocol, results were obtained that are in agreement with estimates of numbers of dopaminergic SNc neurons in C57BL6/J mice using other methods (Baquet et al., 2009).

TH and Ube3a immunofluorescence colocalization. 2 WT and 2 *Ube3a*$^{m-/p+}$ mice were transcardially perfused with 4% paraformaldehyde, and their brains were post-fixed, cryoprotected, and sectioned on a sliding microtome as described above. Tissue sections were rinsed thoroughly in Tris-buffered saline plus 0.3% Triton X-100 (TBST, pH 7.5) prior to being incubated at 80°C for 20 minutes in 10 mM sodium citrate buffer (pH 6.0) for antigen retrieval. Subsequently, sections were rinsed in TBST and blocked for 25 minutes in TBST containing 4% nonfat dry milk. Blocked sections were then incubated for 2 days at 4°C in the same blocking solution containing sheep anti-TH (1:1,000; Pel-Freez) and mouse anti-Ube3a (1:200; clone 330, Sigma-Aldrich) primary antibodies. Sections were then rinsed

with fresh blocking solution prior to incubation for 1 hour at room temperature in biotinylated donkey anti-mouse IgG (1:250; Jackson ImmunoResearch Laboratories Inc.) and Alexa Fluor 488 donkey anti-sheep secondary antibodies (Invitrogen). Following several rinses in TBST, sections were incubated for 1 hour at room temperature in Alexa Fluor 568–streptavidin (2 μg/ml in TBST). Tissue was mounted on subbed slides and coverslipped with DPX. Images were taken using confocal microscopy (LSM710, Zeiss).

Tissue punches. Mice were deeply anesthetized with sodium pentobarbital, and brains were snap frozen in methylbutane on dry ice. Brains were serially sectioned on a cryostat, until reaching the rostral pole of the NAc. Tissue punches (pooled from both hemispheres) were taken from the NAc and dorsolateral striatum (17 and 15 gauge, respectively). Punches were stored at –80°C until use.

Western blotting. Tissue punches from the NAc and striatum (8 WT and 8 *Ube3a*$^{m-/p+}$ mice) were treated with 100 μl lysis buffer (50 mM Tris-HCl, 8.0 pH, 150 mM NaCl, 1% Triton X-100, 0.1% SDS, 0.5% sodium deoxycholate). To assess TH protein levels, 20 μg of total protein lysates from WT and *Ube3a*$^{m-/p+}$ tissue homogenate were separated by 4%–12% SDS-polyacrylamide gel electrophoresis. Proteins were then transferred to nitrocellulose membranes, and immunoblotting was performed using a sheep anti-TH antibody (1:1,000; Pel-Freez), followed by IRDye800CW-conjugated donkey anti-sheep IgG (1:1,000; Rockland) and mouse anti–β-actin antibody (1:1,000; Sigma-Aldrich), followed by Alexa Fluor 680–conjugated goat anti-mouse IgG (1:5,000; Invitrogen). Protein bands were visualized by an Odyssey system (LI-COR Biosciences). To control for protein loading, TH protein levels were normalized to β-actin levels detected in each sample.

HPLC. Tissue punches from the NAc and dorsal striatum (5 WT and 6 *Ube3a*$^{m-/p+}$ mice) were weighed and mixed with 200 µl 0.1 N $HClO_4$ containing 1 µM hydroquinone, the internal standard. Tissue was homogenized using a sonic dismembrator (model 60; Fisher Scientific). The homogenate was then centrifuged at 10,000 *g* for 10 minutes, and the supernatant was removed and filtered using a 0.2-µm syringe filter (Millex-LG; Millipore). HPLC was employed, using a modified method of Mefford (Mefford, 1981). Briefly, 20 µl injections were made onto a revered-phase column (5 µm, 4.6 mm × 5 mm; Waters Atlantis). The mobile phase contained 0.1 M citric acid, 1 mM sodium hexylsulfate, 0.1 mM EDTA (pH = 3), and 10% methanol as the organic modifier at a flow rate of 1.0 ml/min. Neurotransmitters were detected with a thin-layer radial electrochemical cell (BASi) at a potential of +800 mV vs. the Ag/AgCl reference electrode. Data were collected at 60 Hz using a LabVIEW strip chart recorder program (Jorgenson Lab; University of North Carolina at Chapel Hill) and homebuilt electronics. The peak area of the analyte was ratioed to the peak area of the internal standard, and the analyte concentration in the tissue was calculated. Stock solutions were made to be 10 mM in 0.1 N $HClO_4$, and response ratios were determined daily using 2 µM solution mixtures.

FSCV. Mice (NAc, 11 WT and 8 *Ube3a*$^{m-/p+}$ mice; dorsal striatum, 7 WT and 9 *Ube3a*$^{m-/p+}$ mice) were anesthetized with urethane (1.5 g/kg body) and affixed in a stereotaxic frame (David Kopf Instruments). Stereotaxic craniotomies were performed, and a carbon-fiber microelectrode was implanted in either the NAc (from bregma, A/P +1.1, M/L +1.2, D/V from skull surface –3.5 to –4.0) or dorsal striatum (from bregma, A/P +0.5, M/L +2.5, D/V from skull surface –2.5 to –3.0) (Paxinos G, 2001). A bipolar stainless steel stimulating electrode, insulated to the tip (0.2-mm diameter; Plastics One), was implanted

into the MFB (bregma, A/P –1.2, M/L +1.0, D/V from skull surface –5.0), and an Ag/AgCl reference electrode was implanted into the contralateral hemisphere. Computer-generated biphasic pulse trains, 2 ms in width and 325 μA each phase, were applied through constant current stimulators (NL 800A; Neurolog, Medical Systems Corp.), for 24 pulses at 20, 30, 40, 50, and 60 Hz to evoke dopamine release. Stimulation-evoked release was recorded during and after the stimulation. GBR 12909 (20 mg/mg, Sigma-Aldrich) was dissolved in saline and injected i.p. at a volume of 1 ml/kg.

Glass-encased, cylindrical carbon-fiber microelectrodes and Ag/AgCl reference electrodes were prepared as described previously (Cahill et al., 1996). Briefly, carbon-fiber microelectrodes were constructed by vacuum aspiration of a single T-650 carbon fiber (Thornel, Amoco Co.) into a glass capillary of 0.6-mm external diameter and 0.4-mm internal diameter (A-M Systems, Inc.). A micropipette puller (Narishige) was used to taper the glass and form a carbon-glass seal. The exposed carbon fiber was cut to approximately 100 μm in length and was soaked for 30 minutes in isopropyl alcohol to clean the surface. Application of the voltage waveform and data collection for FSCV were computer controlled and have been described in detail previously (Heien et al., 2003). Briefly, a triangular scan (–0.4 to +1.3 V, 400 V/s) was repeated every 100 ms. Data were digitized and stored on a computer using software written in LABVIEW (National Instruments). Background-subtracted cyclic voltammograms were obtained by digitally subtracting voltammograms collected during baseline recording from those collected during stimulation. A custom-built UEI potentiostat (Department of Chemistry Electronics Facility, University of North Carolina at Chapel Hill) was used. All potentials are reported compared with the Ag/AgCl reference electrode. Signal processing (background subtraction, signal averaging, and digital

filtering) (4-pole Bessel Filter, 2 kHz) was also performed by the software. All signals were verified as dopaminergic by the shape of their cyclic voltammogram as well as by their response to GBR 12909, a selective inhibitor of the DAT. Data were analyzed and plotted using TH-1 software.

ICSS and FSCV electrode placement verification. Mice used for ICSS were deeply anesthetized with sodium pentobarbital and intracardially perfused with 0.9% saline followed by 4% paraformaldehyde in 0.1 M PBS. Mice used for FSCV were anesthetized with sodium pentobarbital, and brains were removed and drop fixed in 4% paraformaldehyde in 0.1 M PBS. The brains were sectioned (50 μm) on a sliding microtome, stained with cresyl violet for Nissl, and viewed under low-powered (×4) light microscopy to determine the location of the most ventral electrode tip placements (Supplemental Figures 5 and 6).

Statistics. SigmaPlot (Systat Software) was used for statistical analysis. Mann-Whitney tests were run to compare baseline reward thresholds (EF50), baseline maximum response rates, or basal locomotor activity between genotypes. All other comparisons were based on a repeated-measures model that included a genotype-by-dose (ICSS), genotype-by-day (locomotor activity), genotype-by-second (FSCV), or genotype-by-stimulation frequency (FSCV) interaction. All genotype contrasts (Holm-Sidak) were performed based on these models and reported when significant. An additional comparison between day 1 and challenge was performed for locomotor activity experiments to determine whether sensitization occurred. Corrections for multiple comparisons were made for FSCV experiments based on the genotype-by-second model. Level of significance for all reported effects was placed at $P < 0.05$.

Study approval. All experimental animal procedures were carried out according to the NIH *Guide for the Care and Use of Laboratory Animals* and the Society for Neuroscience *Policy on the Use of Animals in Neuroscience Research* and were approved by the Institutional Animal Care and Use Committee at the University of North Carolina at Chapel Hill.

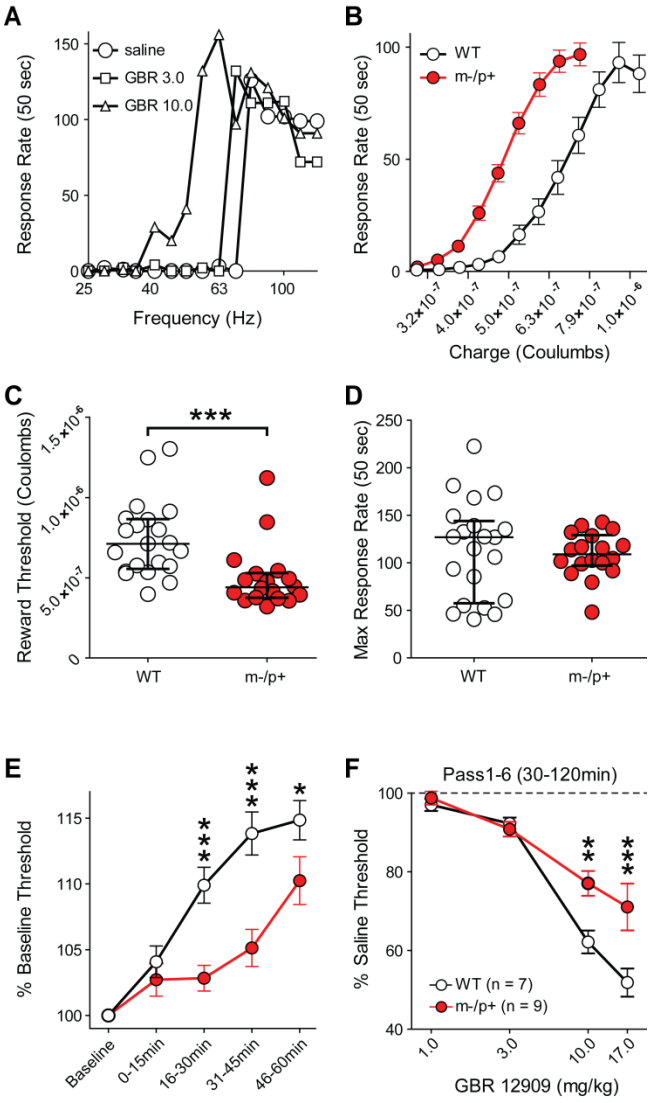

Figure 4-1: *Ube3a*$^{m-/p+}$ mice are more sensitive to BSR but less sensitive to dopaminergic potentiation of BSR. (**A**) Representative ICSS rate-frequency curves in a WT mouse. Injection (i.p.) of the DAT antagonist GBR 12909 dose-dependently increases responding for rewarding electrical current at lower stimulus frequencies. (**B**) Rate-frequency curves expressed as charge (Q) delivery at each frequency (Hz) from *Ube3a*$^{m-/p+}$ mice are shifted to the left compared with those of WT littermates. (**C**) *Ube3a*$^{m-/p+}$ mice require significantly less (***$P < 0.001$) charge to evoke the same degree of responding as WT mice at reward threshold frequencies (EF50). (**D**) The maximum rate of operant responding for rewarding brain stimulation is comparable between genotypes ($P > 0.05$). (**E**) *Ube3a*$^{m-/p+}$ mice maintain a lower reward threshold over time (16–30 minutes, ***$P < 0.001$; 31–45 minutes, ***$P < 0.001$; 46–60 minutes, *$P = 0.026$). (**F**) WT mice exhibit greater potentiation of rewarding brain stimulation expressed as lower reward thresholds than *Ube3a*$^{m-/p+}$ mice following 10.0 mg/kg (**$P = 0.002$) and 17.0 mg/kg (***$P < 0.001$) GBR 12909 (i.p.). Error bars indicate ± SEM in **B**, **E**, and **F** and the median and interquartile ranges in **C** and **D**.

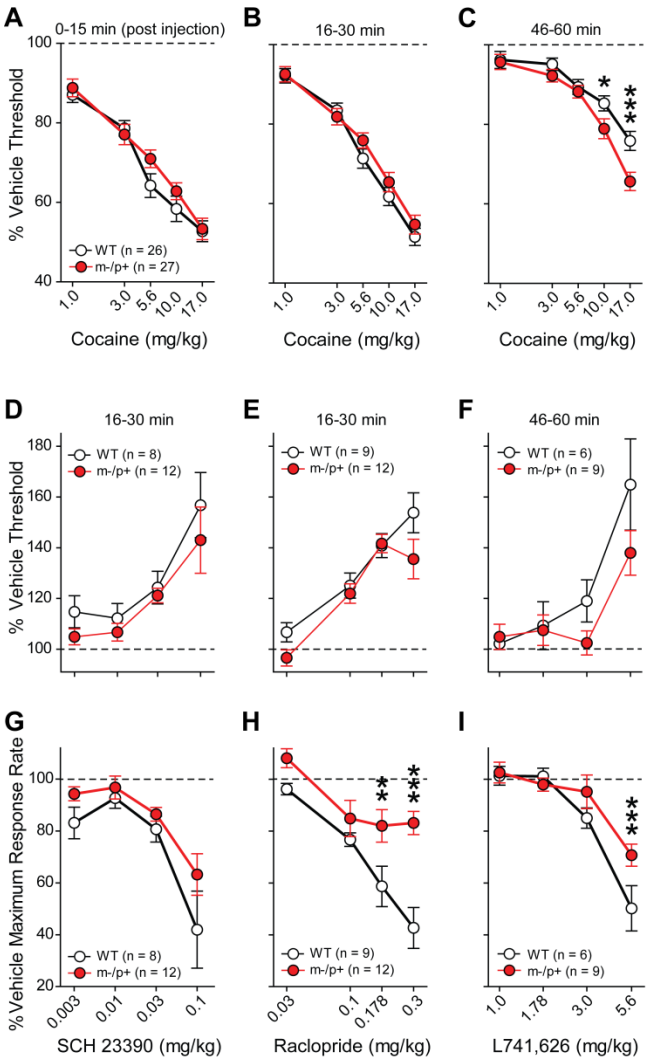

Figure 4-2: *Ube3a*$^{m-/p+}$ mice exhibit normal BSR threshold responses to cocaine and selective D1 and D2 dopamine receptor antagonists but decreased sensitivity to D2-dependent motor impairment. BSR threshold was determined following i.p. administration of (**A**–**C**) cocaine, (**D**) the D1 receptor antagonist SCH 23390, or the D2-selective antagonists (**E**) raclopride or (**F**) L741,626. (**A**–**C**) Cocaine had similar potency on BSR threshold in both genotypes at its peak effect (0–15 minutes), but its rewarding effects decayed more slowly in *Ube3a*$^{m-/p+}$ mice (46–60 minutes, 10.0 mg/kg, $*P = 0.025$; 17.0 mg/kg, $^{\#}P < 0.001$). (**D**) The D1 antagonist SCH 23390, (**E**) the D2-like antagonist raclopride, or (**F**) the highly D2-selective antagonist L741,626 equally elevated reward thresholds of WT and mutant mice. (**G**) However, while D1 receptor antagonism had similar depressant effects on maximum operant response rates of both genotypes, antagonism of D2 receptors with either (**H**) raclopride (0.178 mg/kg, $**P = 0.005$; 0.3 mg/kg, $^{\#}P < 0.001$) or (**I**) L741,626 (5.6 mg/kg, $^{\#}P < 0.001$) had greater depressant effects on maximum response rates of WT mice. Error bars indicate ± SEM.

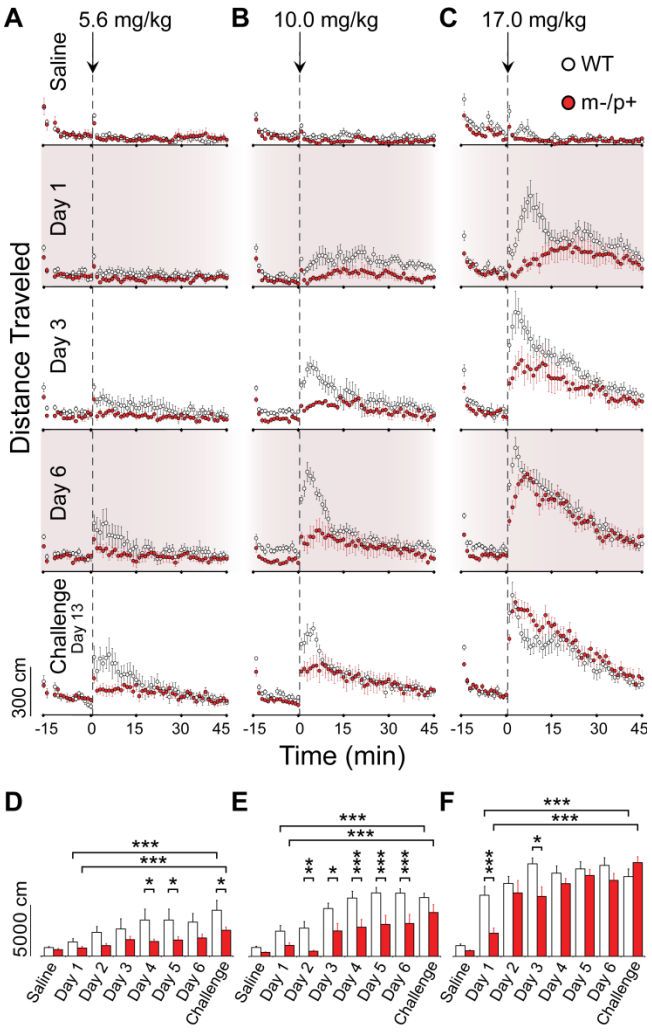

Figure 4-3: Cocaine-stimulated locomotion is lower in *Ube3a*$^{m-/p+}$ mice. Psychostimulant-induced locomotion in 3 separate groups of mice (12 WT and 12 *Ube3a*$^{m-/p+}$ mice per group) injected with 5.6, 10.0 or 17.0 mg/kg i.p. cocaine for 6 consecutive days and a final challenge dose 1 week later. (**A**–**C**) Distance traveled is binned in 1-minute increments. (**D**–**F**) The sum of the first 15 minutes following injection is plotted below each of their respective treatment groups. (**D**) A deficit in the locomotive response of *Ube3a*$^{m-/p+}$ mice emerges after 3 days of 5.6 mg/kg cocaine administration ($P = 0.02$; day 5, $P = 0.031$; challenge, $P = 0.031$) and (**E**) by the second day of 10.0 mg/kg cocaine ($P = 0.009$; day 3, $P = 0.012$; day 4–6, $P < 0.001$). (**F**) High-dose (17.0 mg/kg) cocaine elicits an attenuated response after the first administration in *Ube3a*$^{m-/p+}$ mice that is gone by the fourth day. (**D**–**F**) Cocaine-induced sensitization occurred at all 3 doses for both genotypes (day 1 vs. challenge, $P < 0.001$). Error bars indicate SEM. $^{*}P < 0.05$; $^{\#}P < 0.01$; $^{\dagger}P < 0.001$.

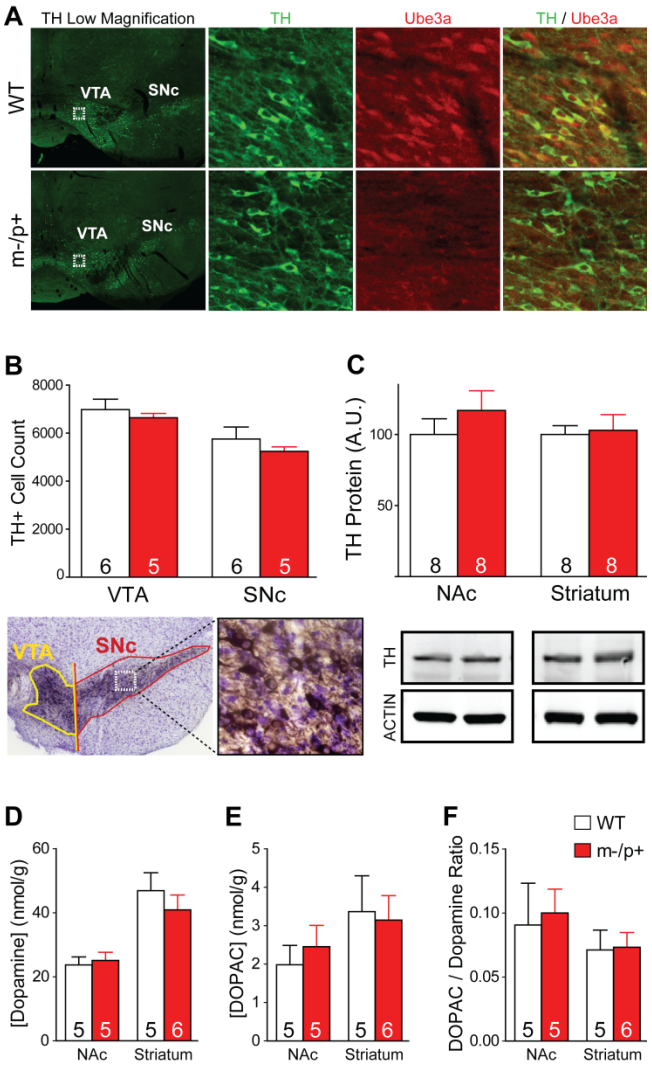

Figure 4-4: Biochemical and anatomical markers of the mesolimbic and nigrostriatal dopaminergic pathways are normal in *Ube3a*$^{m-/p+}$ mice. (**A**) Immunohistochemistry showing imprinting of UBE3A in the mesencephalic VTA and SNc and colocalization with TH in WT mice (original magnification, ×4). Boxed regions are shown at higher magnification in the second, third, and fourth columns (original magnification, ×40). (**B**) Numbers of TH-positive cells in the VTA and SNc estimated with design-based stereology show no differences between WT and *Ube3a*$^{m-/p+}$ mice. Ventral midbrain image is magnified (original magnification, ×4) and the boxed region is shown at higher magnification to the right (original magnification, ×40). (**C**) Quantification of TH, the rate-limiting enzyme in dopamine biosynthesis, from NAc and striatal tissue punches by immunoblotting shows similar levels between the 2 genotypes. (**D**) HPLC analysis of concentrations of dopamine and (**E**) its primary acid metabolite DOPAC in NAc and striatal punches from WT and *Ube3a*$^{m-/p+}$ mice shows similar tissue content of dopamine and DOPAC. (**F**) Dopamine/DOPAC ratios are also equivalent between genotypes in NAc and striatum. Error bars indicate SEM. Numbers in bars represent numbers of mice.

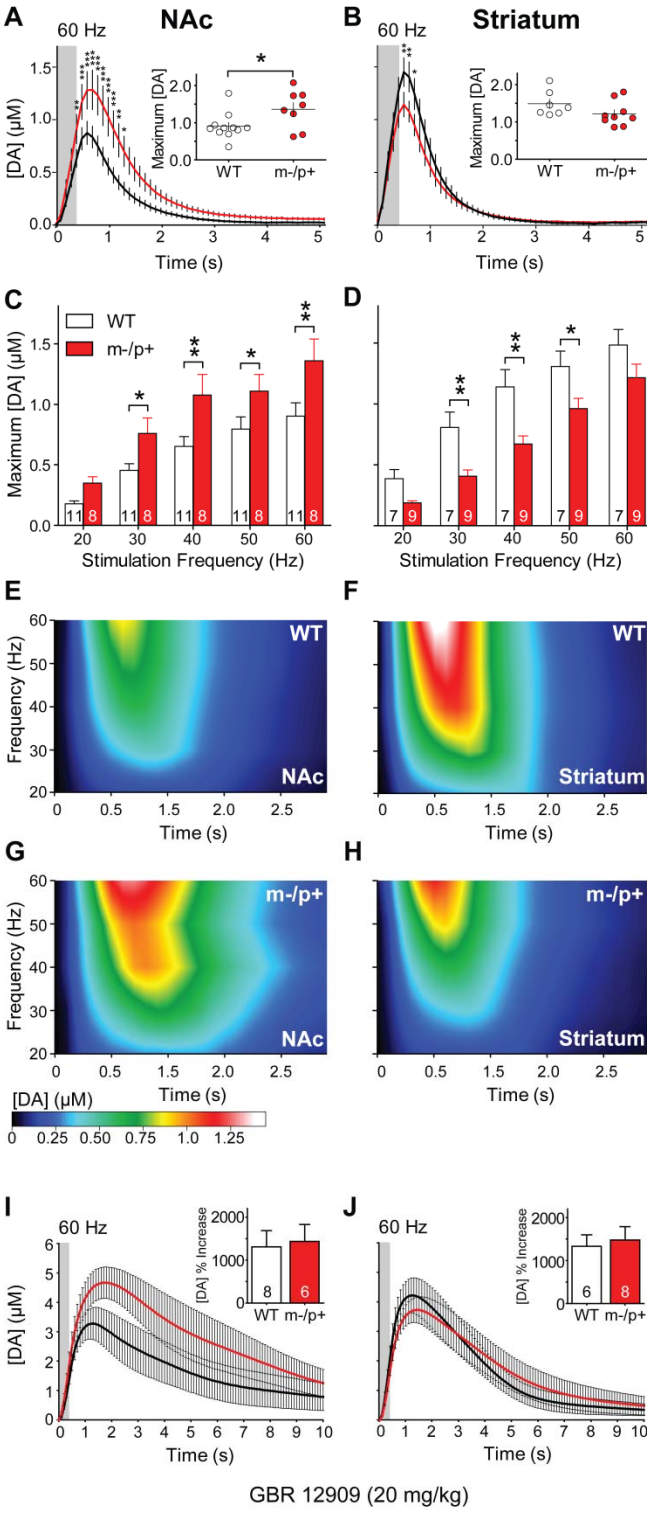

Figure 4-5: Dopamine release is enhanced in NAc and reduced in dorsal striatum of *Ube3a*$^{m-/p+}$ mice. Comparison of dopamine (DA) release measured with in vivo FSCV in the (**A**) NAc (on left throughout) and (**B**) dorsal striatum (on right throughout) of *Ube3a*$^{m-/p+}$ mice and their WT littermates. (**A** and **B**) Traces represent changes in dopamine

concentration evoked by 60-Hz stimulation (stimulus duration shaded gray). Insets show peak concentration of evoked dopamine in individual animals. (**C** and **D**) Average of peak concentrations evoked by stimulation frequencies, ranging from 20 to 60 Hz (NAc, 30 Hz, $P = 0.05$; 40 Hz, $P = 0.008$; 50 Hz, $P = 0.045$; 60 Hz, $P = 0.004$; striatum, 30 Hz, $P = 0.006$; 40 Hz, $P = 0.002$; 50 Hz, $P = 0.015$). (**E**–**H**) Extracellular dopamine concentrations following 5 discrete frequency stimulation steps, ranging from 20 to 60 Hz in the (**E** and **G**) NAc or (**F** and **H**) dorsal striatum. (**I** and **J**) Response of electrically stimulated (60 Hz) dopamine release to GBR 12909 (20 mg/kg), 30 minutes after i.p. injection. Insets show the relative increase in dopamine release (area under the curve) following GBR 12909. Error bars indicate SEM. Numbers in bars represent numbers of mice. $^{*}P < 0.05$; $^{\#}P < 0.01$; $^{\dagger}P < 0.001$.

Table 1
Anatomical markers of dopamine

	VTA		Substantia nigra	
	WT	*Ube3a*$^{m-/p+}$	WT	*Ube3a*$^{m-/p+}$
TH$^+$ cell no.	6,986 ± 427.9 (n = 6)	6,645 ± 174.9 (n = 5)	5,754 ± 500.2 (n = 6)	5,245 ± 182.2 (n = 5)

No significant genotype differences were found (mean ± SEM).

Table 1: Anatomical markers of dopamine

Table 2
Biochemical markers of dopamine

	NAc		Dorsal striatum	
	WT	***Ube3a*$^{m-/p+}$**	**WT**	***Ube3a*$^{m-/p+}$**
TH protein (% WT)	100 ± 10.99 (n = 8)	116.8 ± 13.89 (n = 8)	100 ± 6.16 (n = 8)	102.9 ± 11.10 (n = 8)
Dopamine (nmol/g)	23.72 ± 2.49	25.13 ± 2.52	46.93 ± 5.60	40.93 ± 4.63
DOPAC (nmol/g)	1.98 ± 0.51	2.46 ± 0.55	3.37 ± 0.93	3.15 ± 0.64
Dopamine/DOPAC	0.091 ± 0.03 (n = 5)	0.100 ± 0.02 (n = 5)	0.071 ± 0.02 (n = 5)	0.073 ± 0.01 (n = 5)

No significant genotype differences were found (mean ± SEM).

Table 2: Biochemical markers of dopamine

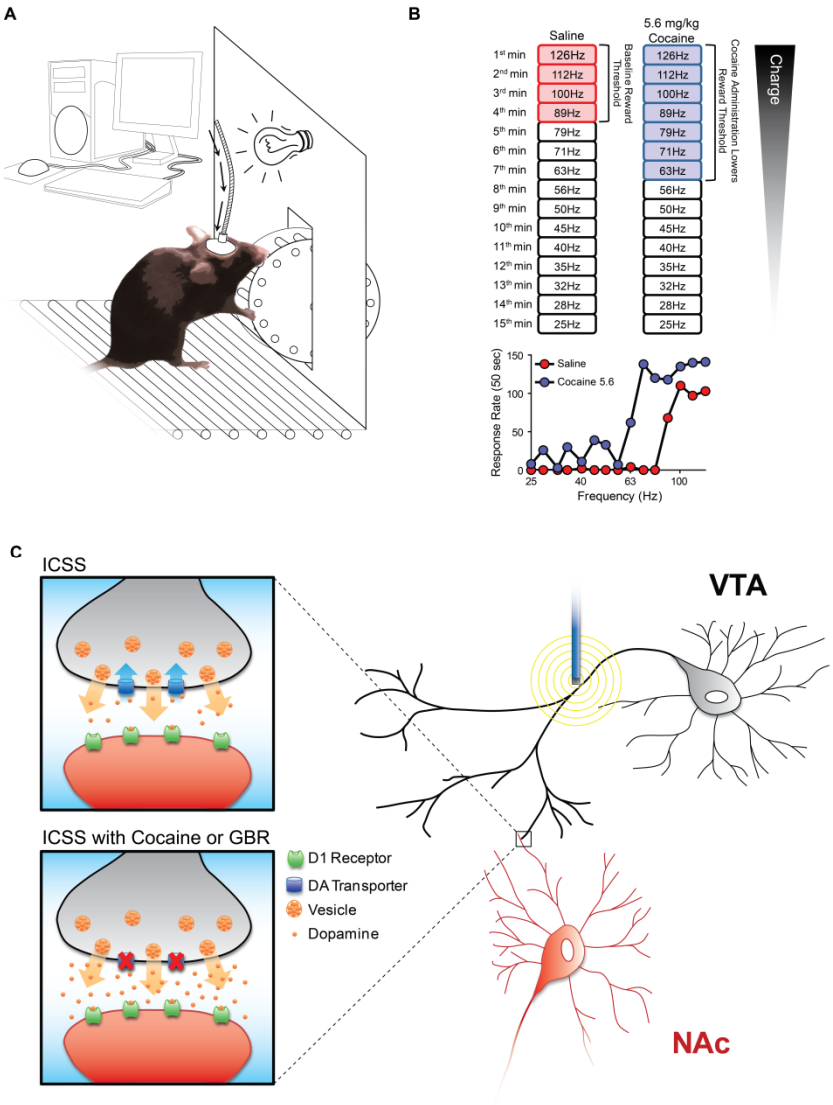

Supplemental Figure 4-1: Schematic of rate-dependent intracranial self-stimulation (ICSS). (A) Mice implanted with monopolar stimulating electrodes to the medial forebrain bundle (MFB) at the level of the lateral hypothalamus receive rewarding brain stimulation (BSR) for every quarter wheel turn, accompanied by illumination of the house light (500 ms). **(B)** Mice are presented with 15 discrete descending frequency steps (0.05 inverse log units) over 15 minutes. Mice have ad libitum access to BSR for 50 seconds during each frequency presentation. The minimum stimulus amplitude (μA) needed to initiate wheel turning for the top 3-5 frequencies is determined for each mouse and kept constant for the rest of the experiment. Injection of drugs that increase forebrain dopamine release (e.g., 5.6 mg/kg cocaine) decrease reward threshold (EF50) such that lower frequency stimulation sustains responding. **(C)** Schematic of the VTA-NAc reward circuit. Stimulation of ascending axons

(MFB) from the VTA results in the release of dopamine from their terminal fields in the NAc. Dopaminergic release in the NAc can be increased pharmacologically by blocking dopamine transporters with cocaine or GBR 12909, increasing extracellular dopamine availability.

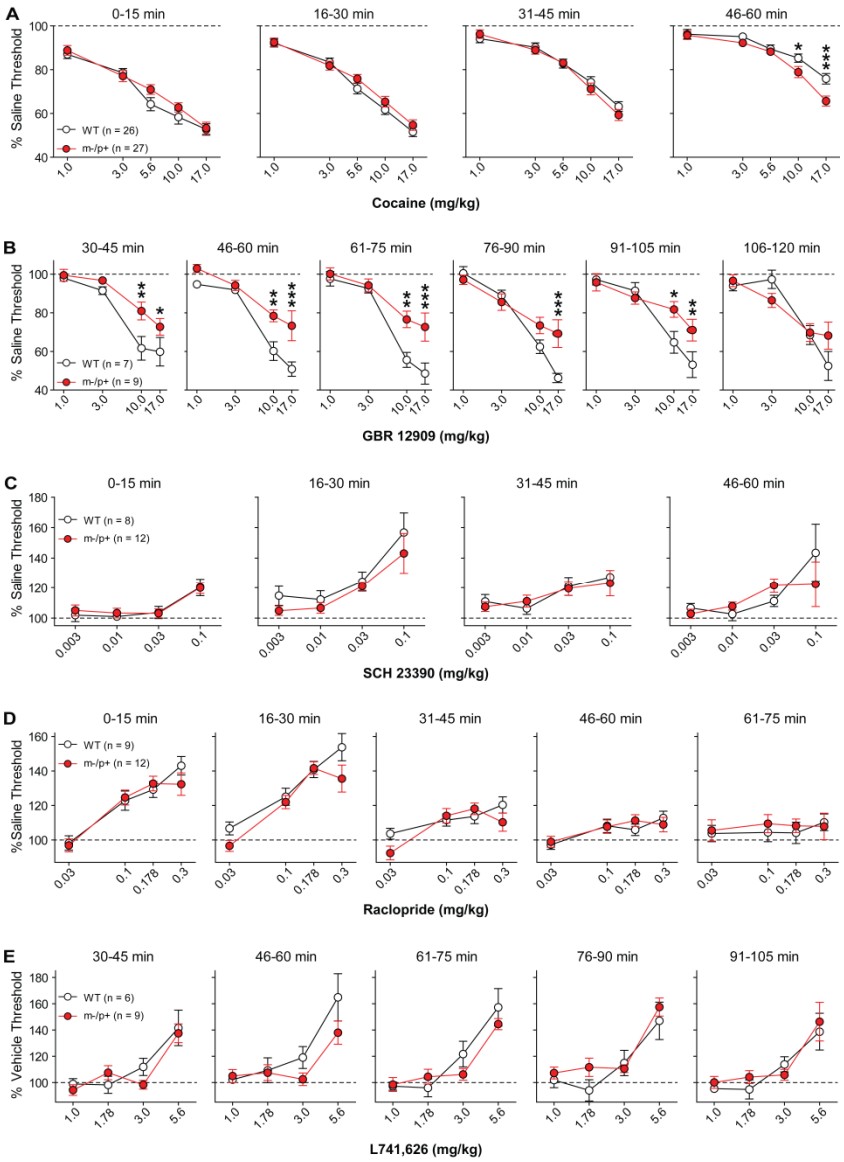

Supplemental Figure 4-2: Changes in BSR threshold following pharmacological treatment Reward threshold (EF50) was determined following i.p. administration of drugs that affect dopaminergic neurotransmission. (A) Cocaine lowered BSR threshold to the same extent in both *Ube3a*$^{m-/p+}$ and WT mice (0-45 min), but its effect decayed more rapidly in WT mice by 45-60 min (10 mg/kg, *p = 0.025; 17 mg/kg, ***p < 0.001). **(B)** The highly-selective (DAT) blocker GBR 12909 consistently lowered reward threshold more in WT mice than m-/p+ littermates for the first 105 minutes following injection (30-45 min, 10.0 mg/kg, **p = 0.002, 17.0 mg/kg, *p < 0.036; 46-60 min, 10.0 mg/kg, **p = 0.003, 17.0 mg/kg ***p < 0.001; 61-75 min, 10.0 mg/kg, **p = 0.002, 17.0 mg/kg, ***p < 0.001; 76-90 min, 17.0 mg/kg, ***p < 0.001; 91-105 min, 10.0 mg/kg, *p = 0.014, 17.0 mg/kg, **p =

0.01). **(C)** There were no significant genotype differences in the threshold-elevating effects of the dopamine D1-receptor antagonist SCH 23390 Neither administration of the D2/D3 antagonist raclopride **(D)** nor the D2-selective antagonist L741,626 **(E)** elevated reward threshold to a greater extent in either genotype. Error bars indicate ±SEM.

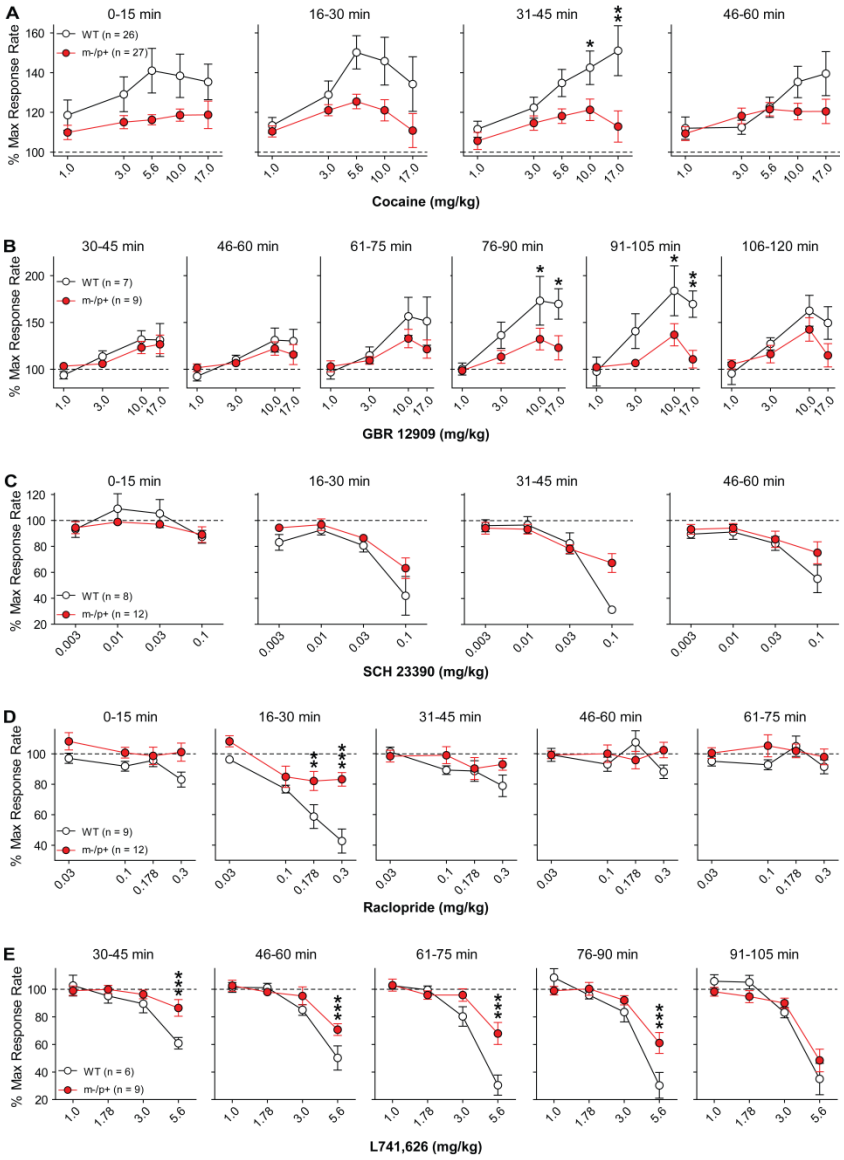

Supplemental Figure 4-3: Maximum operant response rate following pharmacological treatment. (**A**) WT mice exhibited a significantly larger increase in their maximum response rate 31-45 min after i.p. cocaine injection (10 mg/kg, *p = 0.028; 17 mg/kg, **p = 0.001). (**B**) WT mice also exhibited a significantly larger increase in their maximum response rate 76-105 min after i.p. GBR 12909 injection (76-90 min, 10 mg/kg, *p = 0.032, 17 mg/kg, *p = 0.015; 91-105 min, 10 mg/kg, *p = 0.018, 17 mg/kg, **p = 0.004). (**C**) There was no significant difference in reduction of maximum operant response rate following SCH 23350 injection between genotypes at any time point after i.p. administration. (**D**) *Ube3a*$^{m-/p+}$ mice were significantly less sensitive than WT littermates to the depressant effects of the D2/D3 antagonist raclopride on maximum operant response rate (16-30 min, 0.178 mg/kg, **p =

0.005, 0.3 mg/kg, ***p < 0.001). (**E**) *Ube3a*$^{m-/p+}$ mice were also less sensitive to the effects of the selective D2 antagonist L741,626 on maximum response rate (30-45 min, 5.6 kg/mg, ***p < 0.001; 46-60 min, 5.6 kg/mg, ***p < 0.001; 61-75 min, 5.6 kg/mg, ***p < 0.001; 76-90 min, 5.6 kg/mg, ***p < 0.001). Error bars indicate ±SEM.

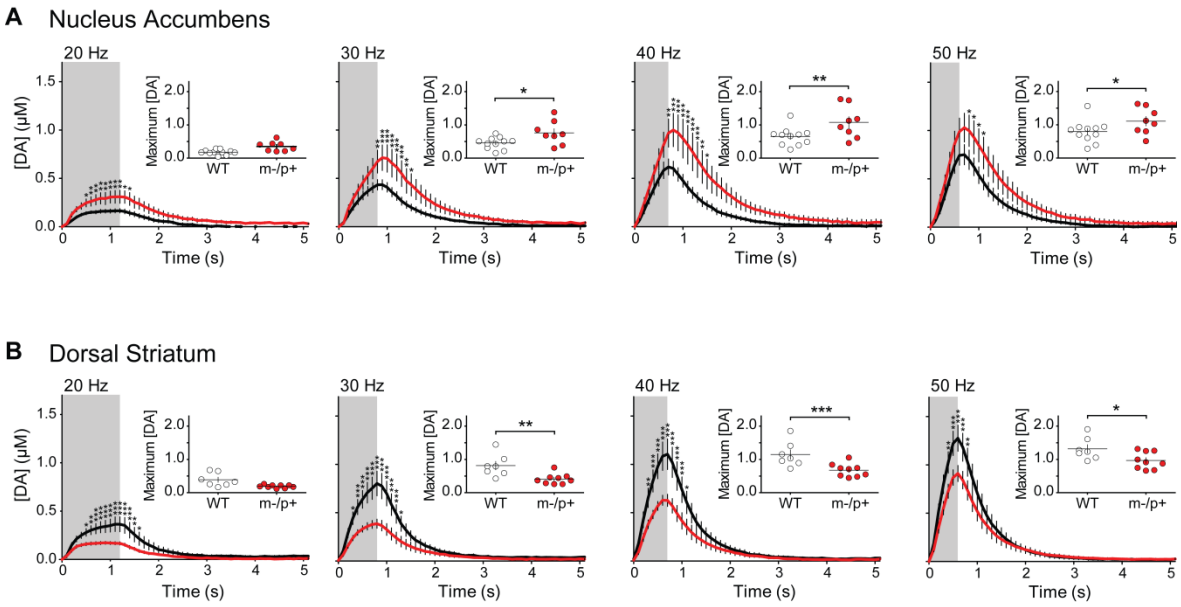

Supplemental Figure 4-4: Enhanced extracellular dopamine in the NAc and reduced extracellular dopamine in the dorsal striatum of *Ube3a*$^{m-/p+}$ mice. Change in extracellular dopamine concentration measured by voltammetry following electrical stimulation of the ascending dopaminergic fibers to either the NAc **(A)** or dorsal striatum **(B)**. Insets show the peak dopamine concentration recorded from each mouse. The stimulus duration is shown in gray shading. **(A)** *Ube3a*$^{m-/p+}$ mice consistently exhibited greater accumbal NAc dopamine concentrations across all stimulation frequencies (20-50 Hz, above, and 60 Hz in Figure 5A). **(B)** Conversely, in the dorsal striatum extracellular dopamine was reduced in *Ube3a*$^{m-/p+}$ mice (20-50 Hz, above, and 60 Hz in Figure 5B). *p < 0.05, **p < 0.01, ***p < 0.001. Error bars indicate ±SEM.

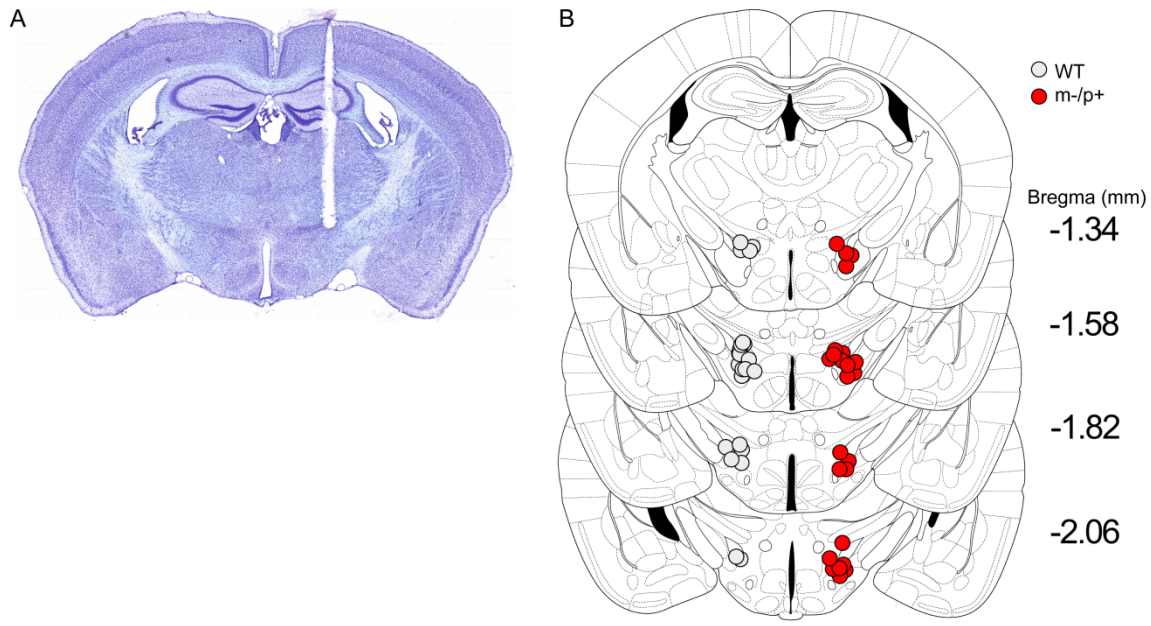

Supplemental Figure 4-5: ICSS electrode placement. Mice used for ICSS experiments were perfused and their brains sectioned and stained for Nissl to determine electrode tip placements. **(A)** Representative coronal section (4x magnification) with a stimulating electrode tract directly above the MFB. **(B)** All electrodes were implanted on the right. The most ventral point of each electrode tract was determined and plotted on the left for WT mice (gray circles) and on the right for *Ube3a*$^{m-/p+}$ mice (red circles) for clarity.

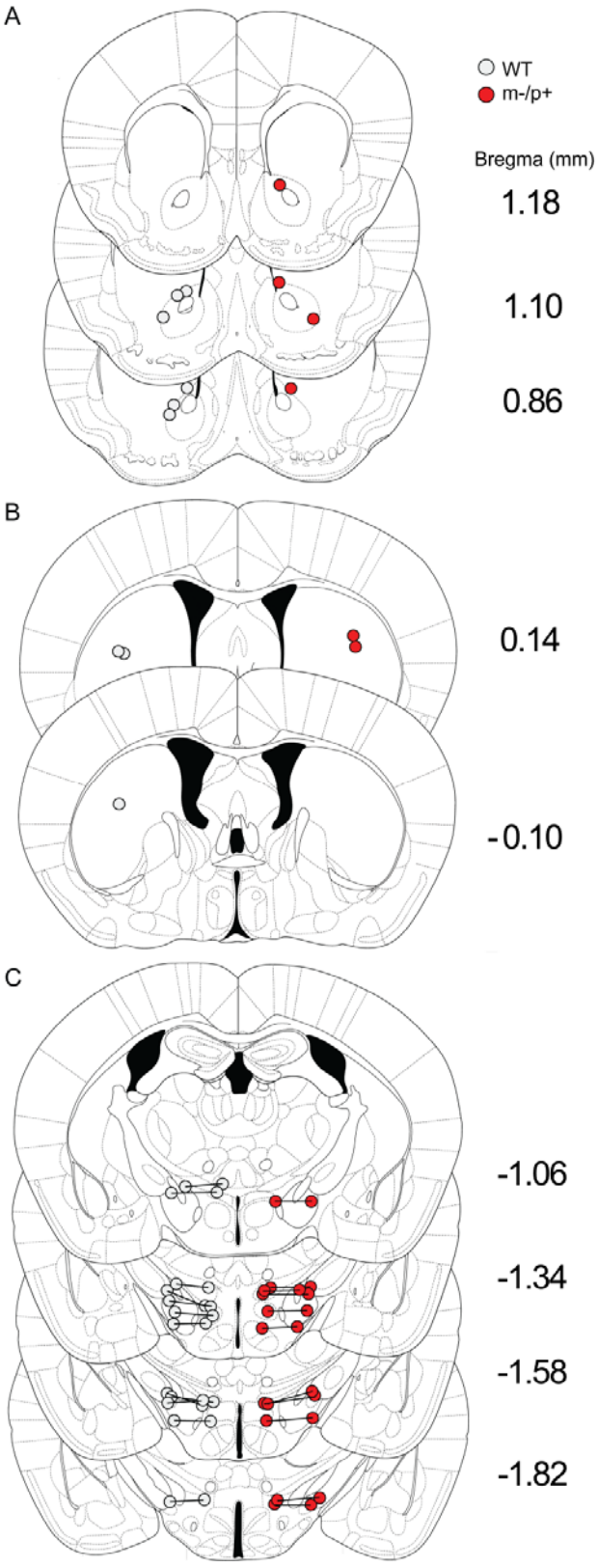

Supplemental Figure 4-6: FSCV electrode placement. Mice used for FSCV experiments were perfused and their brains sectioned and Nissl stained to determine electrode tip

placements. **(A)** Representative placements for carbon-fiber microelectrodes in the NAc. **(B)** Representative placements for carbon-fiber microelectrodes in the dorsal striatum. **(C)** Representative placements for bipolar stimulating electrodes in the MFB. The two tips of each bipolar electrode are connected with horizontal lines. The most ventral point of each electrode tract was determined and plotted on the left for WT mice (gray circles) and on the right for *Ube3a*$^{m-/p+}$ mice (red circles).

CHAPTER 5

5. Concluding Remarks and Future Directions

5.1. Experience-dependent plasticity in Angelman syndrome

We discovered a reduction in neocortical plasticity in Angelman syndrome (AS) model mice. Both long-term potentiation and depression (LTP and LTD respectively) of layer IV to II/III field excitatory postsynaptic potentials (fEPSC) were severely impaired in visual cortical brain slices. The *in vitro* LTD deficit was associated with impaired critical period ocular dominance plasticity, an LTD-contingent form of experience-dependent plasticity. However, while AS mice also exhibited impaired LTP of layer IV to II/III fEPSCs during the critical period (~P25), there were no deficits in stimulus-specific response potentiation (SRP), an LTP-contingent form of experience-dependent plasticity. Furthermore, while the deficit in LTP of layer IV to II/III synapses was even more profound in adult mice (~P100), experience-dependent potentiation was surprisingly enhanced, relative to wild-type (WT) mice.

5.1.1. *In vitro* LTP versus *In vivo* experience-dependent potentiation

There are several possible reasons for the apparent inconsistency between *in vitro* electrically-induced potentiation and *in vivo* visual experience-induced potentiation in AS mice. Field recordings conducted in brain slices measured LTP of layer IV to II/III synapses, but visual evoked potentials (VEP) were recorded from electrodes implanted in layer IV and consist primarily of thalamocortical responses (Muhammad et al., 2009). It is conceivable

that there are layer specific deficits in LTP induction in AS, and that thalamocortical LTP induction is spared. This seems unlikely to account for the discrepancy. Although the negative component of the VEP response is attributed mostly to layer IV pyramidal cells, the positive component is believed to represent intracortical activity driven in part by layer II/III activity (Khibnik et al., 2010). One might therefore expect that a deficit in layer II/III LTP induction would manifest in a smaller VEP amplitude (trough to peak), specifically in the peak amplitude, following SRP. Both the increase in peak and trough components of the VEP were greater in AS mice. However, because layer IV afferents directly activate layer II/III, it is difficult to rule out the possibility of layer IV compensation.

A second factor that has to be considered is tetanic electrical stimulation versus sensory stimulation. The method of stimulation can have a large impact on the magnitude of inhibition. When stimulation consists of patterned sensory input, cortical inhibitory postsynaptic potentials lag behind excitatory postsynaptic potentials, whereas with electrical stimulation, inhibition and excitation are activated concurrently (Okun and Lampl, 2008; Logothetis et al., 2010). Visual stimulation with spatio-temporally structured input patterns more naturally engages the visual circuit, than electrical stimulation, and may have had a profound influence on LTP induction in AS mice. This gets at the greater point that while there may be advantages of *in vitro* slice preparations, such as a relative ease of obtaining stable recordings from an isolated circuit, there are also disadvantages. Neurons in a slice preparation lack many of the normal afferent input and efferent targets present *in vivo*, and so observations made in slice experiments have to be considered in light of their artificial setting, as opposed to the more complex environment of the intact brain.

Another striking difference between the electrical tetanus and sensory LTP induction is timing. Two to three seconds of tetanic electrical stimulation is sufficient to immediately induce LTP. On the other hand, potentiation of the VEP response, following presentation of patterned visual stimuli, takes at least 24 hours, and does not plateau until after 7-11 days of visual stimulation. This leads to the question of whether SRP is an endogenous form of LTP analogous to that induced by tetanic electrical stimulation. There are in fact several lines of evidence to suggest that SRP and electrical induced LTP share common molecular mechanisms. Electrical stimulation of the dorsal lateral geniculate nucleus (dLGN) *in vivo* has been shown to significantly increase the amplitude of VEP responses (Heynen and Bear, 2001), and remained stable for least 5 days (Cooke and Bear, 2010). The augmented VEP response also occluded SRP. Mice that received unilateral electrical stimulation of the dLGN, initially exhibited larger VEP responses in the stimulated hemisphere. However after five days of subsequent visual stimulation, VEP amplitudes were no longer significantly different between the two hemispheres, indicating that the ceiling level for potentiation following electrically inducted LTP and SRP combined was equal to that of SRP alone (Cooke and Bear, 2010). The reverse was also demonstrated following SRP, with electrical stimulation of the dLGN failing to further increase the VEP amplitude (Cooke and Bear, 2010).

In addition to SRP's functional mimicry and occlusion of electrical LTP induction, SRP shares a number of molecular mechanisms with canonical LTP. SRP is blocked by preinjection of the competitive NMDA receptor antagonist 3-(2-Carboxypiperazin-4-yl)propyl-1-phosphonic acid (CPP), which also blocks LTP in visual cortical slices (Kirkwood et al., 1993; Frenkel et al., 2006). Additionally, SRP is blocked by preventing

AMPA receptor insertion into the postsynaptic membrane, by transfection of the GluR1 C-terminal domain, shown to exert a dominant negative effect on AMPA receptor insertion, and block LTP induction in hippocampal slices (Shi et al., 2001; Frenkel et al., 2006). Lastly, maintenance of NMDA-dependent LTP is reliant of the persistently active protein kinase, protein kinase Mζ (PKMζ; (Pastalkova et al., 2006). Local infusion of the ζ-inhibitory peptide (ZIP), which inhibits PKMζ, abolished the enhanced VEP response following SRP (Cooke and Bear, 2010). These studies suggest that SRP likely represents an endogenous form thalamocortical LTP.

5.1.2. Visual cortical inhibition

Several recent studies have revealed a developmental decline in inhibition within the cerebellum and visual cortex of AS model mice (Egawa et al., 2012; Wallace et al., 2012). Adult (~P80) AS mice exhibited a deficit in inhibitory drive onto pyramidal neurons in layer II/III of the visual cortex, which was not present during the critical period (~P25). The decline in visual cortical inhibition observed by Wallace et al. (2012) corresponded with the developmental augmentation of SRP that I had witnessed in AS mice. To determine how loss of *Ube3a* expression in inhibitory neurons contributed to experience-dependent potentiation, I utilized CRE-LOX technology to limit maternal *Ube3a* expression to inhibitory neurons, using the GAD2 promoter (GAD2-CRE:$Ube3a^{stop/+}$). Interestingly, when SRP was assessed in adult GAD2-CRE:$Ube3a^{stop/+}$ mice, the rate and degree of VEP potentiation was comparable to WT mice. This further suggests that the enhanced adult SRP in AS mice may be due to the loss of *Ube3a* function in inhibitory neurons specifically. Electrophysiological recordings still need to be carried out to confirm that normal inhibitory drive onto excitatory neurons is present in the GAD2-CRE:$Ube3a^{stop/+}$ mice.

The documented deficits in both visual cortical inhibition and excitation in AS, led us to hypothesize that solely restoring inhibition would tip the balance of cortical activity in the direction of reduced excitatory drive. It was therefore somewhat surprising that the magnitude of experience-dependent potentiation in GAD2-CRE:*Ube3a*$^{stop/+}$ mice was comparable to WT mice, and not attenuated. However, the magnitude of potentiation to the orthogonal visual stimulus was diminished in the GAD2-CRE:*Ube3a*$^{stop/+}$ mice relative to WT mice. It is difficult to decipher the meaning of this finding since very little of the SRP literature focuses on adult mice, when there is both stimulus-specific and nonspecific components to experience-dependent potentiation. Determining the role of *Ube3a* in excitatory neurons and sensory experience will benefit from future studies that utilize CRE-LOX system. Using the same approach as the GAD2-CRE:*Ube3a*$^{stop/+}$ mice, *Ube3a* expression can be limited to excitatory neurons by having CRE recombinase under control of the CaMKII promoter.

5.1.3. Orientation Selectivity

Cortical inhibition plays an important role in turning orientation selectivity (Borg-Graham et al., 1998; Shapley et al., 2003). Elegant experiments that pharmacologically block cortical inhibition have been shown to reduce orientation selectivity (Sato et al., 1996). The reduction in cortical inhibition observed in AS may similarly result in broader tuning of orientation selectivity, but future single-unit recordings will have to be carried out to test this hypothesis. A reduction in orientation selectivity of AS mice could result in a greater number of active neurons at any given stimulus orientation. A greater number of active cells during SRP might further enhance the VEP response. But a greater number of active cells would also presumably contribute to a larger baseline VEP response, which was not

observed. The other factor that has to be kept in mind is the reduction in excitation. While the reduction in inhibition might contribute to a greater number of responsive cells, the reduction in excitation could mean that each of those responsive cells is less active, and together generate a local field potential of comparable amplitude to WT mice at baseline.

5.2. Inversely affected mesolimbic/nigrostriatal dopamine release

Angelman syndrome has numerous characteristics that are potentially germane to dopaminergic function. AS phenotypes like ataxia, tremor, and stereotypies, including hand-flapping, tongue-thrusting, excessive chewing and mouthing behaviors, can be caused by an imbalance of dopamine in the nigrotriatal pathway. On the other hand, AS phenotypes such as hyperactivity, excitable personality, reduced need for sleep, and happy demeanor can be related to dopaminergic transmission in the mesolimbic system. Despite the potential relevance of dopamine function in AS, exploration of the basal ganglia has not been thoroughly pursued.

I used fast-scan cyclic voltammetry (FSCV) to investigate the possibility that dopamine is dysregulated in AS model mice. Voltammetric analysis revealed that stimulated release of dopamine was attenuated in the nigrostriatal system, and augmented in the mesolimbic system. The enhanced stimulated dopamine release within the nucleus accumbens (NAc) corresponded behaviorally with an increased sensitivity to rewarding electrical stimulation. It is tempting to speculate that the enhanced sensitivity to mesolimbic reward/pleasure may be related to the characteristic happy demeanor of AS. Additionally, drugs that increase dopaminergic tone in the mesolimbic pathway are known to promote hyperactivity and wakefulness, observed in AS (Costall et al., 1984; Wisor et al., 2001). The reduction in dopaminergic tone within the striatum can lead to tremor, and motor

impairments including cogwheel rigidity and bradykinesia, also reported in AS (Harbord, 2001). These reports of Parkinson-like motor impairments in AS have led to a clinical trial using dopamine replacement therapy (Harbord, 2001; Tan, 2012). However, boosting dopamine synthesis with pharmaceuticals such as levodopa, not only increases dopaminergic tone in the nigrostriatal system to ameliorate motor function, it also increases dopamine synthesis in the ventral tegmental area (VTA) which could further exacerbate behaviors linked to mesolimbic function in AS (Macdonald and Monchi, 2011). Therefore it is important to understand why stimulated dopamine release is inversely impacted in the mesolimbic/nigrostriatal pathways of AS.

The differential release of dopamine in the mesolimbic/nigrostriatal pathways of AS mice could not be attributed to changes in dopamine cell number or dopamine availability. The number of tyrosine hydroxylase (TH) positive cells, the precursor and marker for dopamine, was unaltered in the VTA and substantia nigra pars compacta (SNc). Furthermore, the concentrations of TH, dopamine, and DOPAC, the metabolite of dopamine, in the terminal fields of the NAc and striatum were also unchanged in AS mice. Extracellular dopamine availability is also determined by the rate of neurotransmitter uptake through dopamine transporters (DAT), but this aspect of neurotransmission was also unaltered. Neither the rate of dopamine clearance following stimulation, nor the increased concentration of extracellular dopamine following administration of the DAT blocker GBR 12909, were different in AS mice using voltammetric analysis.

5.2.1. D2 receptor function

With differences in dopamine uptake, neuroanatomy and synthesis ruled out, another possibility is that the electrophysiological properties of the dopamine cells are altered in AS.

Because the VTA and SNc are highly modulated by inputs from several dozen brain structures, a reductionistic approach is required to evaluate the cell-autonomous properties of dopamine neurons (Zahm et al., 2011). This can be achieved by recording from brain slices containing the VTA/SNc, in which the majority of inputs have been severed. Dopamine neurons in this region can be identified based upon anatomical landmarks, and with the aid of transgenic mice that express EGFP under the TH promoter (Sawamoto et al., 2001; Matsushita et al., 2002). Dopamine neurons also exhibit a characteristic large inward current (I_h) upon hyperpolarization of the membrane potential, detectable in whole-cell recordings (Johnson and North, 1992). Once patched onto a dopamine neuron, its intrinsic excitability can be evaluated by measuring the input/output and frequency/current relationships. Dopaminergic excitability is regulated in part by D2 autoreceptors, which appears to be affected in AS. While assessing brain stimulation reward (BSR), I discovered that AS mice were less sensitive to the motor disruptive effects of D2 antagonists, but equally sensitive to the depotentiating effects on reward threshold compared to WT mice. This suggests D2 function might be specifically affected in the nigrostriatal pathway. However, it is difficult to rule out the possibility that D2 receptor function is altered in the mesolimbic system as well, since the BSR paradigm is sensitive to changes in motor function. In addition, the antagonists were administered systemically, so that the reduction in sensitivity could be due to changes in D2 receptor function/availability in other brain regions that innervate the motor pathway.

Questions of how and where D2 receptor function might be modified can be addressed by recordings from slice preparations. Dendritic D2 receptors present in the VTA and SNc, and are activated by somatodentric dopamine release (Beart et al., 1979; Cheramy

et al., 1981). Somatodendritic D2 receptor function can be evaluated by whole-cell recordings of dopamine-mediated inhibitory postsynaptic currents from midbrain slices. Dopamine release is also regulated by presynaptic D2 autoreceptors in the terminal fields of the striatum and NAc (Starke et al., 1989; Wolf and Roth, 1990). Presynaptic D2 receptor function can be isolated from somatodendritic D2 receptors, in striatal coronal slices containing denervated dopamine terminals. It is then possible to electrically stimulate the axon fibers and use FSCV to measure dopamine release following D2 agonist/antagonist bath application. FSCV recordings from denervated slices may also help clarify whether the changes in dopamine release in AS are cell autonomous, circuit-dependent or a combination of the two.

5.2.2. *Ube3a* substrate *α-synuclein*

α-Synuclein was identified as a tentative *Ube3a* substrate in culture, but changes in α-synuclein protein levels have yet to be verified in the AS mouse model (Mulherkar et al., 2009). The endogenous role of α-synuclein is unknown, but aggregation of the protein has been implicated in dopaminergic neurodegeneration and the pathogenesis of Parkinson's disease (Lee and Lee, 2002; Recchia et al., 2004). It is hypothesized that α-synuclein may help maintain homeostasis of dopamine metabolism, and that diseases such as Parkinson's are caused by disruption of this homeostasis (Yu et al., 2005). α-Synuclein affects several processes involved in dopamine metabolism; 1) regulates dopamine biosynthesis by inhibiting TH activity (Perez et al., 2002), 2) inhibits DAT trafficking to the plasma membrane (Wersinger et al., 2003; Wersinger et al., 2004), 3) disrupted vesicular recycling (Nemani et al., 2010). If α-synuclein is a *Ube3a* substrate, I would predict elevated levels of α-synuclein in AS, resulting in a reduction of dopamine and membrane bound DAT.

However, when I took frozen tissue punches from the dorsal striatum and NAc and analyzed them with high-performance liquid chromatography there was no detectable difference in dopamine content in AS mice. There was also no evidence of reduced membrane-bound DAT, when functionally assessed by FSCV. Elevated α-synuclein levels have been shown to inhibit dopamine release by disrupting vesicle reclustering following endocytosis (Nemani et al., 2010). Coincidentally, reductions in vesicular availability have also been observed at inhibitory and excitatory synapses in the cortex of AS mice (Wallace et al., 2012). Deficits in the reclustering of vesicles are observed with modest overexpression of α-synuclein that precedes degeneration, and could account for the decrease in striatal dopamine release seen in AS mice.

5.2.3. GABAergic inhibition of dopamine neurons

Reduced inhibitory drive has been described in the visual cortex and the cerebellum of AS mice, however little is known about inhibitory function in the basal ganglia of AS (Cheron et al., 2005; Egawa et al., 2012; Wallace et al., 2012). Considering the anatomical and functional connections between dopamine and GABAergic systems in the mesolimbic and nigrostriatal pathways, it seems likely that inhibitory dysfunction in the basal ganglion would directly influence dopamine neurotransmission. Both active and spontaneous dopamine release is modulated by local GABAergic interneurons in the VTA and SNc (Kosaka et al., 1987; Hajos and Greenfield, 1994; Westerink et al., 1996). Dopamine release is also inhibited by descending GABAergic projections from the striatal complex, composed of the NAc, striatum, ventral pallidum and globus pallidus (Smith and Bolam, 1990). A reduction in inhibition would be expected to increase dopaminergic transmission

5.2.4. Ube3a reinstatement in dopamine neurons

Dopamine neurons play an important role in various brain functions including motivation, reinforcement learning, and motor control. The dopaminergic activity that guides these behaviors is modulated by synaptic projections from dozens of brain regions throughout the neocortex, thalamus, basal ganglia, midbrain and hindbrain (Watabe-Uchida et al., 2012). The heavy modulation of dopamine activity makes it more difficult to determine what changes in dopaminergic function, due to loss of *Ube3a* expression, are because of cell autonomous changes rather than alterations in other ascending circuits. One strategy already talked about, is severing synaptic inputs in brain slices, but this does not preclude developmental influences from other afflicted brain regions. A more novel approach is restricted reinstatement of *Ube3a* in dopamine neurons, made possible by the Cre/loxP gene expression system. This can be accomplished by using an established CRE line under the TH promotor, and a novel genetic tool that allows for CRE-dependent reinstatement of *Ube3a* (TH-Cre;lox-Stop-lox-Ube3a). An AS mouse model with dopaminergic *Ube3a* expression would be invaluable in parsing out which AS deficits are specifically due to dopamine neurons. Determining the contribution of dopaminergic dysfunction to AS is important in better understanding the value of dopamine replacement therapy.

REFERENCES

Abrahams, B.S., and Geschwind, D.H. (2008). Advances in autism genetics: on the threshold of a new neurobiology. Nature reviews Genetics 9, 341-355.

Albrecht, U., Sutcliffe, J.S., Cattanach, B.M., Beechey, C.V., Armstrong, D., Eichele, G., and Beaudet, A.L. (1997). Imprinted expression of the murine Angelman syndrome gene, Ube3a, in hippocampal and Purkinje neurons. Nature genetics 17, 75-78.

Allensworth, M., Saha, A., Reiter, L.T., and Heck, D.H. (2011). Normal social seeking behavior, hypoactivity and reduced exploratory range in a mouse model of Angelman syndrome. BMC genetics 12, 7.

Arieli, A., Shoham, D., Hildesheim, R., and Grinvald, A. (1995). Coherent spatiotemporal patterns of ongoing activity revealed by real-time optical imaging coupled with single-unit recording in the cat visual cortex. Journal of neurophysiology 73, 2072-2093.

Arieli, A., Sterkin, A., Grinvald, A., and Aertsen, A. (1996). Dynamics of ongoing activity: explanation of the large variability in evoked cortical responses. Science 273, 1868-1871.

Baquet, Z.C., Williams, D., Brody, J., and Smeyne, R.J. (2009). A comparison of model-based (2D) and design-based (3D) stereological methods for estimating cell number in the substantia nigra pars compacta (SNpc) of the C57BL/6J mouse. Neuroscience 161, 1082-1090.

Basar, E., Basar-Eroglu, C., Karakas, S., and Schurmann, M. (2001). Gamma, alpha, delta, and theta oscillations govern cognitive processes. International journal of psychophysiology : official journal of the International Organization of Psychophysiology 39, 241-248.

Baudry, M., Kramar, E., Xu, X., Zadran, H., Moreno, S., Lynch, G., Gall, C., and Bi, X. (2012). Ampakines promote spine actin polymerization, long-term potentiation, and learning in a mouse model of Angelman syndrome. Neurobiology of disease 47, 210-215.

Beart, P.M., McDonald, D., and Gundlach, A.L. (1979). Mesolimbic dopaminergic neurones and somatodendritic mechanisms. Neuroscience letters 15, 165-170.

Bello, E.P., Mateo, Y., Gelman, D.M., Noain, D., Shin, J.H., Low, M.J., Alvarez, V.A., Lovinger, D.M., and Rubinstein, M. (2011). Cocaine supersensitivity and enhanced motivation for reward in mice lacking dopamine D2 autoreceptors. Nature neuroscience 14, 1033-1038.

Benuck, M., Lajtha, A., and Reith, M.E. (1987). Pharmacokinetics of systemically administered cocaine and locomotor stimulation in mice. The Journal of pharmacology and experimental therapeutics 243, 144-149.

Borg-Graham, L.J., Monier, C., and Fregnac, Y. (1998). Visual input evokes transient and strong shunting inhibition in visual cortical neurons. Nature 393, 369-373.

Bourgeron, T. (2009). A synaptic trek to autism. Current opinion in neurobiology 19, 231-234.

Bramham, C.R., Worley, P.F., Moore, M.J., and Guzowski, J.F. (2008). The immediate early gene arc/arg3.1: regulation, mechanisms, and function. The Journal of neuroscience : the official journal of the Society for Neuroscience 28, 11760-11767.

Browne, C.E., Dennis, N.R., Maher, E., Long, F.L., Nicholson, J.C., Sillibourne, J., and Barber, J.C. (1997). Inherited interstitial duplications of proximal 15q: genotype-phenotype correlations. American journal of human genetics 61, 1342-1352.

Bruni, O., Ferri, R., D'Agostino, G., Miano, S., Roccella, M., and Elia, M. (2004). Sleep disturbances in Angelman syndrome: a questionnaire study. Brain & development 26, 233-240.

Cahill, P.S., Walker, Q.D., Finnegan, J.M., Mickelson, G.E., Travis, E.R., and Wightman, R.M. (1996). Microelectrodes for the measurement of catecholamines in biological systems. Analytical chemistry 68, 3180-3186.

Cattanach, B.M., Barr, J.A., Beechey, C.V., Martin, J., Noebels, J., and Jones, J. (1997). A candidate model for Angelman syndrome in the mouse. Mammalian genome : official journal of the International Mammalian Genome Society 8, 472-478.

Charles A. Williams, S.U.P., Stephen N. Calculator (2009). Facts about Angelman syndrome, 7th Edition edn (Angelman Syndrome Foundation).

Chausmer, A.L., Elmer, G.I., Rubinstein, M., Low, M.J., Grandy, D.K., and Katz, J.L. (2002). Cocaine-induced locomotor activity and cocaine discrimination in dopamine D2 receptor mutant mice. Psychopharmacology 163, 54-61.

Cheramy, A., Leviel, V., and Glowinski, J. (1981). Dendritic release of dopamine in the substantia nigra. Nature 289, 537-542.

Cheron, G., Servais, L., Wagstaff, J., and Dan, B. (2005). Fast cerebellar oscillation associated with ataxia in a mouse model of Angelman syndrome. Neuroscience 130, 631-637.

Choi, P., Snyder, H., Petrucelli, L., Theisler, C., Chong, M., Zhang, Y., Lim, K., Chung, K.K., Kehoe, K., D'Adamio, L.*, et al.* (2003). SEPT5_v2 is a parkin-binding protein. Brain research Molecular brain research 117, 179-189.

Clayton-Smith, J., and Laan, L. (2003). Angelman syndrome: a review of the clinical and genetic aspects. Journal of medical genetics 40, 87-95.

Colas, D., Wagstaff, J., Fort, P., Salvert, D., and Sarda, N. (2005). Sleep disturbances in Ube3a maternal-deficient mice modeling Angelman syndrome. Neurobiology of disease 20, 471-478.

Colledge, M., Snyder, E.M., Crozier, R.A., Soderling, J.A., Jin, Y., Langeberg, L.K., Lu, H., Bear, M.F., and Scott, J.D. (2003). Ubiquitination regulates PSD-95 degradation and AMPA receptor surface expression. Neuron 40, 595-607.

Cooke, S.F., and Bear, M.F. (2010). Visual experience induces long-term potentiation in the primary visual cortex. The Journal of neuroscience : the official journal of the Society for Neuroscience 30, 16304-16313.

Cooke, S.F., and Bear, M.F. (2012). Stimulus-selective response plasticity in the visual cortex: an assay for the assessment of pathophysiology and treatment of cognitive impairment associated with psychiatric disorders. Biological psychiatry 71, 487-495.

Cooper, B.R., and Breese, G.R. (1975). A role for dopamine in the psychopharmacology of electrical self-stimulation. National Institute on Drug Abuse research monograph series, 63-70.

Costall, B., Domeney, A.M., and Naylor, R.J. (1984). Locomotor hyperactivity caused by dopamine infusion into the nucleus accumbens of rat brain: specificity of action. Psychopharmacology 82, 174-180.

Crozier, R.A., Wang, Y., Liu, C.H., and Bear, M.F. (2007). Deprivation-induced synaptic depression by distinct mechanisms in different layers of mouse visual cortex. Proceedings of the National Academy of Sciences of the United States of America 104, 1383-1388.

Dekker, M., Bonifati, V., van Swieten, J., Leenders, N., Galjaard, R.J., Snijders, P., Horstink, M., Heutink, P., Oostra, B., and van Duijn, C. (2003). Clinical features and neuroimaging of PARK7-linked parkinsonism. Movement disorders : official journal of the Movement Disorder Society 18, 751-757.

DeLorey, T.M., Handforth, A., Anagnostaras, S.G., Homanics, G.E., Minassian, B.A., Asatourian, A., Fanselow, M.S., Delgado-Escueta, A., Ellison, G.D., and Olsen, R.W. (1998). Mice lacking the beta3 subunit of the GABAA receptor have the epilepsy phenotype and many of the behavioral characteristics of Angelman syndrome. The Journal of neuroscience : the official journal of the Society for Neuroscience 18, 8505-8514.

Desai, N.S., Cudmore, R.H., Nelson, S.B., and Turrigiano, G.G. (2002). Critical periods for experience-dependent synaptic scaling in visual cortex. Nature neuroscience 5, 783-789.

Dindot, S.V., Antalffy, B.A., Bhattacharjee, M.B., and Beaudet, A.L. (2008). The Angelman syndrome ubiquitin ligase localizes to the synapse and nucleus, and maternal deficiency results in abnormal dendritic spine morphology. Human molecular genetics 17, 111-118.

Egawa, K., Kitagawa, K., Inoue, K., Takayama, M., Takayama, C., Saitoh, S., Kishino, T., Kitagawa, M., and Fukuda, A. (2012). Decreased tonic inhibition in cerebellar granule cells causes motor dysfunction in a mouse model of angelman syndrome. Science translational medicine 4, 163ra157.

Elmer, G.I., Pieper, J.O., Levy, J., Rubinstein, M., Low, M.J., Grandy, D.K., and Wise, R.A. (2005). Brain stimulation and morphine reward deficits in dopamine D2 receptor-deficient mice. Psychopharmacology 182, 33-44.

Fagiolini, M., Katagiri, H., Miyamoto, H., Mori, H., Grant, S.G., Mishina, M., and Hensch, T.K. (2003). Separable features of visual cortical plasticity revealed by N-methyl-D-aspartate receptor 2A signaling. Proceedings of the National Academy of Sciences of the United States of America 100, 2854-2859.

Fang, P., Lev-Lehman, E., Tsai, T.F., Matsuura, T., Benton, C.S., Sutcliffe, J.S., Christian, S.L., Kubota, T., Halley, D.J., Meijers-Heijboer, H.*, et al.* (1999). The spectrum of mutations in UBE3A causing Angelman syndrome. Human molecular genetics 8, 129-135.

Feldman, D.E., Nicoll, R.A., and Malenka, R.C. (1999). Synaptic plasticity at thalamocortical synapses in developing rat somatosensory cortex: LTP, LTD, and silent synapses. Journal of neurobiology 41, 92-101.

Fellinger, R., Klimesch, W., Gruber, W., Freunberger, R., and Doppelmayr, M. (2011). Pre-stimulus alpha phase-alignment predicts P1-amplitude. Brain research bulletin 85, 417-423.

Ferdousy, F., Bodeen, W., Summers, K., Doherty, O., Wright, O., Elsisi, N., Hilliard, G., O'Donnell, J.M., and Reiter, L.T. (2011). Drosophila Ube3a regulates monoamine synthesis by increasing GTP cyclohydrolase I activity via a non-ubiquitin ligase mechanism. Neurobiology of disease 41, 669-677.

Fish, E.W., Riday, T.T., McGuigan, M.M., Faccidomo, S., Hodge, C.W., and Malanga, C.J. (2010). Alcohol, cocaine, and brain stimulation-reward in C57Bl6/J and DBA2/J mice. Alcoholism, clinical and experimental research 34, 81-89.

Fonseca, R., Vabulas, R.M., Hartl, F.U., Bonhoeffer, T., and Nagerl, U.V. (2006). A balance of protein synthesis and proteasome-dependent degradation determines the maintenance of LTP. Neuron 52, 239-245.

Frankland, P.W., O'Brien, C., Ohno, M., Kirkwood, A., and Silva, A.J. (2001). Alpha-CaMKII-dependent plasticity in the cortex is required for permanent memory. Nature 411, 309-313.

Frenkel, M.Y., Sawtell, N.B., Diogo, A.C., Yoon, B., Neve, R.L., and Bear, M.F. (2006). Instructive effect of visual experience in mouse visual cortex. Neuron 51, 339-349.

Gabriel, J.M., Merchant, M., Ohta, T., Ji, Y., Caldwell, R.G., Ramsey, M.J., Tucker, J.D., Longnecker, R., and Nicholls, R.D. (1999). A transgene insertion creating a heritable chromosome deletion mouse model of Prader-Willi and angelman syndromes. Proceedings of the National Academy of Sciences of the United States of America 96, 9258-9263.

Gatenby J.B., B.H.W. (1950). The Microtomist's Vade-mecum; A Handbook of the Methods of Animal and Plant Microscopic Technique, 11th Edition edn (J. & A. Churchill).

Gianfranceschi, L., Siciliano, R., Walls, J., Morales, B., Kirkwood, A., Huang, Z.J., Tonegawa, S., and Maffei, L. (2003). Visual cortex is rescued from the effects of dark rearing by overexpression of BDNF. Proceedings of the National Academy of Sciences of the United States of America 100, 12486-12491.

Gibson, J.R., Bartley, A.F., Hays, S.A., and Huber, K.M. (2008). Imbalance of neocortical excitation and inhibition and altered UP states reflect network hyperexcitability in the mouse model of fragile X syndrome. Journal of neurophysiology 100, 2615-2626.

Gispert, S., Ricciardi, F., Kurz, A., Azizov, M., Hoepken, H.H., Becker, D., Voos, W., Leuner, K., Muller, W.E., Kudin, A.P.*, et al.* (2009). Parkinson phenotype in aged PINK1-deficient mice is accompanied by progressive mitochondrial dysfunction in absence of neurodegeneration. PloS one 4, e5777.

Goel, A., and Lee, H.K. (2007). Persistence of experience-induced homeostatic synaptic plasticity through adulthood in superficial layers of mouse visual cortex. The Journal of neuroscience : the official journal of the Society for Neuroscience 27, 6692-6700.

Goldberg, M.S., Fleming, S.M., Palacino, J.J., Cepeda, C., Lam, H.A., Bhatnagar, A., Meloni, E.G., Wu, N., Ackerson, L.C., Klapstein, G.J.*, et al.* (2003). Parkin-deficient mice exhibit nigrostriatal deficits but not loss of dopaminergic neurons. The Journal of biological chemistry 278, 43628-43635.

Goldberg, M.S., Pisani, A., Haburcak, M., Vortherms, T.A., Kitada, T., Costa, C., Tong, Y., Martella, G., Tscherter, A., Martins, A.*, et al.* (2005). Nigrostriatal dopaminergic deficits and hypokinesia caused by inactivation of the familial Parkinsonism-linked gene DJ-1. Neuron 45, 489-496.

Gordon, J.A., and Stryker, M.P. (1996). Experience-dependent plasticity of binocular responses in the primary visual cortex of the mouse. The Journal of neuroscience : the official journal of the Society for Neuroscience 16, 3274-3286.

Greer, P.L., Hanayama, R., Bloodgood, B.L., Mardinly, A.R., Lipton, D.M., Flavell, S.W., Kim, T.K., Griffith, E.C., Waldon, Z., Maehr, R.*, et al.* (2010). The Angelman Syndrome protein Ube3A regulates synapse development by ubiquitinating arc. Cell 140, 704-716.

Gundersen, H.J., and Jensen, E.B. (1987). The efficiency of systematic sampling in stereology and its prediction. Journal of microscopy 147, 229-263.

Hajos, M., and Greenfield, S.A. (1994). Synaptic connections between pars compacta and pars reticulata neurones: electrophysiological evidence for functional modules within the substantia nigra. Brain research 660, 216-224.

Harauzov, A., Spolidoro, M., DiCristo, G., De Pasquale, R., Cancedda, L., Pizzorusso, T., Viegi, A., Berardi, N., and Maffei, L. (2010). Reducing intracortical inhibition in the adult visual cortex promotes ocular dominance plasticity. The Journal of neuroscience : the official journal of the Society for Neuroscience 30, 361-371.

Harbord, M. (2001). Levodopa responsive Parkinsonism in adults with Angelman Syndrome. Journal of clinical neuroscience : official journal of the Neurosurgical Society of Australasia 8, 421-422.

He, H.Y., Hodos, W., and Quinlan, E.M. (2006). Visual deprivation reactivates rapid ocular dominance plasticity in adult visual cortex. The Journal of neuroscience : the official journal of the Society for Neuroscience 26, 2951-2955.

Heck, D.H., Zhao, Y., Roy, S., LeDoux, M.S., and Reiter, L.T. (2008). Analysis of cerebellar function in Ube3a-deficient mice reveals novel genotype-specific behaviors. Human molecular genetics 17, 2181-2189.

Heien, M.L., Phillips, P.E., Stuber, G.D., Seipel, A.T., and Wightman, R.M. (2003). Overoxidation of carbon-fiber microelectrodes enhances dopamine adsorption and increases sensitivity. The Analyst 128, 1413-1419.

Heynen, A.J., and Bear, M.F. (2001). Long-term potentiation of thalamocortical transmission in the adult visual cortex in vivo. The Journal of neuroscience : the official journal of the Society for Neuroscience 21, 9801-9813.

Heynen, A.J., Yoon, B.J., Liu, C.H., Chung, H.J., Huganir, R.L., and Bear, M.F. (2003). Molecular mechanism for loss of visual cortical responsiveness following brief monocular deprivation. Nature neuroscience 6, 854-862.

Hislop, J.N., and von Zastrow, M. (2011). Role of ubiquitination in endocytic trafficking of G-protein-coupled receptors. Traffic 12, 137-148.

Huibregtse, J.M., Scheffner, M., and Howley, P.M. (1991). A cellular protein mediates association of p53 with the E6 oncoprotein of human papillomavirus types 16 or 18. The EMBO journal 10, 4129-4135.

Imai, Y., Soda, M., Inoue, H., Hattori, N., Mizuno, Y., and Takahashi, R. (2001). An unfolded putative transmembrane polypeptide, which can lead to endoplasmic reticulum stress, is a substrate of Parkin. Cell 105, 891-902.

Itier, J.M., Ibanez, P., Mena, M.A., Abbas, N., Cohen-Salmon, C., Bohme, G.A., Laville, M., Pratt, J., Corti, O., Pradier, L.*, et al.* (2003). Parkin gene inactivation alters behaviour and dopamine neurotransmission in the mouse. Human molecular genetics 12, 2277-2291.

Jay, V., Becker, L.E., Chan, F.W., and Perry, T.L., Sr. (1991). Puppet-like syndrome of Angelman: a pathologic and neurochemical study. Neurology 41, 416-422.

Jiang, B., Trevino, M., and Kirkwood, A. (2007). Sequential development of long-term potentiation and depression in different layers of the mouse visual cortex. The Journal of neuroscience : the official journal of the Society for Neuroscience 27, 9648-9652.

Jiang, Y.H., Armstrong, D., Albrecht, U., Atkins, C.M., Noebels, J.L., Eichele, G., Sweatt, J.D., and Beaudet, A.L. (1998). Mutation of the Angelman ubiquitin ligase in mice causes increased cytoplasmic p53 and deficits of contextual learning and long-term potentiation. Neuron 21, 799-811.

Jiang, Y.H., Pan, Y., Zhu, L., Landa, L., Yoo, J., Spencer, C., Lorenzo, I., Brilliant, M., Noebels, J., and Beaudet, A.L. (2010). Altered ultrasonic vocalization and impaired learning and memory in Angelman syndrome mouse model with a large maternal deletion from Ube3a to Gabrb3. PloS one 5, e12278.

Johnson, S.W., and North, R.A. (1992). Two types of neurone in the rat ventral tegmental area and their synaptic inputs. The Journal of physiology 450, 455-468.

Johnstone, K.A., DuBose, A.J., Futtner, C.R., Elmore, M.D., Brannan, C.I., and Resnick, J.L. (2006). A human imprinting centre demonstrates conserved acquisition but diverged maintenance of imprinting in a mouse model for Angelman syndrome imprinting defects. Human molecular genetics 15, 393-404.

Jordan, C., and Francke, U. (2006). Ube3a expression is not altered in Mecp2 mutant mice. Human molecular genetics 15, 2210-2215.

Kahana, M.J. (2006). The cognitive correlates of human brain oscillations. The Journal of neuroscience : the official journal of the Society for Neuroscience 26, 1669-1672.

Kaphzan, H., Hernandez, P., Jung, J.I., Cowansage, K.K., Deinhardt, K., Chao, M.V., Abel, T., and Klann, E. (2012). Reversal of impaired hippocampal long-term potentiation and contextual fear memory deficits in Angelman syndrome model mice by ErbB inhibitors. Biological psychiatry 72, 182-190.

Khan, N.L., Graham, E., Critchley, P., Schrag, A.E., Wood, N.W., Lees, A.J., Bhatia, K.P., and Quinn, N. (2003). Parkin disease: a phenotypic study of a large case series. Brain : a journal of neurology 126, 1279-1292.

Khan, N.L., Valente, E.M., Bentivoglio, A.R., Wood, N.W., Albanese, A., Brooks, D.J., and Piccini, P. (2002). Clinical and subclinical dopaminergic dysfunction in PARK6-linked parkinsonism: an 18F-dopa PET study. Annals of neurology 52, 849-853.

Khibnik, L.A., Cho, K.K., and Bear, M.F. (2010). Relative contribution of feedforward excitatory connections to expression of ocular dominance plasticity in layer 4 of visual cortex. Neuron 66, 493-500.

Kirik, D., Rosenblad, C., Burger, C., Lundberg, C., Johansen, T.E., Muzyczka, N., Mandel, R.J., and Bjorklund, A. (2002). Parkinson-like neurodegeneration induced by targeted overexpression of alpha-synuclein in the nigrostriatal system. The Journal of neuroscience : the official journal of the Society for Neuroscience 22, 2780-2791.

Kirkwood, A., Dudek, S.M., Gold, J.T., Aizenman, C.D., and Bear, M.F. (1993). Common forms of synaptic plasticity in the hippocampus and neocortex in vitro. Science 260, 1518-1521.

Kirkwood, A., Rioult, M.C., and Bear, M.F. (1996). Experience-dependent modification of synaptic plasticity in visual cortex. Nature 381, 526-528.

Kirkwood, A., Silva, A., and Bear, M.F. (1997). Age-dependent decrease of synaptic plasticity in the neocortex of alphaCaMKII mutant mice. Proceedings of the National Academy of Sciences of the United States of America 94, 3380-3383.

Kishino, T., Lalande, M., and Wagstaff, J. (1997a). UBE3A/E6-AP mutations cause Angelman syndrome. Nature genetics 15, 70-73.

Kishino, T., Lalande, M., and Wagstaff, J. (1997b). UBE3A/E6-AP mutations cause Angelman syndrome (vol 15, pg 70, 1997). Nature genetics 15, 411-411.

Kitada, T., Pisani, A., Porter, D.R., Yamaguchi, H., Tscherter, A., Martella, G., Bonsi, P., Zhang, C., Pothos, E.N., and Shen, J. (2007). Impaired dopamine release and synaptic plasticity in the striatum of PINK1-deficient mice. Proceedings of the National Academy of Sciences of the United States of America 104, 11441-11446.

Kleijnen, M.F., Alarcon, R.M., and Howley, P.M. (2003). The ubiquitin-associated domain of hPLIC-2 interacts with the proteasome. Molecular biology of the cell 14, 3868-3875.

Kleijnen, M.F., Shih, A.H., Zhou, P., Kumar, S., Soccio, R.E., Kedersha, N.L., Gill, G., and Howley, P.M. (2000). The hPLIC proteins may provide a link between the ubiquitination machinery and the proteasome. Molecular cell 6, 409-419.

Knoll, J.H., Nicholls, R.D., Magenis, R.E., Graham, J.M., Jr., Lalande, M., and Latt, S.A. (1989). Angelman and Prader-Willi syndromes share a common chromosome 15 deletion but differ in parental origin of the deletion. American journal of medical genetics 32, 285-290.

Ko, H.S., von Coelln, R., Sriram, S.R., Kim, S.W., Chung, K.K., Pletnikova, O., Troncoso, J., Johnson, B., Saffary, R., Goh, E.L*., et al.* (2005). Accumulation of the authentic parkin substrate aminoacyl-tRNA synthetase cofactor, p38/JTV-1, leads to catecholaminergic cell death. The Journal of neuroscience : the official journal of the Society for Neuroscience 25, 7968-7978.

Kosaka, T., Kosaka, K., Hataguchi, Y., Nagatsu, I., Wu, J.Y., Ottersen, O.P., Storm-Mathisen, J., and Hama, K. (1987). Catecholaminergic neurons containing GABA-like and/or glutamic acid decarboxylase-like immunoreactivities in various brain regions of the rat. Experimental brain research Experimentelle Hirnforschung Experimentation cerebrale 66, 191-210.

Kuhne, C., and Banks, L. (1998). E3-ubiquitin ligase/E6-AP links multicopy maintenance protein 7 to the ubiquitination pathway by a novel motif, the L2G box. The Journal of biological chemistry 273, 34302-34309.

Kumar, S., Talis, A.L., and Howley, P.M. (1999). Identification of HHR23A as a substrate for E6-associated protein-mediated ubiquitination. The Journal of biological chemistry 274, 18785-18792.

Lalande, M., and Calciano, M.A. (2007). Molecular epigenetics of Angelman syndrome. Cellular and molecular life sciences : CMLS 64, 947-960.

Lee, H.J., and Lee, S.J. (2002). Characterization of cytoplasmic alpha-synuclein aggregates. Fibril formation is tightly linked to the inclusion-forming process in cells. The Journal of biological chemistry 277, 48976-48983.

Lee, J.Y., Song, J., Kwon, K., Jang, S., Kim, C., Baek, K., Kim, J., and Park, C. (2012). Human DJ-1 and its homologs are novel glyoxalases. Human molecular genetics 21, 3215-3225.

Li, L., Li, Z., Howley, P.M., and Sacks, D.B. (2006a). E6AP and calmodulin reciprocally regulate estrogen receptor stability. The Journal of biological chemistry 281, 1978-1985.

Li, Y., Fitzpatrick, D., and White, L.E. (2006b). The development of direction selectivity in ferret visual cortex requires early visual experience. Nature neuroscience 9, 676-681.

Logothetis, N.K., Augath, M., Murayama, Y., Rauch, A., Sultan, F., Goense, J., Oeltermann, A., and Merkle, H. (2010). The effects of electrical microstimulation on cortical signal propagation. Nature neuroscience 13, 1283-1291.

Lossie, A.C., Whitney, M.M., Amidon, D., Dong, H.J., Chen, P., Theriaque, D., Hutson, A., Nicholls, R.D., Zori, R.T., Williams, C.A., and Driscoll, D.J. (2001). Distinct phenotypes distinguish the molecular classes of Angelman syndrome. Journal of medical genetics 38, 834-845.

Louria-Hayon, I., Alsheich-Bartok, O., Levav-Cohen, Y., Silberman, I., Berger, M., Grossman, T., Matentzoglu, K., Jiang, Y.H., Muller, S., Scheffner, M.*, et al.* (2009). E6AP promotes the degradation of the PML tumor suppressor. Cell death and differentiation 16, 1156-1166.

Lu, Y., Wang, F., Li, Y., Ferris, J., Lee, J.A., and Gao, F.B. (2009). The Drosophila homologue of the Angelman syndrome ubiquitin ligase regulates the formation of terminal dendritic branches. Human molecular genetics 18, 454-462.

Mabb, A.M., Judson, M.C., Zylka, M.J., and Philpot, B.D. (2011). Angelman syndrome: insights into genomic imprinting and neurodevelopmental phenotypes. Trends in neurosciences 34, 293-303.

Macdonald, P.A., and Monchi, O. (2011). Differential effects of dopaminergic therapies on dorsal and ventral striatum in Parkinson's disease: implications for cognitive function. Parkinson's disease 2011, 572743.

Maingay, M., Romero-Ramos, M., Carta, M., and Kirik, D. (2006). Ventral tegmental area dopamine neurons are resistant to human mutant alpha-synuclein overexpression. Neurobiology of disease 23, 522-532.

Majdan, M., and Shatz, C.J. (2006). Effects of visual experience on activity-dependent gene regulation in cortex. Nature neuroscience 9, 650-659.

Malenka, R.C., and Bear, M.F. (2004). LTP and LTD: an embarrassment of riches. Neuron 44, 5-21.

Manning, J.R., Jacobs, J., Fried, I., and Kahana, M.J. (2009). Broadband shifts in local field potential power spectra are correlated with single-neuron spiking in humans. The Journal of neuroscience : the official journal of the Society for Neuroscience 29, 13613-13620.

Mao, R., Jalal, S.M., Snow, K., Michels, V.V., Szabo, S.M., and Babovic-Vuksanovic, D. (2000). Characteristics of two cases with dup(15)(q11.2-q12): one of maternal and one of paternal origin. Genetics in medicine : official journal of the American College of Medical Genetics 2, 131-135.

Mardirossian, S., Rampon, C., Salvert, D., Fort, P., and Sarda, N. (2009). Impaired hippocampal plasticity and altered neurogenesis in adult Ube3a maternal deficient mouse model for Angelman syndrome. Experimental neurology 220, 341-348.

Margolis, S.S., Salogiannis, J., Lipton, D.M., Mandel-Brehm, C., Wills, Z.P., Mardinly, A.R., Hu, L., Greer, P.L., Bikoff, J.B., Ho, H.Y.*, et al.* (2010). EphB-mediated degradation of the RhoA GEF Ephexin5 relieves a developmental brake on excitatory synapse formation. Cell 143, 442-455.

Martinez-Noel, G., Galligan, J.T., Sowa, M.E., Arndt, V., Overton, T.M., Harper, J.W., and Howley, P.M. (2012). Identification and proteomic analysis of distinct UBE3A/E6AP protein complexes. Molecular and cellular biology 32, 3095-3106.

Matsushita, N., Okada, H., Yasoshima, Y., Takahashi, K., Kiuchi, K., and Kobayashi, K. (2002). Dynamics of tyrosine hydroxylase promoter activity during midbrain dopaminergic neuron development. Journal of neurochemistry 82, 295-304.

Mefford, I.N. (1981). Application of high performance liquid chromatography with electrochemical detection to neurochemical analysis: measurement of catecholamines, serotonin and metabolites in rat brain. Journal of neuroscience methods 3, 207-224.

Miano, S., Bruni, O., Leuzzi, V., Elia, M., Verrillo, E., and Ferri, R. (2004). Sleep polygraphy in Angelman syndrome. Clinical neurophysiology : official journal of the International Federation of Clinical Neurophysiology 115, 938-945.

Miller, K.J. (2010). Broadband spectral change: evidence for a macroscale correlate of population firing rate? The Journal of neuroscience : the official journal of the Society for Neuroscience 30, 6477-6479.

Minassian, B.A., DeLorey, T.M., Olsen, R.W., Philippart, M., Bronstein, Y., Zhang, Q., Guerrini, R., Van Ness, P., Livet, M.O., and Delgado-Escueta, A.V. (1998). Angelman syndrome: correlations between epilepsy phenotypes and genotypes. Annals of neurology 43, 485-493.

Mishra, A., Godavarthi, S.K., and Jana, N.R. (2009). UBE3A/E6-AP regulates cell proliferation by promoting proteasomal degradation of p27. Neurobiology of disease 36, 26-34.

Miura, K., Kishino, T., Li, E., Webber, H., Dikkes, P., Holmes, G.L., and Wagstaff, J. (2002). Neurobehavioral and electroencephalographic abnormalities in Ube3a maternal-deficient mice. Neurobiology of disease 9, 149-159.

Moncla, A., Malzac, P., Voelckel, M.A., Auquier, P., Girardot, L., Mattei, M.G., Philip, N., Mattei, J.F., Lalande, M., and Livet, M.O. (1999). Phenotype-genotype correlation in 20 deletion and 20 non-deletion Angelman syndrome patients. European journal of human genetics : EJHG 7, 131-139.

Muhammad, R., Brain, M.I.o.T.D.o., and Sciences, C. (2009). The Mouse Visually Evoked Potential: Neural Correlates and Functional Applications (Massachusetts Institute of Technology, Department of Brain and Cognitive Sciences).

Mulherkar, S.A., and Jana, N.R. (2010). Loss of dopaminergic neurons and resulting behavioural deficits in mouse model of Angelman syndrome. Neurobiology of disease 40, 586-592.

Mulherkar, S.A., Sharma, J., and Jana, N.R. (2009). The ubiquitin ligase E6-AP promotes degradation of alpha-synuclein. Journal of neurochemistry 110, 1955-1964.

Mulkey, R.M., Endo, S., Shenolikar, S., and Malenka, R.C. (1994). Involvement of a calcineurin/inhibitor-1 phosphatase cascade in hippocampal long-term depression. Nature 369, 486-488.

Mullen, R.J., Buck, C.R., and Smith, A.M. (1992). NeuN, a neuronal specific nuclear protein in vertebrates. Development 116, 201-211.

Nasu, J., Murakami, K., Miyagawa, S., Yamashita, R., Ichimura, T., Wakita, T., Hotta, H., Miyamura, T., Suzuki, T., Satoh, T., and Shoji, I. (2010). E6AP ubiquitin ligase mediates ubiquitin-dependent degradation of peroxiredoxin 1. Journal of cellular biochemistry 111, 676-685.

Nemani, V.M., Lu, W., Berge, V., Nakamura, K., Onoa, B., Lee, M.K., Chaudhry, F.A., Nicoll, R.A., and Edwards, R.H. (2010). Increased expression of alpha-synuclein reduces neurotransmitter release by inhibiting synaptic vesicle reclustering after endocytosis. Neuron 65, 66-79.

Nguyen, L., Besson, A., Heng, J.I., Schuurmans, C., Teboul, L., Parras, C., Philpott, A., Roberts, J.M., and Guillemot, F. (2006). p27kip1 independently promotes neuronal differentiation and migration in the cerebral cortex. Genes Dev 20, 1511-1524.

Nimchinsky, E.A., Sabatini, B.L., and Svoboda, K. (2002). Structure and function of dendritic spines. Annual review of physiology 64, 313-353.

Nuber, U., Schwarz, S.E., and Scheffner, M. (1998). The ubiquitin-protein ligase E6-associated protein (E6-AP) serves as its own substrate. Eur J Biochem 254, 643-649.

Oda, H., Kumar, S., and Howley, P.M. (1999). Regulation of the Src family tyrosine kinase Blk through E6AP-mediated ubiquitination. Proceedings of the National Academy of Sciences of the United States of America 96, 9557-9562.

Ohta, T., Buiting, K., Kokkonen, H., McCandless, S., Heeger, S., Leisti, H., Driscoll, D.J., Cassidy, S.B., Horsthemke, B., and Nicholls, R.D. (1999). Molecular mechanism of angelman syndrome in two large families involves an imprinting mutation. American journal of human genetics 64, 385-396.

Okun, M., and Lampl, I. (2008). Instantaneous correlation of excitation and inhibition during ongoing and sensory-evoked activities. Nature neuroscience 11, 535-537.

Pastalkova, E., Serrano, P., Pinkhasova, D., Wallace, E., Fenton, A.A., and Sacktor, T.C. (2006). Storage of spatial information by the maintenance mechanism of LTP. Science 313, 1141-1144.

Paxinos G, F.K. (2001). The Mouse Brain In Stereotaxic Coordinates. 2nd ed San Diego, California, USA: Academic Press.

Pelc, K., Boyd, S.G., Cheron, G., and Dan, B. (2008). Epilepsy in Angelman syndrome. Seizure : the journal of the British Epilepsy Association 17, 211-217.

Perez, R.G., Waymire, J.C., Lin, E., Liu, J.J., Guo, F., and Zigmond, M.J. (2002). A role for alpha-synuclein in the regulation of dopamine biosynthesis. The Journal of neuroscience : the official journal of the Society for Neuroscience 22, 3090-3099.

Peters, S.U., Beaudet, A.L., Madduri, N., and Bacino, C.A. (2004). Autism in Angelman syndrome: implications for autism research. Clinical genetics 66, 530-536.

Philpot, B.D., Cho, K.K., and Bear, M.F. (2007). Obligatory role of NR2A for metaplasticity in visual cortex. Neuron 53, 495-502.

Philpot, B.D., Sekhar, A.K., Shouval, H.Z., and Bear, M.F. (2001). Visual experience and deprivation bidirectionally modify the composition and function of NMDA receptors in visual cortex. Neuron 29, 157-169.

Philpot, B.D., Thompson, C.E., Franco, L., and Williams, C.A. (2011). Angelman syndrome: advancing the research frontier of neurodevelopmental disorders. Journal of neurodevelopmental disorders 3, 50-56.

Recchia, A., Debetto, P., Negro, A., Guidolin, D., Skaper, S.D., and Giusti, P. (2004). Alpha-synuclein and Parkinson's disease. FASEB journal : official publication of the Federation of American Societies for Experimental Biology 18, 617-626.

Robinson, W.P., Christian, S.L., Kuchinka, B.D., Penaherrera, M.S., Das, S., Schuffenhauer, S., Malcolm, S., Schinzel, A.A., Hassold, T.J., and Ledbetter, D.H. (2000). Somatic segregation errors predominantly contribute to the gain or loss of a paternal chromosome leading to uniparental disomy for chromosome 15. Clinical genetics 57, 349-358.

Ross, C.A., and Pickart, C.M. (2004). The ubiquitin-proteasome pathway in Parkinson's disease and other neurodegenerative diseases. Trends in cell biology 14, 703-711.

Rouge-Pont, F., Usiello, A., Benoit-Marand, M., Gonon, F., Piazza, P.V., and Borrelli, E. (2002). Changes in extracellular dopamine induced by morphine and cocaine: crucial control by D2 receptors. The Journal of neuroscience : the official journal of the Society for Neuroscience 22, 3293-3301.

Rougeulle, C., Glatt, H., and Lalande, M. (1997). The Angelman syndrome candidate gene, UBE3A/E6-AP, is imprinted in brain. Nature genetics 17, 14-15.

Rubenstein, J.L., and Merzenich, M.M. (2003). Model of autism: increased ratio of excitation/inhibition in key neural systems. Genes, brain, and behavior 2, 255-267.

Sato, H., Katsuyama, N., Tamura, H., Hata, Y., and Tsumoto, T. (1996). Mechanisms underlying orientation selectivity of neurons in the primary visual cortex of the macaque. The Journal of physiology 494 (Pt 3), 757-771.

Sato, M., and Stryker, M.P. (2010). Genomic imprinting of experience-dependent cortical plasticity by the ubiquitin ligase gene Ube3a. Proceedings of the National Academy of Sciences of the United States of America 107, 5611-5616.

Sawamoto, K., Nakao, N., Kobayashi, K., Matsushita, N., Takahashi, H., Kakishita, K., Yamamoto, A., Yoshizaki, T., Terashima, T., Murakami, F.*, et al.* (2001). Visualization, direct isolation, and transplantation of midbrain dopaminergic neurons. Proceedings of the National Academy of Sciences of the United States of America 98, 6423-6428.

Scherfler, C., Khan, N.L., Pavese, N., Eunson, L., Graham, E., Lees, A.J., Quinn, N.P., Wood, N.W., Brooks, D.J., and Piccini, P.P. (2004). Striatal and cortical pre- and postsynaptic dopaminergic dysfunction in sporadic parkin-linked parkinsonism. Brain : a journal of neurology 127, 1332-1342.

Schroer, R.J., Phelan, M.C., Michaelis, R.C., Crawford, E.C., Skinner, S.A., Cuccaro, M., Simensen, R.J., Bishop, J., Skinner, C., Fender, D., and Stevenson, R.E. (1998). Autism and maternally derived aberrations of chromosome 15q. American journal of medical genetics 76, 327-336.

Shapley, R., Hawken, M., and Ringach, D.L. (2003). Dynamics of orientation selectivity in the primary visual cortex and the importance of cortical inhibition. Neuron 38, 689-699.

Shenoy, S.K., and Lefkowitz, R.J. (2003). Multifaceted roles of beta-arrestins in the regulation of seven-membrane-spanning receptor trafficking and signalling. The Biochemical journal 375, 503-515.

Shi, S., Hayashi, Y., Esteban, J.A., and Malinow, R. (2001). Subunit-specific rules governing AMPA receptor trafficking to synapses in hippocampal pyramidal neurons. Cell 105, 331-343.

Shimoji, T., Murakami, K., Sugiyama, Y., Matsuda, M., Inubushi, S., Nasu, J., Shirakura, M., Suzuki, T., Wakita, T., Kishino, T.*, et al.* (2009). Identification of annexin A1 as a novel

substrate for E6AP-mediated ubiquitylation. Journal of cellular biochemistry 106, 1123-1135.

Shimura, H., Schlossmacher, M.G., Hattori, N., Frosch, M.P., Trockenbacher, A., Schneider, R., Mizuno, Y., Kosik, K.S., and Selkoe, D.J. (2001). Ubiquitination of a new form of alpha-synuclein by parkin from human brain: implications for Parkinson's disease. Science 293, 263-269.

Silva, A.J., Stevens, C.F., Tonegawa, S., and Wang, Y. (1992). Deficient hippocampal long-term potentiation in alpha-calcium-calmodulin kinase II mutant mice. Science 257, 201-206.

Smith, A., Marks, R., Haan, E., Dixon, J., and Trent, R.J. (1997). Clinical features in four patients with Angelman syndrome resulting from paternal uniparental disomy. Journal of medical genetics 34, 426-429.

Smith, A.D., and Bolam, J.P. (1990). The neural network of the basal ganglia as revealed by the study of synaptic connections of identified neurones. Trends in neurosciences 13, 259-265.

Smith, S.E., Zhou, Y.D., Zhang, G., Jin, Z., Stoppel, D.C., and Anderson, M.P. (2011). Increased gene dosage of Ube3a results in autism traits and decreased glutamate synaptic transmission in mice. Science translational medicine 3, 103ra197.

Snyder, H., Mensah, K., Theisler, C., Lee, J., Matouschek, A., and Wolozin, B. (2003). Aggregated and monomeric alpha-synuclein bind to the S6' proteasomal protein and inhibit proteasomal function. The Journal of biological chemistry 278, 11753-11759.

Starke, K., Gothert, M., and Kilbinger, H. (1989). Modulation of neurotransmitter release by presynaptic autoreceptors. Physiological reviews 69, 864-989.

Steffenburg, S., Gillberg, C.L., Steffenburg, U., and Kyllerman, M. (1996). Autism in Angelman syndrome: a population-based study. Pediatric neurology 14, 131-136.

Sutcliffe, J.S., Jiang, Y.H., Galijaard, R.J., Matsuura, T., Fang, P., Kubota, T., Christian, S.L., Bressler, J., Cattanach, B., Ledbetter, D.H., and Beaudet, A.L. (1997a). The E6-Ap ubiquitin-protein ligase (UBE3A) gene is localized within a narrowed Angelman syndrome critical region. Genome research 7, 368-377.

Sutcliffe, J.S., Jiang, Y.H., Galjaard, R.J., Christian, S.L., Matsuura, T., Fang, P., Kubota, T., Bressler, J., Cattanach, B., Ledbetter, D.H., and Beaudet, A.L. (1997b). The E6-AP ubiquitin-protein ligase (UBE3A) gene is localized within a narrowed angelman syndrome critical region. Genome research 7, 368-377.

Tan, W.-H. (2012). A Trial of Levodopa in Angelman Syndrome. In NIH Web site http://clinicaltrialsgov/ct2/show/NCT01281475.

Tanaka, Y., Engelender, S., Igarashi, S., Rao, R.K., Wanner, T., Tanzi, R.E., Sawa, A., V, L.D., Dawson, T.M., and Ross, C.A. (2001). Inducible expression of mutant alpha-synuclein decreases proteasome activity and increases sensitivity to mitochondria-dependent apoptosis. Human molecular genetics 10, 919-926.

Thompson, D.A., Kriss, A., Cottrell, S., and Taylor, D. (1999). Visual evoked potential evidence of albino-like chiasmal misrouting in a patient with Angelman syndrome with no ocular features of albinism. Developmental medicine and child neurology 41, 633-638.

Torii, N., Kamishita, T., Otsu, Y., and Tsumoto, T. (1995). An inhibitor for calcineurin, FK506, blocks induction of long-term depression in rat visual cortex. Neuroscience letters 185, 1-4.

Tropea, D., Kreiman, G., Lyckman, A., Mukherjee, S., Yu, H., Horng, S., and Sur, M. (2006). Gene expression changes and molecular pathways mediating activity-dependent plasticity in visual cortex. Nature neuroscience 9, 660-668.

Van Splunder, J., Stilma, J.S., and Evenhuis, H.M. (2003). Visual performance in specific syndromes associated with intellectual disability. European journal of ophthalmology 13, 566-574.

van Woerden, G.M., Harris, K.D., Hojjati, M.R., Gustin, R.M., Qiu, S., de Avila Freire, R., Jiang, Y.H., Elgersma, Y., and Weeber, E.J. (2007). Rescue of neurological deficits in a mouse model for Angelman syndrome by reduction of alphaCaMKII inhibitory phosphorylation. Nature neuroscience 10, 280-282.

Vu, T.H., and Hoffman, A.R. (1997). Imprinting of the Angelman syndrome gene, UBE3A, is restricted to brain. Nature genetics 17, 12-13.

Wallace, M.L., Burette, A.C., Weinberg, R.J., and Philpot, B.D. (2012). Maternal loss of Ube3a produces an excitatory/inhibitory imbalance through neuron type-specific synaptic defects. Neuron 74, 793-800.

Wallace, W., and Bear, M.F. (2004). A morphological correlate of synaptic scaling in visual cortex. The Journal of neuroscience : the official journal of the Society for Neuroscience 24, 6928-6938.

Walz, N.C., and Baranek, G.T. (2006). Sensory processing patterns in persons with Angelman syndrome. The American journal of occupational therapy : official publication of the American Occupational Therapy Association 60, 472-479.

Wang, H.Q., Imai, Y., Inoue, H., Kataoka, A., Iita, S., Nukina, N., and Takahashi, R. (2008). Pael-R transgenic mice crossed with parkin deficient mice displayed progressive and selective catecholaminergic neuronal loss. Journal of neurochemistry 107, 171-185.

Watabe-Uchida, M., Zhu, L., Ogawa, S.K., Vamanrao, A., and Uchida, N. (2012). Whole-brain mapping of direct inputs to midbrain dopamine neurons. Neuron 74, 858-873.

Weeber, E.J., Jiang, Y.H., Elgersma, Y., Varga, A.W., Carrasquillo, Y., Brown, S.E., Christian, J.M., Mirnikjoo, B., Silva, A., Beaudet, A.L., and Sweatt, J.D. (2003). Derangements of hippocampal calcium/calmodulin-dependent protein kinase II in a mouse model for Angelman mental retardation syndrome. The Journal of neuroscience : the official journal of the Society for Neuroscience 23, 2634-2644.

Welter, M., Vallone, D., Samad, T.A., Meziane, H., Usiello, A., and Borrelli, E. (2007). Absence of dopamine D2 receptors unmasks an inhibitory control over the brain circuitries activated by cocaine. Proceedings of the National Academy of Sciences of the United States of America 104, 6840-6845.

Wersinger, C., Prou, D., Vernier, P., Niznik, H.B., and Sidhu, A. (2003). Mutations in the lipid-binding domain of alpha-synuclein confer overlapping, yet distinct, functional properties in the regulation of dopamine transporter activity. Molecular and cellular neurosciences 24, 91-105.

Wersinger, C., Vernier, P., and Sidhu, A. (2004). Trypsin disrupts the trafficking of the human dopamine transporter by alpha-synuclein and its A30P mutant. Biochemistry 43, 1242-1253.

West, M.J. (1999). Stereological methods for estimating the total number of neurons and synapses: issues of precision and bias. Trends in neurosciences 22, 51-61.

Westerink, B.H.C., Kwint, H.F., and deVries, J.B. (1996). The pharmacology of mesolimbic dopamine neurons: A dual-probe microdialysis study in the ventral tegmental area and nucleus accumbens of the rat brain. Journal of Neuroscience 16, 2605-2611.

Wiesel, T.N., and Hubel, D.H. (1963). Single-Cell Responses in Striate Cortex of Kittens Deprived of Vision in One Eye. Journal of neurophysiology 26, 1003-1017.

Williams, C.A., Beaudet, A.L., Clayton-Smith, J., Knoll, J.H., Kyllerman, M., Laan, L.A., Magenis, R.E., Moncla, A., Schinzel, A.A., Summers, J.A., and Wagstaff, J. (2006). Angelman syndrome 2005: updated consensus for diagnostic criteria. American journal of medical genetics Part A 140, 413-418.

Williams, C.A., Driscoll, D.J., and Dagli, A.I. (2010). Clinical and genetic aspects of Angelman syndrome. Genetics in medicine : official journal of the American College of Medical Genetics 12, 385-395.

Williams, C.A., Zori, R.T., Stone, J.W., Gray, B.A., Cantu, E.S., and Ostrer, H. (1990). Maternal origin of 15q11-13 deletions in Angelman syndrome suggests a role for genomic imprinting. American journal of medical genetics 35, 350-353.

Wise, R.A. (2002). Brain reward circuitry: insights from unsensed incentives. Neuron 36, 229-240.

Wise, R.A., and Rompre, P.P. (1989). Brain dopamine and reward. Annual review of psychology 40, 191-225.

Wisor, J.P., Nishino, S., Sora, I., Uhl, G.H., Mignot, E., and Edgar, D.M. (2001). Dopaminergic role in stimulant-induced wakefulness. The Journal of neuroscience : the official journal of the Society for Neuroscience 21, 1787-1794.

Wolf, M.E., and Roth, R.H. (1990). Autoreceptor regulation of dopamine synthesis. Annals of the New York Academy of Sciences 604, 323-343.

Wu, M.Y., Chen, K.S., Bressler, J., Hou, A., Tsai, T.F., and Beaudet, A.L. (2006). Mouse imprinting defect mutations that model Angelman syndrome. Genesis 44, 12-22.

Wu, Y., Bolduc, F.V., Bell, K., Tully, T., Fang, Y., Sehgal, A., and Fischer, J.A. (2008). A Drosophila model for Angelman syndrome. Proceedings of the National Academy of Sciences of the United States of America 105, 12399-12404.

Xia, Z., and Storm, D.R. (2005). The role of calmodulin as a signal integrator for synaptic plasticity. Nature reviews Neuroscience 6, 267-276.

Xiong, H., Wang, D., Chen, L., Choo, Y.S., Ma, H., Tang, C., Xia, K., Jiang, W., Ronai, Z., Zhuang, X., and Zhang, Z. (2009). Parkin, PINK1, and DJ-1 form a ubiquitin E3 ligase complex promoting unfolded protein degradation. The Journal of clinical investigation 119, 650-660.

Yamamoto, Y., Huibregtse, J.M., and Howley, P.M. (1997). The human E6-AP gene (UBE3A) encodes three potential protein isoforms generated by differential splicing. Genomics 41, 263-266.

Yashiro, K., Riday, T.T., Condon, K.H., Roberts, A.C., Bernardo, D.R., Prakash, R., Weinberg, R.J., Ehlers, M.D., and Philpot, B.D. (2009). Ube3a is required for experience-dependent maturation of the neocortex. Nature neuroscience 12, 777-783.

Yasuda, H., Barth, A.L., Stellwagen, D., and Malenka, R.C. (2003). A developmental switch in the signaling cascades for LTP induction. Nature neuroscience 6, 15-16.

Yi, J.J., and Ehlers, M.D. (2005). Ubiquitin and protein turnover in synapse function. Neuron 47, 629-632.

Yi, J.J., and Ehlers, M.D. (2007). Emerging roles for ubiquitin and protein degradation in neuronal function. Pharmacological reviews 59, 14-39.

Yizhar, O., Fenno, L.E., Prigge, M., Schneider, F., Davidson, T.J., O'Shea, D.J., Sohal, V.S., Goshen, I., Finkelstein, J., Paz, J.T.*, et al.* (2011). Neocortical excitation/inhibition balance in information processing and social dysfunction. Nature 477, 171-178.

Yu, S., Ueda, K., and Chan, P. (2005). Alpha-synuclein and dopamine metabolism. Molecular neurobiology 31, 243-254.

Zaaroor-Regev, D., de Bie, P., Scheffner, M., Noy, T., Shemer, R., Heled, M., Stein, I., Pikarsky, E., and Ciechanover, A. (2010). Regulation of the polycomb protein Ring1B by self-ubiquitination or by E6-AP may have implications to the pathogenesis of Angelman syndrome. Proceedings of the National Academy of Sciences of the United States of America 107, 6788-6793.

Zahm, D.S., Cheng, A.Y., Lee, T.J., Ghobadi, C.W., Schwartz, Z.M., Geisler, S., Parsely, K.P., Gruber, C., and Veh, R.W. (2011). Inputs to the midbrain dopaminergic complex in the rat, with emphasis on extended amygdala-recipient sectors. The Journal of comparative neurology 519, 3159-3188.

Zhang, Y., Gao, J., Chung, K.K., Huang, H., Dawson, V.L., and Dawson, T.M. (2000). Parkin functions as an E2-dependent ubiquitin- protein ligase and promotes the degradation of the synaptic vesicle-associated protein, CDCrel-1. Proceedings of the National Academy of Sciences of the United States of America 97, 13354-13359.

Zheng, L., Ding, H., Lu, Z., Li, Y., Pan, Y., Ning, T., and Ke, Y. (2008). E3 ubiquitin ligase E6AP-mediated TSC2 turnover in the presence and absence of HPV16 E6. Genes to cells : devoted to molecular & cellular mechanisms 13, 285-294.

Zoghbi, H.Y. (2003). Postnatal neurodevelopmental disorders: meeting at the synapse? Science 302, 826-830.